University of Crete

School of Sciences and Engineering

Department of Materials Science and Engineering

Master Thesis

«Synthesis and characterization of acid- and photo-degradable star polymers»

Niki Iliadi

Registration number 151

Supervisor: Professor Maria Vamvakaki

Heraklion, October 2018

Abstract

This Master Thesis focused on the synthesis and characterization of star polymers, specifically tailored to be acid- and photo-degradable. In order to achieve that, two novel cross-linkers were synthesized via acid-catalysed condensation reactions, that were later used for the synthesis of two different polymers each. The polymerization method employed for the synthesis of the star polymers was group transfer polymerization with an arm-first approach for all star polymers. The molecular weight of the polymers was determined by size exclusion chromatography, and their molecular structure was verified via ^{1}H nuclear magnetic resonance spectroscopy. The size of the polymers was also measured with dynamic light scattering, and finally the polymers were imaged by scanning electron microscopy. Following their characterization, their degradation needed to be proven. Both cross-linkers were sensitive to a decrease in the pH value due to the characteristic acetal groups they carry, and their degradation after treatment with a hydrochloric acid solution was proven by size exclusion chromatography, nuclear magnetic resonance spectroscopy, as well as dynamic light scattering and scanning electron microscopy. One of the synthesized cross-linkers was also proven to be photo-degradable under irradiation at 254 nm, due to the aromatic groups it carries along with its characteristic acetal bonds. The photo-degradation of the star polymers was also proven using the same characterization techniques as described above.

Περίληψη

Σκοπός της παρούσας μεταπτυχιακής εργασίας ήταν η σύνθεση αστεροειδών πολυμερών, τα οποία θα είναι ικανά να υποστούν διάσπαση μετά την εφαρμογή κάποιου εξωτερικού παράγοντα. Για τον σκοπό αυτό πραγματοποιήθηκε σύνθεση μέσω όξινα καταλυώμενης αντίδρασης συμπύκνωσης δύο διαφορετικών μορίων με την ικανότητα να δράσουν ως διασταυρωτές, τα οποία έχουν ως βάση τον ακεταλικό δεσμό για να αποδώσουν τις επιθυμητές ιδιότητες στο τελικό πολυμερές, καθώς και διπλούς δεσμούς στα άκρα τους ώστε να μπορούν να λειτουργήσουν ως διασταυρωτές. Και οι δύο διασταυρωτές απαλλάχθηκαν από ακαθαρσίες και τυχόν υλικά που δεν καταναλώθηκαν κατά τη διάρκεια της αντίδρασης για την σύνθεσή τους με διέλευσή τους από στήλη χρωματογραφίας και στη συνέχεια πραγματοποιήθηκε ο χαρακτηρισμός τους με τη βοήθεια φασματοσκοπίας πυρηνικού μαγνητικού συντονισμού. Οι διασταυρωτές αυτοί χρησιμοποιήθηκαν στη συνέχεια για τη σύνθεση αστεροειδών πολυμερών, στα οποία αποτελούν τον πυρήνα, μέσω συμπολυμερισμού τους με συγκεκριμένα μονομερή, τα οποία είναι αυτά που υπόκεινται πρώτα πολυμερισμό και σχηματίζουν τα άκρα του αστέρα. Η μέθοδος πολυμερισμού που χρησιμοποιήθηκε ήταν ο πολυμερισμός μεταφοράς ομάδας (GTP) και τα μονομερή που χρησιμοποιήθηκαν για την σύνθεση των άκρων του αστεριού είναι ο μεθακρυλικός μεθυλεστέρας (methyl methacrylate, MMA) και ο μεθακρυλικός (2-διμέθυλοαμινο)αιθυλεστέρας (2-(dimethylamino)ethyl methacrylate, DMAEMA) με διαφορετική διάταξη. Για τον κάθε διασταυρωτή συντέθηκαν δύο αστεροειδή πολυμερή, το ένα εκ των οποίων περιείχε συσταδικά συμπολυμερή για άκρα, ενώ το δεύτερο τυχαία συμπολυμερή. Το μοριακό βάρος όλων των πολυμερών, καθώς και των άκρων τους πριν το τελικό στάδιο του πολυμερισμού λάβει χώρα, προσδιορίστηκε μέσω χρωματογραφίας αποκλεισμού μεγεθών και η τελική τους σύσταση επιβεβαιώθηκε με τη βοήθεια φασματοσκοπίας πυρηνικού μαγνητικού συντονισμού. Η υδροδυναμική διάμετρος των αστεροειδών πολυμερών μετρήθηκε επίσης μέσω δυναμικής σκέδασης φωτός, ενώ η διάταξη η οποία υιοθετούν τα μόρια του πολυμερούς στο χώρο παρατηρήθηκε μέσω σαρωτικής ηλεκτρονιακής μικροσκοπίας.

Στη συνέχεια, κρίθηκε απαραίτητο να αποδειχθεί το γεγονός ότι κατεργασία των πολυμερών, ανεξαρτήτως του διασταυρωτή που χρησιμοποιήθηκε για τη σύνθεσή τους, με διάλυμα οξέος, μπορεί να οδηγήσει στην διάσπαση του ακεταλικού δεσμού που φέρουν οι διασταυρωτές, και κατά συνέπεια στη διάσπαση των αστεριών. Διαλύματα δειγμάτων από το κάθε πολυμερές λοιπόν αναμείχθηκαν με διάλυμα υδροχλωρικού οξέος, και ύστερα ελέγχθηκαν με χρωματογραφία αποκλεισμού μεγεθών η οποία και επιβεβαίωσε την διάσπαση του αστεροειδούς πολυμερούς. Μετρήσεις φασματοσκοπίας πυρηνικού μαγνητικού συντονισμού στήριξαν το γεγονός αυτό. Η υδροδυναμική διάμετρος των διεσπασμένων πολυμερών μετρήθηκε επίσης, μερικές φορές ανεπιτυχώς, μέσω δυναμικής σκέδασης φωτός και η μορφή τους παρατηρήθηκε για άλλη μια φορά μέσω σαρωτικής ηλεκτρονιακής μικροσκοπίας, όπου οι αλλαγές που υπέστη το πολυμερές ήταν παραπάνω από προφανείς.

Τέλος, ο ένας από του δύο διασταυρωτές που συντέθηκαν φέρει επίσης μια αρωματική ομάδα, η οποία και τον καθιστά ικανό να απορροφήσει ακτινοβολία και να οδηγήσει στη διάσπαση του ακεταλικού δεσμού, και συνεπώς στη διάσπαση του αστεροειδούς πολυμερούς. Διαλύματα δειγμάτων από τα πολυμερή εκτέθηκαν σε ακτινοβολία 254 nm για χρονικό διάστημα 12 ωρών, και η πορεία της διάσπασης παρακολουθήθηκε με χρωματογραφία αποκλεισμού μεγεθών καθώς και με φασματοσκοπία πυρηνικού μαγνητικού συντονισμού. Τα τελικά διεσπασμένα προϊόντα απεικονίστηκαν για ακόμα μια φορά μέσω ηλεκτρονιακού μικροσκοπίου σάρωσης.

Συνοψίζοντας, κατά τη διάρκεια της παρούσας μεταπτυχιακής εργασίας, συντέθηκαν επιτυχώς δύο διασταυρωτές με βάση τον ακεταλικό δεσμό, ο ένας εκ των οποίων και ήταν αρωματικός. Αστεροειδή πολυμερή συντέθηκαν μέσω πολυμερισμού μεταφοράς ομάδας με τους διασταυρωτές αυτούς να παίζουν τον ρόλο του πυρήνα. Όλα τα πολυμερή χαρακτηρίστηκαν με τη βοήθεια χρωματογραφίας αποκλεισμού μεγεθών, φασματοσκοπίας πυρηνικού μαγνητικού συντονισμού, δυναμικής σκέδασης φωτός και σαρωτικής ηλεκτρονιακής μικροσκοπίας. Στη συνέχεια αποδείχθηκε η επιτυχής διάσπασή τους μετά από κατεργασία τους με όξινα μέσα, η οποία και επιβεβαιώθηκε με τις προαναφερθείς μεθόδους. Τέλος, τα πολυμερή που συντέθηκαν με τον αρωματικό διασταυρωτή υπέστησαν επίσης διάσπαση μετά από έκθεσή τους σε φως μήκους κύματος 254 nm, με την διάσπασή τους να επιβεβαιώνεται για άλλη μια φορά από τις παραπάνω μεθόδους χαρακτηρισμού.

Acknowledgements

First and foremost, I would like to thank Prof. Maria Vamvakaki for giving me the opportunity to work in her laboratory for the duration of my Master Thesis and further my education in that new field that I chose to work in, and for her guidance whenever and wherever was needed. I would also like to thank Dr. Theodore Manouras for his help and guidance during my stay in the Polymer Laboratory.

I would also like to thank all the members of our research group, with very special thanks to Lucille Chambon for her invaluable help while conducting my experiments, both in the form of general advice and guidance, as well as specific advice on my work in the lab whenever was needed. Also, I want to thank Maria Psarrou, for sharing with me her experience on polyacetals during the last stages of my experiments, as well as Eva Vasilaki for their help whenever I needed it for the duration of my thesis, in addition to the support of every one of them outside of the lab.

Furthermore, I want to give a very special and large thank you to my parents, Maria and Dionysis, and my brother Vasilis, for being there for me and supporting me all these years, as well as all my friends, and especially Rigas, Theodora and Eleni for their support and encouragement these lasts few years.

Finally, I would also like to thank Assistant Professor Maria Chatzinikolaidou from the Department of Materials Science and Engineering, as well as Assistant Professor Vaggelis Harmandaris from the Department of Mathematics and Applied Mathematics for honoring me by participating in the examination committee for the presentation of my Master Thesis.

Table of Contents

1. Introduction

1.1 Polymers

Polymers are macromolecules comprising a large number of covalently bound repeat units. They can be divided into two general categories: i) Natural polymers, such as RNA and DNA, and in general polymers that can be found in nature, and ii) Synthetic polymers. The high molecular mass of the polymers leads to unique physical properties, including toughness, viscoelasticity and a tendency to form glasses and semicrystalline structures, rather than crystals. Because of their broad range of properties, both synthetic and natural polymers play an essential role in everyday life. [1,2]

The term "polymer" was coined in 1833 by Jöns Jacob Berzelius, to describe organic compounds which shared identical empirical formulas, but which differed in the overall molecular weight, the larger of the compounds being described as "polymers" of the smallest, viewing for example glucose ($C_6H_{12}O_6$) as a polymer of formaldehyde (CH_2O), a definition that greatly differs from the modern IUPAC definition. In the beginning of the 1900s, Baekeland, while exploring possible combinations of phenol and formaldehyde by controlling the temperature and pressure applied to them, managed to synthesize the first completely synthetic and moldable plastic, Bakelite, thus marking the beginning of the age of plastics. The modern concept of polymers as covalently bonded macromolecular structures was proposed in 1920 by Hermann Staudinger, who spent the next decade finding experimental evidence to support his hypothesis, since leading organic chemists at the time, such as Emil Fischer and Heinrich Wieland, believed that the high molecular weights that were being measured, were the result of the aggregation of smaller molecules into colloids. The evidence Staudinger was expecting though, emerged in the 1930s, as the high molecular weight of the polymers was confirmed by membrane osmometry, as well as viscosity measurements in solution. Herman Mark's studies in X-ray diffraction also gave direct evidence for long chains consisting of repeated molecular units, and the synthetic work that Carothers was conducting at the time demonstrated clearly that polymers such as nylon, could be prepared by well-understood organic reactions. Staudinger's theory set a solid basis for further development of Polymer Science, eventually leading to his being awarded the Nobel Prize in Chemistry in 1953 for "his discoveries in the field of macromolecular chemistry".

Polymer Properties

As mentioned above, a polymer is a large molecule, or macromolecule, composed of many repeated units. Every synthesized polymer has different properties, owing to a number of factors, and depending on the properties that the final polymer is expected

to have, its synthesis can be tailored specifically so that the desired properties can be achieved.

The most basic property of a polymer is the identity of its constituent *monomers*, while a second set of properties, called *microstructure* or *configuration*, describes the way the repeat units are arranged in a single polymeric chain. Depending on the identity of monomer used, the polymers can be separated into categories. Homopolymers consist of a single type of repeat unit, while polymers containing two or more types of repeat units, are called copolymers. Polymers containing three types of repeat units are called terpolymers. The configuration of the polymer refers to the physical way the repeat units are arranged along the backbone of the polymeric chain. For example, in the case of copolymers, the possible configurations of the different repeat units could be:

- Alternating copolymers: they contain two, regularly alternating repeat units

  -A-B-A-B-A-B-A-B-A-B-A-B-A-B-A-B-A-B-A-B-A-B-A-B-A-B-

- Random (or statistical) copolymers: the different types of repeat units along the backbone are alternating in a completely random way

  -A-A-A-B-A-B-B-B-B-B-A-A-A-A-B-A-B-A-A-B-A-B-A-B-A-B-B-B-

- Block copolymers: they consist of long sequences of different repeat units. Block copolymers with two or three different types of repeat units, are called diblocks and triblock copolymers respectively.

  -A-A-A-A-A-A-A-A-A-A-A-B-B-B-B-B-B-B-B-B-B-B-B-B-B-

- Graft copolymers: they contain side chains, or branches, that are of a different composition or configuration than the main chain, and they are typically added on a preformed polymeric backbone.

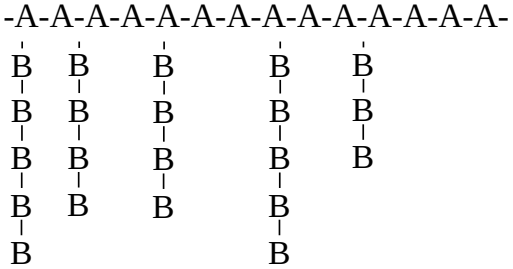

It is also possible to have polymeric mixtures, that can be either miscible, or immiscible.

Overall, the properties of the copolymers typically differ in comparison to the corresponding homopolymers. The properties of any given polymer are also depended on its topology, also known as *polymer architecture*, and they can be divided into categories based on it. These categories are:

- Linear polymers: They consist of a single chain of repeat units, with no pendant groups. A representative example of this category, is high density polyethylene (HDPE), that consists of more than a thousand CH_2 units, $-[-CH_2-CH_2-]_n-$.
- Branched polymers: The polymers of this category have branches of different sizes spaced along the backbone at irregular intervals, and so they are thought to be non-linear. Main example is low density polyethylene (LDPE). The branches that these polymers have, tend to act as an obstacle, and the polymer chains cannot be closely packed, resulting in a polymer with lower density in comparison to its linear counterpart. Brush, ladder, dendritic and hyperbranched polymers also belong in this general category. Star polymers also represent a class of branched polymers with linear "arms" bound onto a single central branching point, that is referred to as the "core"[3].
- Crosslinked polymers: When there are cross-links between chains of the polymer, a three-dimensional network is created. This leads to high density polymers, the chains of which have minimal mobility, thus a very rigid material is created.

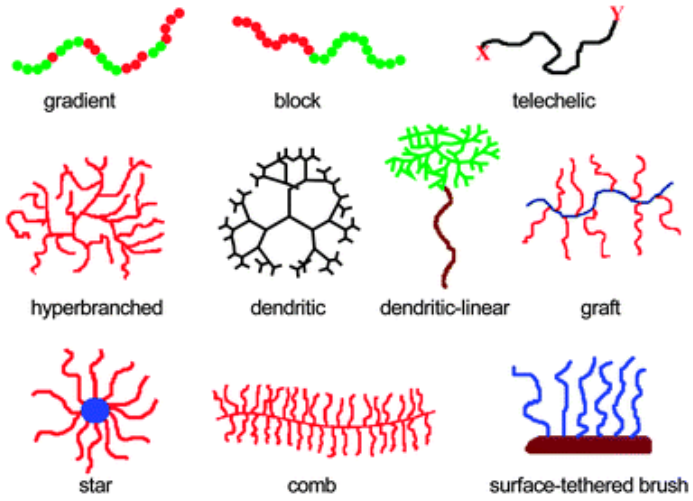

Figure 1 - Schematic representation of polymer chain architectures [4]

In the case of linear polymers, when the repeat units are not symmetric, there is another factor that influences the properties of the polymer, and that is *tacticity*, or in other words, the steric order. If all the chiral centers have the same configuration, the arrangement of the side groups is considered *isotactic*. In case every other chiral center has the same arrangement, then it is called *syndiotactic*, and lastly, when the side groups are arranged in a completely random order, their arrangement is considered *atactic* or *heterotactic*.

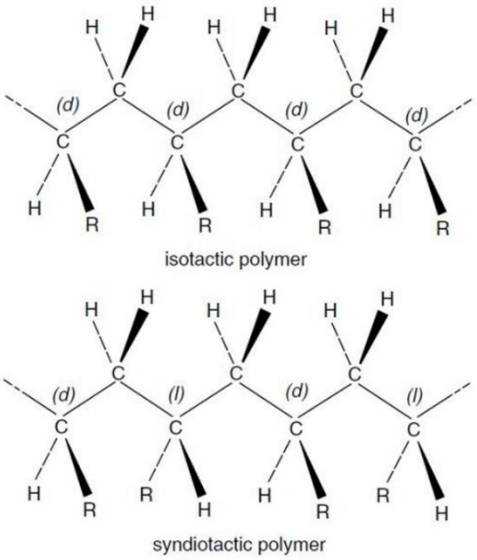

Figure 2 - Representation of polymer Tacticity [5]

The tacticity that each polymer exhibits, greatly influences its properties, as isotactic or syndiotactic polymers can be packed into fibers and crystals with ease, while in atactic polymers, packing cannot occur. Thus, the glass transition temperature (T_g) that each polymer exhibits are different for every configuration.

One of the properties that does not depend either on the architecture or the microstructure of the polymers, but does depend on the chain length, is their molecular weight. Due to the fact that the polymerization process is typically random, the resulting chains are not all of the same length. So, when we refer to molecular weight of a polymer, we are typically talking about an average molecular weight. There are two ways to calculate that:

- Number average molecular weight: It is the total weight of the sample divided by the number of molecules in the sample, or:

$$\overline{\mathrm{M}}_{\mathrm{n}} = \frac{\sum_i N_i M_i}{\sum_i N_i} = \sum_{\mathrm{i}} f_{\mathrm{i}} M_i$$

- Weight average molecular weight: To calculate the weight average molecular weight, the weight fraction of each type of molecule, w_i, needs to be calculated too. The weight fraction is expressed as the weight of one type of molecule divided by the total weight of the sample, and it is different for each type of molecule, so it needs to be calculated separately. After the weight fraction is calculated, the weight average molecular weight of the polymer can be estimated by the following equation:

$$\overline{\mathrm{M}}_{\mathrm{w}} = \frac{\sum_i w_i M_i}{\sum_i w_i} = \frac{\sum_i N_i M_i^2}{\sum_i N_i M_i}$$

As mentioned previously, not all polymeric chains have the same number of repeat units. Apart from the number average and weight average molecular weights, there is another factor we can calculate, that shows us the breadth of the molecular weight distribution: the polydispersity index. The polydispersity index (PDI) is defined as follows:

$$\mathrm{I} = \frac{\overline{M}_w}{\overline{M}_n}$$

Where I=1 when all the chains have the same length, so the polymers are monodisperse (e.g. proteins) or it can be I≥1 for polymers with chains of a different size. The higher the value of the polydispersity index, the broader the distribution of molecular weights in the sample.

The degree of polymerization (DP) also needs to be calculated, and is defined as :

$$DP = \frac{MW_{polymer}}{MW_{repeat\ unit}}$$

1.2 Star polymers

Star polymers consist of numerous linear polymeric chains, the arms, that all connect to a central branching point, typically referred to as the core of the star, that can either be an atom, a molecule, or a macromolecule. They can be divided into two categories based on the chemical composition of the arm species: Homo-arm star polymers and mikto-arm (or heteroarm) star copolymers [6]. Homo-arm star polymers have arms with identical chemical composition and more often than not, similar molecular weights, while miktoarm star polymers contain arms of two or more different compositions and can be further divided into categories based on their asymmetric architecture, that demonstrate their varying molecular weights, topologies, and functional groups [7].

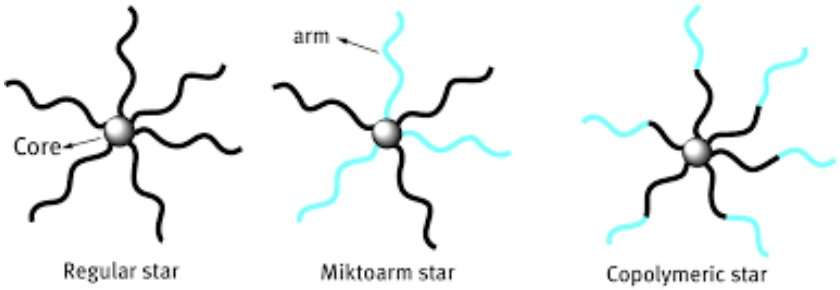

Figure 3 - Representation of structure in star polymers [8]

Due to their unique structure, star polymers exhibit noteworthy properties and characteristics, thus constituting a class of materials that have already been utilized in several industrial applications, while they are still under research for more sophisticated applications. They are used as model materials in rheological studies since they can be synthesized with very narrow dispersities. The effect that the molecular weight of the arms as well as the arm number and core size have on the polymer properties is also being investigated, since viscosity, shear rate, glass transition temperature (T_g), melting temperature (T_m), crystallization temperature (T_c) and decomposition temperature (T_d) have been observed to differentiate when changing the core size or the number of arms. . Industrially they are currently being used as viscosity modifiers in a range of products, and in defoaming applications, while academically they are studied as interfacial stabilizing agents [9, 10], as vectors for gene delivery [11, 12], as carriers for drug encapsulation [13, 14] and delivery [15], for molecular imaging in therapy development [16] and as nanoreactors for catalysis [17].

1.3 Polymerization Methods

Polymerization occurs via a variety of reaction mechanisms that vary in complexity but can be divided into two broad categories: step-growth or polycondensation polymerizations and chain-growth or addition polymerizations. The distinction [18] between polycondensation and addition polymerizations was initially made by Wallace H. Carothers in 1929 [19] based on the final products of the reactions, and was further corroborated by Paul Flory in 1953, who introduced the terms step-growth and chain-growth polymerizations and differentiated between the two based on the mechanism responsible for the polymerization reaction [20]. Specifically:

a. Step-growth or polycondensation polymerization: bifunctional or multifunctional monomers react to form dimers, trimers, oligomers, and eventually polymers. The molecular weight increases slowly, so when high molecular weights are needed, long reaction times are essential. In the case of condensation reactions, two monomers combine to form a dimer while a small molecule, usually water, is released as a byproduct. If the monomers used in the polymerization are bifunctional, then the resulting polymer will be linear. When the monomer's functionality is higher, branching can occur, resulting in a

crosslinked final polymer. The addition of monofunctional monomers terminates the polymerization reaction. Polyesters, polyamides such as nylon, polyurethanes, polycarbonates etc. can be synthesized via polycondensation reactions.

b. Chain-growth or addition polymerization is a polymerization technique in which unsaturated monomers, usually alkenes, are added on the active site of a growing polymer chain one at a time. Growth of the polymeric chain occurs only at one end (or ends if we refer to branched polymers), and every repeated unit that is added, regenerates the active site so that the chains keep on growing. Chain-growth polymerizations usually have three steps: initiation, propagation and termination. Chain transfer could be considered as an additional step before termination, that even though it terminates one chain by reacting with the solvent/monomer/another polymer molecule, it can lead to branched polymers. The speed of the reaction depends on the concentration of the initiator, so high molecular weight polymers can be formed throughout the reaction. Polymers such as polyvinylchloride (PVC), polystyrene and polytetrafluoroethylene (Teflon) can be synthesized via addition polymerization.

In the case of addition (chain-growth) polymerization, depending on the species of the active site, we can further distinguish the polymerization mechanisms as follows:

- Free radical polymerization: when the active site is a free radical, which is a very reactive atom or molecule with an unpaired electron. Free radical polymerizations do not require extreme temperature or pressure, but they tend to lack control, resulting in branched polymers or in polymers with much shorter chains than desired due to early and random termination.
- Cationic polymerization: when the initiator produces a carbocation that initiates the polymerization, thus the active center is cationic [21].
- Anionic polymerization: when a carbanion acts as an initiator for the polymerization, so the active center of the polymerization is anionic as well [21]. Both cationic and anionic polymerizations require quite stringent conditions since oxygen or water tend to terminate them, so they are not widely used in industrial applications even though they provide much better control over the final product. Both are considered living polymerizations, although free radical living polymerizations have also been developed.
- Coordination polymerization: it usually occurs by pseudo-ionic polymerization, and it involves the preliminary coordination of a monomer with a chain carrier [21].

At this point, it should be noted that “living” polymers, are the polymers that retain their ability to propagate for a long time and grow to a desired maximum size while their degree of termination or chain transfer is negligible [22]. Such behavior has been observed in anionic polymerization, as well as cationic, metathesis and radical reactions.

1.4 Synthetic Approaches to Star Polymers

The advances made in the field of "living"/controlled polymerizations greatly favored the development of star polymers, rendering them more accessible. The synthesis of star polymers via living polymerization methods can follow one of three synthetic routes: (i) the core-first, (ii) the arm-first and (iii) the grafting onto (or coupling onto) strategies [3, 23]. All of these synthetic strategies are well established and are relatively easy to be carried out with the aid of controlled "living" polymerization methods, however, each route has certain advantages and drawbacks that render it suitable for the synthesis of a specific type of polymer over the others. Thus, the final characteristics of the polymer need to be considered before choosing to follow a certain synthetic route.

(i) The Core-First Approach

During the core-first approach, a presynthesized multifunctional initiator, either well-defined with a known number of functional/initiating groups or less defined [24], is used as initiating site to form stars by divergently growing linear polymers [3], the arms. In order for the stars to be well-defined, they need to have the same number of arms, all of which must have the same length and molecular weight. For that to happen, all the functional sites on the core must have equal reactivity and 100% initiation efficiency. Controlled/living polymerizations are extremely useful in this case, since they have a rate of initiation much higher than that of propagation and coupled with a low percentage of chain termination reactions, the degree of polymerization (DP) of each arm can be comparable.

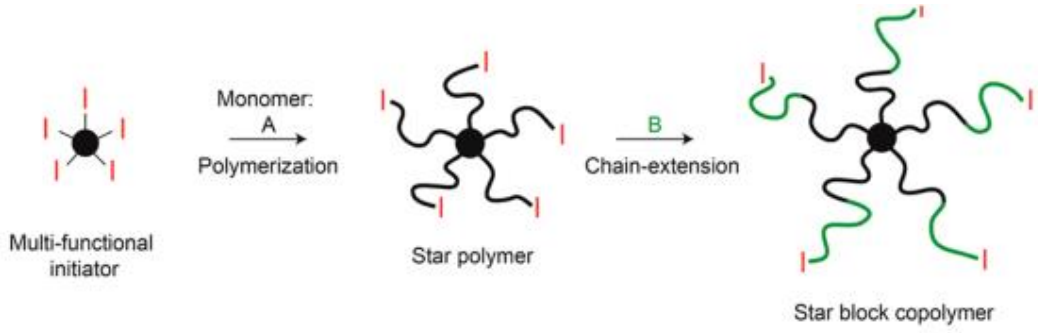

Figure 4 - Schematic representation of the core-first star synthesis [3]

Even though this approach has excellent yields, it also has several limitations. It produces stars with low number of arms (typically from 3 to 8) and a small core, due to the fact that the molecules most commonly used as initiators are small with low number of functional groups, thus the core size and the number of arms, are both limited and defined from the beginning. It is also not suitable for the synthesis of miktoarm stars unless specially designed cores are utilized.

(ii) The Arm-First Approach

In this synthetic approach, star polymers are formed by cross-linking linear polymers via a polymerization or coupling reaction in a convergent manner [3]. So, if the cross-linking mechanism is taken for granted, the synthesis can be further divided into three categories, the (a) macroinitiator (MI), (b) macromonomer (MM) and the (c) self-assemble crosslinking (SC) routes. For the macroinitiator (MI) approach, the polymers are formed by polymerizing a di- (or higher) functional monomer (also referred to as the cross-linker) using as an initiator the polymeric "living" arms, i.e., the arm macroinitiator. A similar process is followed for the macromonomer (MM) synthetic route, the molecule that is used for the initiation of the polymerization of the core being the only difference. While in the MI route the arms act as an initiator for the cross-linker, in the MM route the polymerization is initiated by a small molecular initiator, and the previously formed arms take part in the polymerization as macromonomers. In the case of self-assemble cross-linking (SC) routes, instead of polymerization, coupling chemistries are most often used. The star polymer is formed by connecting the presynthesized arm copolymers with a cross-linkable block via reaction between the pendant groups and a di-functional compound. Copper click chemistry is highly efficient and is often used for these types of coupling reactions. The cross-linkers used can be designed to respond to certain stimuli, thus being able to either dissociate and reconstruct upon application of the specified stimulus, or even lead to the degradation of the polymer.

The arm-first approach can lead to polymers with very high molecular weight and large number of arms (>100), though that depends on the DP of the arms and their composition, as well as the nature of the cross-linker, its ratio in relation to the arms and the timing of its addition to the reaction mixture. Common feature for the stars synthesized by the arm-first route, is that their core consists of cross-linked network structures with limited mobility and exhibits large molecular sizes, in contrast to the cores of stars prepared via the core-first method, that have almost negligible molecular weight relative to the weight of the whole star. Star polymers synthesized via the arm-first approach are often referred to as core cross-linked star polymers (CCS), a term that gives an indication as to the size of their core.

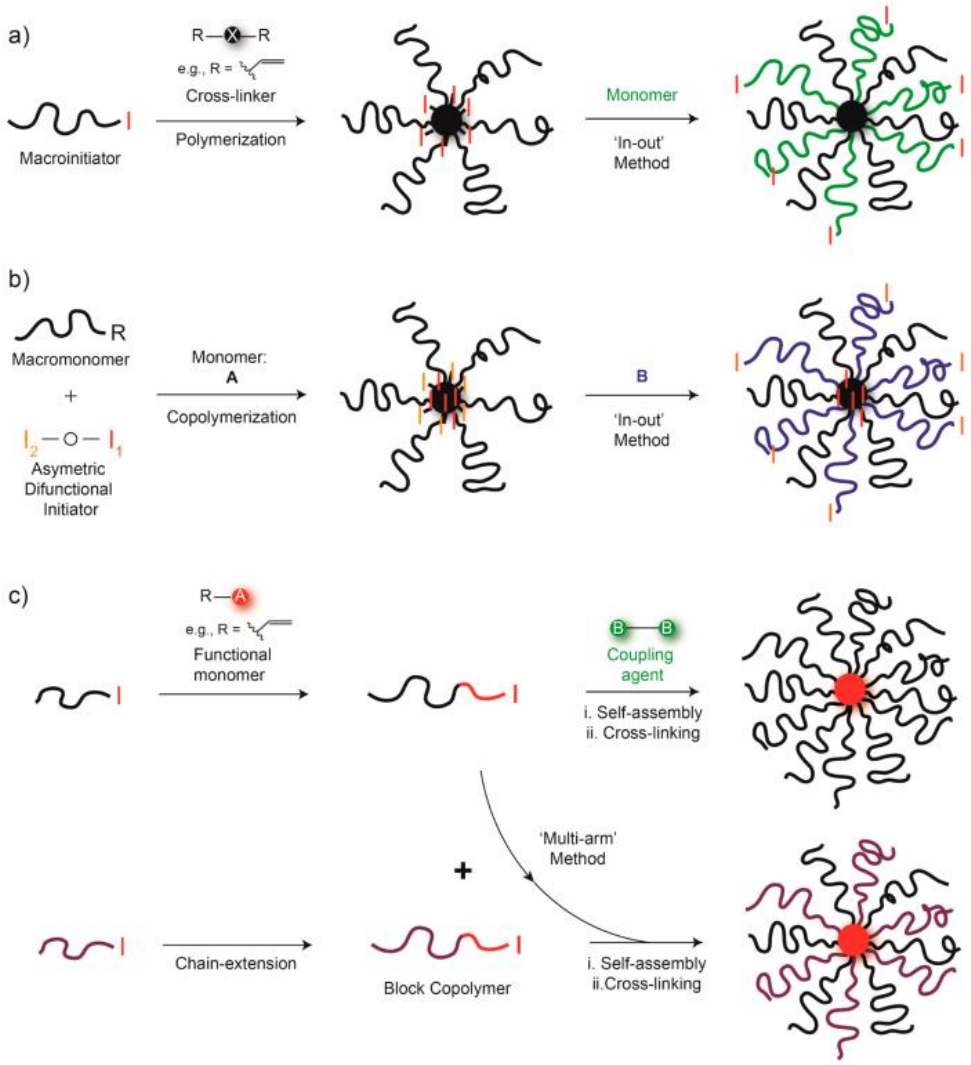

Figure 5 - Arm-first star synthesis via a)macroinitiator approach, b)macromonomer approach, c)self-assembly cross-linking approach [3]

(iii) The Grafting-onto approach:

The grafting-onto synthetic approach is the one that provides the highest level of control on the structure of the final polymeric product among all the previously mentioned synthetic routes. This is a direct result of the fact that the arms and the core are synthesized and characterized independently before the coupling reaction for the formation of the star takes place.

The star polymers prepared via the grafting-onto approach have a number of arms that can be equal to the functionality of the core in the case that the coupling reaction is quantitative, or less than that. Star polymers synthesized in this manner typically have a low number of arms (4-8) and small core size. The synthesis of stars with a large number of arms (>20) that have a high molecular weight is extremely difficult due to steric hindrance.

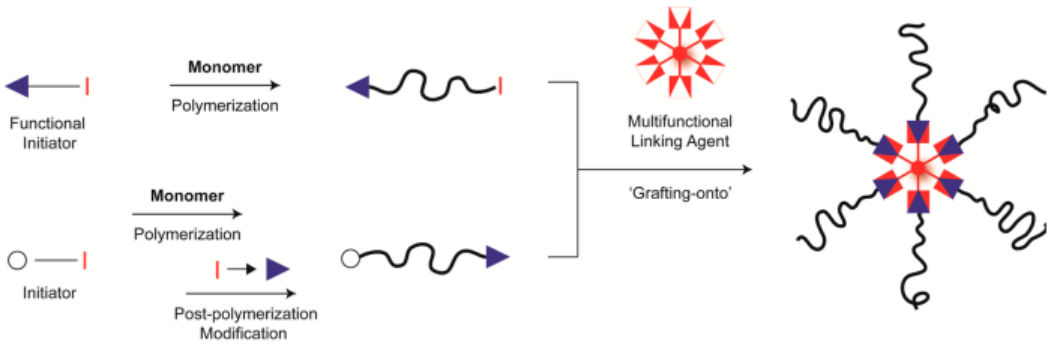

Figure 6 - Schematic representation of the grafting-onto star synthesis approach [3]

1.5 Group Transfer Polymerization (GTP)

Living polymerization techniques provide the maximum possible amount of control over the synthesis of polymers and often lead to well-defined macromolecules. In order to have enough control over the molecular weight of the forming polymer, the rate of initiation need to be higher than the rate of propagation. GTP is a "quasi-living", silicon-mediated oxyanionic polymerization of acrylic esters [25]. It was introduced by Webster and his team at the DuPont's experimental station of Wilmington in the late 1970s, and it was announced in the early 1980s. It utilizes silyl ketene acetals that can be activated by fluoride anions and Lewis acids, to undergo a Michael addition reaction with a methacrylic compound [26]. This reaction introduces the silyl ketene acetal at the chain end, and its repetition leads to the formation of the polymeric chain.

It was named GTP because it was hypothesized that it followed a covalent (nonionic)-concerted mechanism [27], during which the polymer chains preserve the trimethylsilyl group they started with, by transferring it to the incoming monomer. There are two main pathways for the polymerization: the dissociative and the associative pathway. During the dissociative mechanistic route, the catalyst complexes with the silyl ketene acetal end groups and by reversibly cleaving, a reactive enolate end is generated that adds monomers. That can then be capped by the initiator-catalyst complex to generate once again the silyl ketene acetal ends that are needed for the polymerization to proceed.

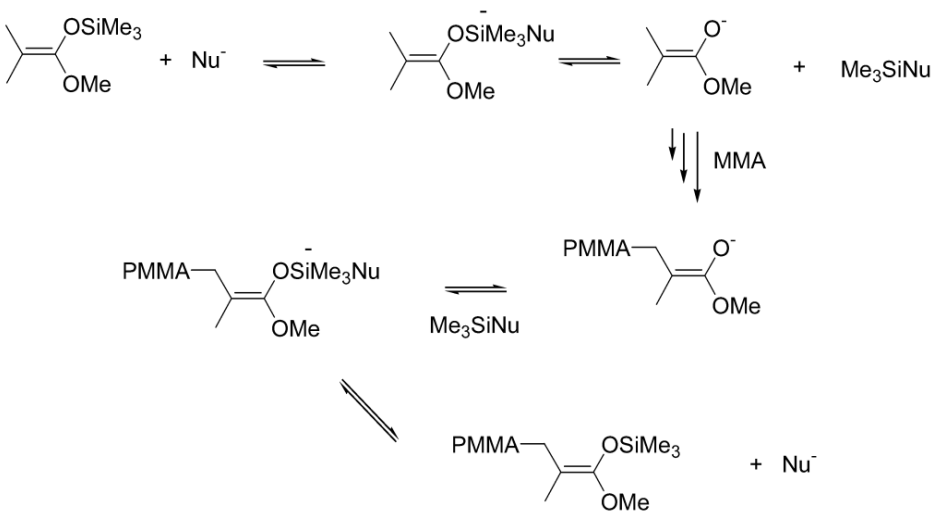

Figure 7 - Dissociative synthetic mechanism [28]

In the associative pathway case, the acetal activates the silyl ketene acetal group and leads to addition of monomer. The silyl group is then transferred to the incoming monomer while it remains on the polymer chain for the length of the polymerization. The silyl end group exchange that takes place, arises from an unknown process.

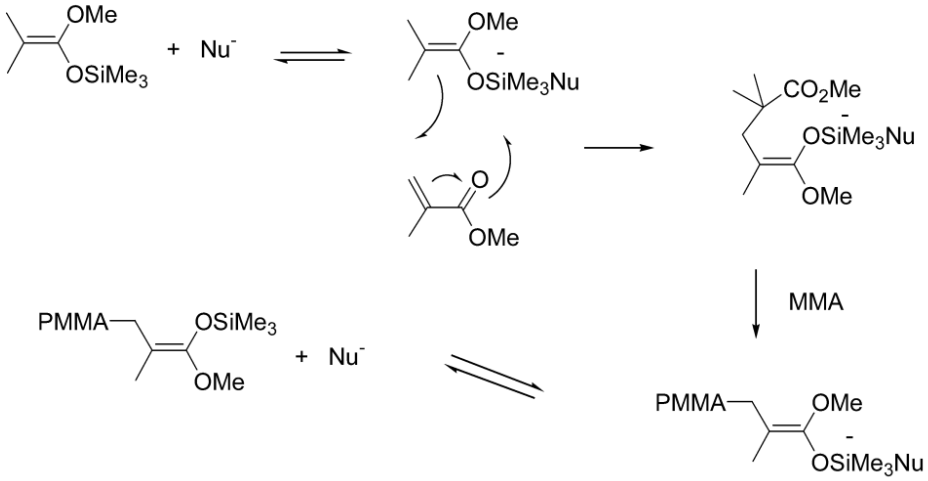

Figure 8 - Associative synthetic mechanism [28]

GTP, just like the classical "living" anionic polymerization methods, is able to prepare block copolymers and polymers of various architectures, as well as end-functionalized polymers, and is inert to functionalities that are susceptible to radical or ring-opening polymerization. GTP has an advantage over the classical anionic polymerization because it can be carried out at ambient temperature and is rapidly completed. The disadvantage of the method though is that it is limited as to the type of monomers that can be polymerized by it (only *α,β*-unsaturated carbonyl compounds can be used) and its products are typically polymers with relatively low molecular weights (less than 20.000 g/mol) and high molecular weight dispersities (~1.2-1.3).

The monomers that work best in GTP are mainly methacrylates and they produce polymers with very narrow molecular weight distributions [29], in contrast to acrylates, that polymerize very quickly via this method, and so produce polymers with low molecular weights and broad molecular weight distributions. GTP is extremely sensitive to the presence of hydrogen, but it can bear with the presence of oxygen. Monomers (and any other compounds) that bear active hydrogens can interfere with GTP and stop the polymerization when they are present in amounts greater than the concentration of the initiator used. However, monomers such as these can be polymerized via GTP as long as protective groups are used prior to the polymerization, that can be removed later on. Monomers with strong intramolecular hydrogen bonds, can be polymerized without the use of protective groups.

The initiator in GTP plays a very important role, as it sets off the polymerization reaction and, in this case, it is also incorporated into the polymer. In living polymerizations in general, the structure of the initiator needs to be the same as that of the growing polymer ends. This also stands for GTP, with the best suited initiators containing 1-alkoxy-1-(trimethylsiloxy)-2-methyl-1-alkene structure that corresponds to that of the polymethacrylate living end of the growing polymeric chains. The simplest of the initiators that can be used in GTP is 1-methoxy-1-trimethylsiloxy-2-methyl-1-propene (MTS).

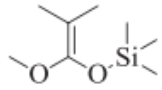

1-Methoxy-1-trimethylsiloxy
-2-methyl-1-propene (**MTS**)

Figure 9 - Initiator chemical structure [25]

If the silicon atom in the initiator is replaced by other elements from group IV of the periodic table, such as Germanium or Tin, the resulting compound can also be used as an initiator for GTP. α-silyl esters are also considered initiators, along with silyl derivatives, since they can be rearranged to silyl ketene acetals and can form silyl ketene acetals when they are added to methacrylates respectively. Also, if specific functional end groups need to be incorporated into the polymer, then specialized initiators can be used.

Another crucial component of GTP is the catalyst used, since without it, silyl ketene acetals are unreactive under normal GTP conditions. The catalysts used for GTP are divided into two categories: Lewis acids and nucleophilic anions. Lewis acids are used to catalyze the polymerization of acrylates and normally high concentrations of them are needed (~10 mol% based on the monomer). Nucleophilic anionic catalysts are largely preferred for GTP, because the amount required for them to work is very small (approximately 0.1% based on the initiator). These catalysts are mostly used in the form of sterically hindered salts, such as tris(dimethyl-amino)sulfonium (TAS) or

tetrabutylammonium (TBA), that being large ions, manage to delay the backbiting termination [28] that may occur during the polymerization in the case it follows a dissociative pathway. Potassium salts of bifluoride and acetate have also been tried as GTP catalysts. Fluorides, difluoromethylsilicates, and bifluorides were used as anionic catalysts during earlier work on GTP because they have a high affinity for organosilanes, however, they tend to deactivate under GTP conditions. Currently, a widely used catalyst for GTP is tetrabutylammonium bibenzoate (TBABB).

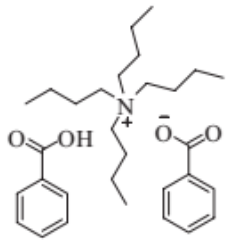

Figure 10 - Catalyst chemical structure [25]

It should be noted that when a monomer is absent from the reaction vessel, the catalyst can react with the initiator and destroy it [28]. The fact that such reactions can take place, supports the theory that the GTP mechanism is dissociative, in which ester enolate can be generated. Had the reaction mechanism been associative, the catalyst would only complex with the initiator and not destroy it. When a low concentration of catalyst relative to the initiator is used, the ester enolate that is generated can easily be stabilized by the larger amounts of initiator, and so the catalyst and the initiator can be combined before the addition of the monomer without killing the polymerization. If large amounts of catalysts are used however, the polymerization does not occur. In the associative mechanism, the addition of larger amounts of catalyst would not only not destroy the initiator and thus kill the polymerization, but it would actually increase the rate of the reaction. In the dissociative mechanism though, by increasing the amount of catalyst, larger amounts of enolate are generated, that the initiator is not able to stabilize with the silyl ketene acetal end groups that are available [30].

The temperature for the polymerization of methacrylates ranges from 0 to 150˚C, and although GTP could be successful if carried out under a temperature that falls in this range, the choice of catalyst must be carefully made, because each catalyst has a range of temperatures within which it can be useful. A suitable temperature range for the polymerization of methacrylates is between 0 and 50˚C, while acrylates are better polymerized in temperatures below 0˚C to diminish their swift polymerization and have better control over the process and thus generate better-defined products. GTP is a relatively fast polymerization reaction that mainly depends on the rate of addition of the monomer.

1.6 Stimuli responsive polymers

Degradable polymers, and in particular stimuli-responsive polymers [31], are constantly gaining further attention in recent years, leading to the development of a wide variety of them that find use in numerous biotechnological fields. Drug delivery, gene delivery and tissue engineering are only a few of the fields that stimuli-responsive and degradable polymers have already proven to be useful in and the number of applications keeps increasing. In applications such as these, the degradation of the polymers needs to be controlled to a high extent, so their design and synthesis is carried out in an extremely careful way. In the majority of cases in drug and gene delivery, the degradation of the polymer, and thus the release of the encapsulated or conjugated drug or gene respectively, must take place in a specific area of the body, leading researchers to exploit specific characteristic of these areas. For example, it is known that cancerous tissue tends to have lower pH values than healthy tissue [32], at such an extent that it can be easily used to regulate or trigger the degradation of the polymers used for delivering the needed drug to that specific area. Another such example of a difference in pH that can be exploited for controlled degradation of a polymer and subsequent release of its cargo, is the pH of endosomes, that ranges from 4 to 6 [33], and is much lower than the pH 7.4 of their surrounding environment.

A great number of studies has been conducted on how polymers can be used in situations such as these, but all of them have as a common denominator the fact that the polymers used must be susceptible to changes in the pH of their environment, either by completely degrading [34], or by changing their configuration [35]. Polymers that are sensitive to acidic pH can result from various synthetic approaches that include acid-labile linkages between the polymer and its cargo, in the main backbone or in side chains, but they can also include acid-labile linkages in the polymer itself [36]. Hydrazone bonds have proven to be selectively cleaved at pH values ranging from 5 to 6 (pH values that correspond to the pH of intracellular vesicles, such as endosomes) and they have already been used for the development of polymeric micelles in which the polymer was conjugated with anticancer drugs, that were efficiently delivered to the desired area and they selectively released their cargo, while under the influence of the decreasing intracellular pH [37]. Another type of linkage that responds to a decrease in the pH and can be exploited for the synthesis of pH-sensitive polymers used as drug carries, is the acetal linkage. Acetals are also known to be hydrolyzable under acidic conditions, though they are stable under neutral and basic conditions [38], and they have the extra advantage that their expected hydrolysis rate is 10 times faster than other acid-cleavable linkages with each unit of pH decrease, because their hydrolysis is generally first order relative to the hydronium ion [39], and also the products of their degradations are mainly alcohols and aldehydes that tend to be biocompatible and do not result in acidosis at the area where the degradation happens, as is the case when polyesters undergo biodegradation [40]. Polymer networks, as well as star polymers, that contain an acetal-based cross-linker have already been synthesized and their degradation under acidic conditions has been proven. What is more, by altering the

chemical structure of the acetals it is also possible to tune the hydrolysis rate they exhibit [41].

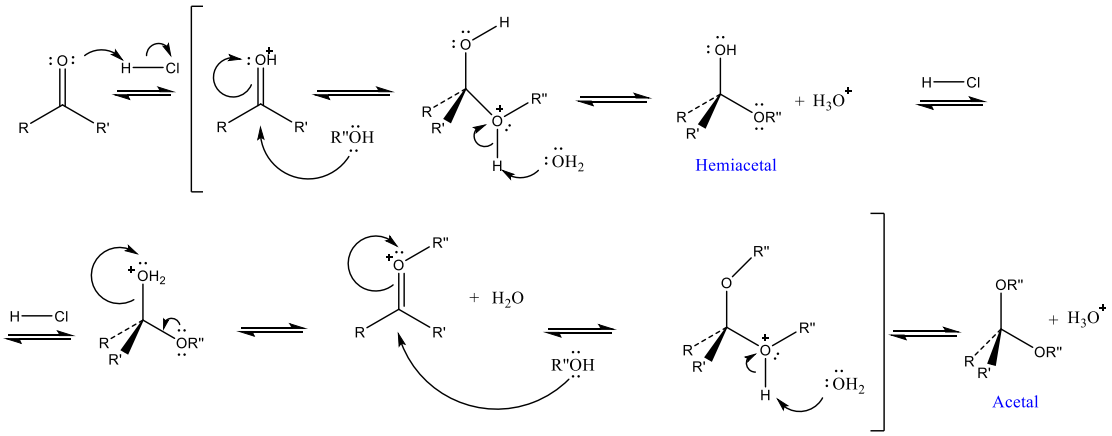

Figure 11 - Mechanism of the synthesis and hydrolysis of acetals [38]

On the other hand, the exploitation of chemical and biochemical stimuli in order to control the properties of a certain material and even to lead to its degradation, as mentioned above, has been thoroughly researched. Physical stimuli have come to the forefront recently, and that interest arises from the need of spatiotemporal, often even remote, control over the materials. Depending on the intensity of the physical stimulus used in conjunction with the material, they can also be considered biocompatible [42, 43]. Physical stimuli that can be utilized for spatiotemporal control over certain materials include the temperature [44] of the solution, as well as the application of an external field, such as magnetic or electric [45], ultrasonic treatment [46], and light irradiation. Photo-responsive polymeric materials in particular, are considered very attractive in the fields of drug delivery and tissue engineering, because they could lead to the development of intelligent systems that would prove extremely useful. Photo-sensitive materials can be divided in two categories, photo-responsive materials that change their physicochemical properties upon irradiation, and photodegradable materials which degrade in response to light irradiation of an appropriate wavelength. Light as an external stimulus has the advantage that is relatively inexpensive and easily available, while it also allows for high spatiotemporal control [47], though the choice of the wavelength used for the irradiation of the polymers needs to be well thought of, so as to avoid adverse effects at the irradiation site [48]. NIR light is preferable for biomedical applications due to its higher tissue penetration, while UV irradiation is highly absorbed by the skin and therefore does not penetrate deep into the tissues [43]. The most commonly used and studied photo-responsive groups until now are azobenzenes [49], as well as spiropyrans [50] and spirooxazines [42].

As far as photo-degradable polymers are concerned, the challenge that needs to be overcome is their design and the range of the electromagnetic spectrum they are

sensitive. In order for polymers to be photo-degradable, they need to carry photo-labile groups that can react to external light sources, either as pendant side-groups, or as part of the polymeric backbone, or as cross-linkers in a polymeric network. Chemical bonds that can be cleaved by irradiation include ester bonds, disulphide bonds, triazine bonds, and of course acetal bonds. These types of bonds typically exhibit no absorbance in the deep UV range, and when used, are normally located close to an absorbing group, widely known as chromophores, that include aromatic groups, coumarin and nitrobenzyl groups. These groups can augment the absorption coefficient of the material, rendering the photo-degradation more efficient, or they can even shift the irradiation wavelength needed to lead to the degradation of the polymer. Even the presence of a single photo-responsive unit in a polymeric chain has been proven sufficient to influence the properties of the polymer upon irradiation [51]. The most widely known absorbing group, is the *ortho*-nitrobenzyl (ONB) group, owing to its great sensitivity, as well as its degradation wavelength (λ=365 nm) [52].

Apart from photo-degradation that occurs on pendant groups of the polymers, polymers that exhibit main chain photo-degradation are attracting a lot of attention owing to the fact that upon irradiation, they tend to break into low molecular weight products that, especially in biotechnological applications, can be easily removed from the body. The polymers that can undergo main-chain photo-degradation are limited and they can be divided into three categories: polyesters, polytriazines and polyacetals [43]. Even though the photochemistry of molecules containing ketal and acetal groups is already known, it was recently shown that main-chain polyketals and polyacetals undergo cleavage when using ultra-fast lasers [42]. In this case, the photo-degradation of the polymer occurred when the aromatic group located next to the ketal/acetal bond was irradiated using 248 nm light at low irradiation thresholds, and it resulted to low molecular weight photodegradation products [53].

1.7 Aim of the present Master Thesis

This Master Thesis focused on the synthesis and characterization of two novel cross-linkers and their further polymerization into stars in organic solvents. Specifically, an acid-degradable cross-linker was synthesized via an acid-catalyzed condensation reaction, and then used to form two types of star polymers via GTP by the arm-first approach. The arms of the stars consisted of block and random copolymers of poly(2-(dimethylamino)ethyl methacrylate) (PDMAEMA) and polymethyl methacrylate (PMMA). The molecular weight of the star polymers was determined using SEC, and they were also characterized by NMR spectroscopy, as well as DLS and SEM. Finally, the degradation of the star polymers was proven by their hydrolysis after treatment with a hydrochloric acid solution. The products of the degradation were characterized by NMR and SEC. An acid- and photo-degradable cross-linker was also synthesized by an acid-catalyzed condensation reaction. Two types of star polymers were again synthesized via GTP comprising block and random PDMAEMA - PMMA arms. The

star polymers were then characterized by SEC, NMR, DLS and SEM. The degradation of the star polymers was proven by separately treating the polymers with a hydrochloric acid solution and UV irradiation at 254 nm. The hydrolyzed, as well as the photoproducts, were characterized by SEC, NMR, DLS and SEM.

1.8 References

[1] Allcock, H.R., Lampe, F.W., Contemporary Polymer Chemistry, 2nd ed., Prentice Hall, Englewood Cliffs, 1990

[2] Hiemenz, P.C., Polymer Chemistry: The basic concepts, Marcel Dekker, NY, 1984

[3] Ren, J. M., McKenzie, T. G., Fu, Q., Wong, E. H. H., Xu, J., An, Z., Qiao, G. G. (2016). Star Polymers. Chemical Reviews, 116(12), 6743–6836. doi:10.1021/acs.chemrev.6b00008

[4] Ye, Z., Xu, L., Dong, Z., & Xiang, P. (2013). Designing polyethylenes of complex chain architectures via Pd–diimine-catalyzed "living" ethylene polymerization. Chemical Communications, 49(56), 6235. doi:10.1039/c3cc42517g

[5] http://polymerdatabase.com/polymer%20physics/Tacticity.html

[6] Atom Transfer Radical Polymerization (ATRP), K. Maryjaszewski and J. Spanswick, Reference Module in Materials Science and Materials Engineering, Carnegie Mellon University, Elsevier, 2016

[7] W. Wu et al. / Progress in Polymer Science 46 (2015) 55–85

[8] Acebo, C., Ramis, X., & Serra, A. (2017). Improved epoxy thermosets by the use of poly(ethyleneimine) derivatives. Physical Sciences Reviews, 2(8). doi:10.1515/psr-2016-0128

[9] Qiu, Q., Liu, G., An, Z., Efficient and Versatile synthesis of star polymers in Water and their use as emulsifiers, *Chem. Commun.* **2011**, 47 (47), 12685-12687

[10] Li, W., Yu, Y., Lamson, M., Silverstein, M.S., Tilton, R. D., Matyjaszewski, K., Peo-based star copolymers as stabilizers for water-in-oil or oil-in-water emulsions, *Macromolecules* 2012, 45 (23), 9419-9426

[11] Cho, H. Y., Averick, S.E., Paredes, E., Wegner, K., Averick, A., Jurga, S., Das, S.R., Matyjaszewski, K., Star polymers with a cationic core prepared by atrp for cellular nucleic acids delivery, *Biomacromolecules* 2013, 14 (5), 1262-1267

[12] Georgiou, T.K., Vamvakaki, M., Patrickios, C. S., Yamasaki, E., Phylactoy, L., Nanoscopic cationic methacrylate star homopolymers: synthesis by group transfer polymerization, characterization and evaluation as transfection reagents, *Biomacromolecules* 2004, 5 (6), 2221-2229

[13] Li, X.J., Qian, Y.F., Liu, T., Hu, X.L., Zhang, G.Y., You, Y.Z., Liu, S.Y., Amphiphilic Multiarm star block copolymer-based multifunctional Unimolecular micelles for cancer targeted drug delivery and Mr imaging, *Biomaterials* 2011, 32 (27), 6595-6605

[14] Qiu, L.Y., Wang, R.J., Zheng, C., Jin, Y., Jin, L.Q., B-cyclodextrin-centered star-shaped amphiphilic polymers for doxorubicin delivery, *Nanomedicine* 2010, 5 (2), 193-208

[15] Jones, M.C., Ranger, M., Leroux, J.C., pH-sensitive unimolecular polymeric micelles: synthesis of a novel drug carrier, *Bioconjugate Chem.* 2003, 14 (4), 774-781

[16] Wu, W., Wang, W., Li, J., Star polymers: advances in biomedical applications, *Prog. Polym. Sci.*, 2015, 46, 55-85

[17] Rodionov V., Gao H., Scroggins S., Unruh D.A., Avestro A.J., Fréchet J.M., Easy access to a family of polymer catalysts from modular star polymers, *J. Am. Che. Soc.*, 2010, 132 (8), 2570-2572

[18] Paul J. Flory, Principles of Polymer Chemistry, Cornell University Press, 1953, p.39. ISBN 0-8014-0134-8

[19] Wallace H. Carothers, *J. Am. Chem. Soc.*, 51, 8, 2548-2559

[20] Susan E. M. Selke, John D. Culter, Ruben J. Hernandez, Plastics packaging: Properties, processing, applications and regulations, Hanser, 2004, p.29, ISBN 1-56990-372-7

[21] Penczek S., Moad G., *Pure Appl. Chem.*, 2008, 80 (10), 2163-2193

[22] Szwarc M., Living polymers. Their discovery, characterization, and properties, J. Polym. Sci., Polym. Chem. 1988, 36, ix-xv

[23] H. Gao, K. Matyjaszewski, Progress in Polymer Science 34 (2009) 317–350

[24] H. Gao, K. Matyjaszewski, Progress in Polymer Science 34 (2009) 317–350

[25] Maria Rikkou-Kolourkoti, Owen W. Webster, Costas S. Patrickios, Group Transfer polymerization, *Encyclopedia of polymer science and technology*, 2013, vol 99, 1-17, doi: 10.1002/0471440264.pst603

[26] Recent progress in organocatalytic group transfer polymerization, Keita Fuchise, Yougen Chen, Toshifumi Satoh, Toyoji Kakuchi, *Polym. Chem.*, 2013, doi: 10.1039/c3py00278k

[27] Owen W. Webster, Science, 22 Feb 1991, Vol. 251, Issue 4996, pp 887-893, doi: 10.1126/science.251.4996.887

[28] Webster, O. W. (2003). Group Transfer Polymerization: A Critical Review of Its Mechanism and Comparison with Other Methods for Controlled Polymerization of Acrylic Monomers. Advances in Polymer Science, 1–34. doi:10.1007/b12303

[29] A review of Group-Transfer Polymerization, William J. Brittain, Rubber Chemistry and Technology, Vol. 65, 580-598

[30] Owen W. Webster, J. Polym. Sci. Part A: Polym. Chem. Vol. 38, 2000, 2855-2860

[31] Pasparakis, G., & Vamvakaki, M. (2011). Multiresponsive polymers: nano-sized assemblies, stimuli-sensitive gels and smart surfaces. Polymer Chemistry, 2(6), 1234. doi:10.1039/c0py00424c

[32] Swietach P, Vaughan-Jones RD, Harris AL, Hulikova A. 2014 The chemistry, physiology and pathology of pH in cancer. *Phil. Trans. R. Soc. B 369*: 20130099. http://dx.doi.org/10.1098/rstb.2013.0099

[33] Seema Agarwal, Yi Zhang, Samarendra Maji, Andreas Greiner, PDMAEMA based gene delivery materials, Materials Today, September 2012, Volume 15, Number 9, 388-393

[34] H. Kostková, L. Schindler, L. Kotrchová, M. Kovář, M. Šírová, L. Kostka, T. Etrych, Star polymer-drug conjugates with pH-controlled drug release and carrier degradation, Hindawi, *Journal of Nanomaterials*, Volume 2017, Article ID 8675435, 10 pages, https://doi.org/10.1155/2017/8675435

[35] Muharrem Seleci, Didem Ag Seleci, Mustafa Ciftci, Dilek Odaci Demirkol, Frank Stahl, Suna Timur, Thomas Scheper, Yusuf Yagci, Nanostructured amphiphilic star-hyperbranched block copolymers for drug delivery, Langmuir, 31(15), 4542–4551. doi:10.1021/acs.langmuir.5b00082

[36] Jin-Ki kim, Vivek Kumar Garripelli, Ui-Hyeon Jeong, Jeong-Sook Park, Michael A. Repka, Seongbong Jo, *Int J Pharm* 2010 November 30, 401 (1-2), 79-86, doi:10.1016/j.ijpharm.2010.08.029

[37] Bae, Y., Fukushima, S., Harada, A., and Kataoka, K. (2003), Design of environment-sensitive supramolecular assemblies for intracellular drug delivery: polymeric micelles that are responsive to intracellular pH change. *Angew. Chem., Int. Ed. 42*, 4640-4643

[38] John E. McMurry, Organic Chemistry, Cengage Learning; 8th edition (2012), ISBN-13: 978-1133152118

[39] Fife, T., and Jao, L. (1965) Substituent effects in acetal hydrolysis. *J. Org. Chem. 30*, 1492-1495

[40] Khaja, S. D., Lee, S., & Murthy, N. (2007). Acid-Degradable Protein Delivery Vehicles Based on Metathesis Chemistry. Biomacromolecules, 8(5), 1391–1395. doi:10.1021/bm061234z

[41] Gillies, E. R., Goodwin, A. P., & Fréchet, J. M. J. (2004). Acetals as pH-Sensitive Linkages for Drug Delivery. Bioconjugate Chemistry, 15(6), 1254–1263. doi:10.1021/bc049853x

[42] Manouras, T., & Vamvakaki, M. (2017). Field responsive materials: photo-, electro-, magnetic- and ultrasound-sensitive polymers. Polymer Chemistry, 8(1), 74–96. doi:10.1039/c6py01455k

[43] Pasparakis, G., Manouras, T., Argitis, P., & Vamvakaki, M. (2011). Photodegradable Polymers for Biotechnological Applications. Macromolecular Rapid Communications, 33(3), 183–198. doi:10.1002/marc.201100637

[44] Mark A. Ward, Theoni K. Georgiou, Thermoresponsive polymers for biomedical applications, *Polymers* 2011, 3, 1215-1242

[45] Zhang, W., & Choi, H. (2014). Stimuli-Responsive Polymers and Colloids under Electric and Magnetic Fields. Polymers, 6(11), 2803–2818. doi:10.3390/polym6112803

[46] Traitel, T., Goldbart, R., & Kost, J. (2008). Smart polymers for responsive drug-delivery systems. Journal of Biomaterials Science, Polymer Edition, 19(6), 755–767. doi:10.1163/156856208784522065

[47] Pasparakis, G., Manouras, T., Vamvakaki, M., & Argitis, P. (2014). Harnessing photochemical internalization with dual degradable nanoparticles for combinatorial photo–chemotherapy. Nature Communications, 5(1). doi:10.1038/ncomms4623

[48] Yan, Q., Han, D., & Zhao, Y. (2013). Main-chain photoresponsive polymers with controlled location of light-cleavable units: from synthetic strategies to structural engineering. Polymer Chemistry, 4(19), 5026. doi:10.1039/c3py00804e

[49] Hu, J., Yu, H., Gan, L. H., & Hu, X. (2011). Photo-driven pulsating vesicles from self-assembled lipid-like azopolymers. Soft Matter, 7(24), 11345. doi:10.1039/c1sm06495a

[50] Ventura, C., Thornton, P., Giordani, S., & Heise, A. (2014). Synthesis and photochemical properties of spiropyran graft and star polymers obtained by “click” chemistry. Polym. Chem., 5(21), 6318–6324. doi:10.1039/c4py00778f

[51] Theato, P. (2011). One is Enough: Influencing Polymer Properties with a Single Chromophoric Unit. Angewandte Chemie International Edition, 50(26), 5804–5806. doi:10.1002/anie.201100975

[52] Olejniczak, J., Nguyen Huu, V. A., Lux, J., Grossman, M., He, S., & Almutairi, A. (2015). Light-triggered chemical amplification to accelerate degradation and release from polymeric particles. Chemical Communications, 51(95), 16980–16983. doi:10.1039/c5cc06143a

[53] Pasparakis, G., Manouras, T., Selimis, A., Vamvakaki, M., & Argitis, P. (2011). Laser-Induced Cell Detachment and Patterning with Photodegradable Polymer Substrates. Angewandte Chemie International Edition, 50(18), 4142–4145. doi:10.1002/anie.201007310

2. Experimental

2.1 Acid – degradable cross-linker synthesis

2.1.1 Materials

For the synthesis of the cross-linker, 1,4-cyclohexanedimethanol divinyl ether (98%) and methacrylic acid (99%) were purchased from Aldrich, pyridinium p-toluenesulfonate (98+%) was purchased from Alfa aesar, while dichloromethane (≥99.9%) was purchased from Sigma Aldrich.

For the purification of the synthesized cross-linker, silica gel (high purity grade, pore size 60Å) was used obtained from Fluka, as well as aluminium oxide 90 basic from Macherey-Nagel, n-hexane (reagent grade, 96%) from Scharlau, and ethyl acetate (analytical reagent grade) from Fisher Chemical. In order for the cross-linkers to be completely dry, calcium hydride (93%) was used, ordered from Acros organics, as well as magnesium sulfate anhydrous, ≥98%, obtained from Fluka.

2.1.2 Synthesis of the acid-degradable cross-linker

The acid-degradable cross-linker was synthesized by an acid-catalyzed condensation reaction (catalyst PPTS, 0.063 gr, 1% with respect to the vinyl ether) of methacrylic acid (46.8 mmol, 3.97 ml) and 1,4-cyclohexanedimethanol divinyl ether (23.4 mmol, 5 ml) in dry dichloromethane, at a 2:1 molar ratio. The reaction scheme for the preparation of the cross-linker is depicted below (Figure 12). The solution was stirred for 3 hours, followed by filtration through basic aluminium oxide and extraction with nanopure water. The structure of the cross-linker was verified via ^{1}H-NMR, and the product was dried over anhydrous magnesium sulfate, and subsequently adsorbed in silica gel, to be purified by column chromatography using hexane: ethyl acetate at a 4:1 ratio as the eluent. The progress of the column was monitored by thin layer chromatography (TLC) in the same solvent. After the product has successfully passed through the column, all the fractions are collected, and the solvent evaporated. The purified cross-linker was stored in the fridge at 4ºC.

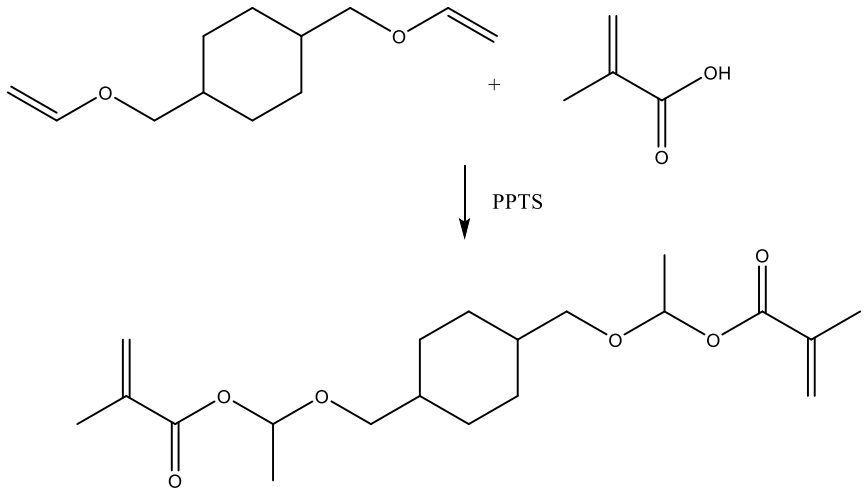

Figure 12 - Synthesis of the acid-degradable cross-linker

2.2 Synthesis of the acid- and photo-degradable cross-linker

2.2.1 Materials

For the synthesis of the photo-degradable cross-linker, 1,4-benzenedimethanol (99%), methacryloyl chloride (97%), and ethylene glycol vinyl ether (97%) were purchased from Aldrich, triethylamine (≥99%) was obtained from Sigma Aldrich, and tetrahydrofuran (for analysis) was ordered from AppliChem Panreac.

For the purification of the synthesized cross-linker, silica gel (high purity grade, pore size 60Å) was used that had been obtained from Fluka, as well as aluminium oxide 90 basic from Macherey-Nagel, n-hexane (reagent grade, 96%) from Scharlau, and ethyl acetate (analytical reagent grade) from Fisher Chemical. In order for the cross-linkers to be completely dry, Calcium hydride (93%) was used, ordered from Acros organics, as well as magnesium sulfate anhydrous, ≥98%, obtained from Fluka.

2.2.2 Synthesis of vinyl ether methacrylate (precursor for the acid- and photo-degradable cross-linker)

The synthesis of the precursor is an esterification reaction between ethylene glycol vinyl ether and methacryloyl chloride in dry THF, in the presence of triethylamine to neutralize the hydrochloric acid produced during the reaction (Figure 13) [1]. All reagents have been distilled under vacuum prior to the reaction. In a 250 ml round bottom flask with side arm that has already been purged with N_2, 40 ml of dry THF are added, along with 9.2 ml (133.7 mmol) ethylene glycol vinyl ether and 15.60 ml (145.8 mmol) triethylamine. The flask is placed in an ice bath and left to purge under constant N_2 flow for 30 min. Extra ice is added to the ice bath as needed, and after 30 min 10 ml (133.7 mmol) of methacryloyl chloride are added dropwise in the mixture. The flask is sealed under N_2 and left to stir for 5 hours. The completion of the reaction was verified

with ^{1}H-NMR spectroscopy. Once completed, the reaction mixture is filtered to remove the salt produced, and then distilled under vacuum to purify the final product. After the purification process, the product is stored in the freezer.

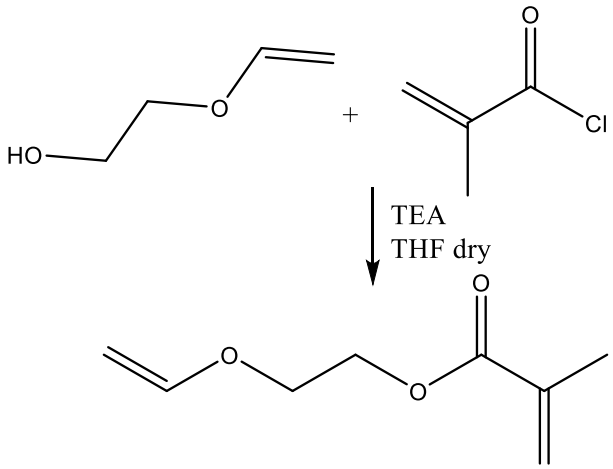

Figure 13 - Synthesis reaction of Vinyl ether methacrylate

2.2.3 Synthesis of the acid- and photo-degradable cross-linker

The cross-linker is synthesized via an acid-catalyzed condensation reaction (catalyst PPTS, 0.36 gr, 0.1% with respect to the diol) between 1,4-benzenedimethanol (2 gr) and vinyl ether methacrylate (4.5 gr) in dry THF (14.5 ml, 1M) in a 1:2 molar ratio. The solution is left to stir for 3 hours at 55˚C, followed by stirring overnight at room temperature. The synthesis reaction is presented below (Figure 14). The progress of the reaction is monitored by ^{1}H-NMR spectroscopy. The excess solvent is then evaporated, and the product adsorbed on silica gel, in order to be purified via column chromatography. A mixture of hexane: ethyl acetate at 4:1 ratio is used as eluent, with 2% added triethylamine to neutralize any acidic protons of the silica and avoid the premature degradation of the cross-linker. The process is followed with thin layer chromatography (TLC). The fractions containing the cross-linker are collected and the solvent is evaporated. The purified product is then stored in the fridge.

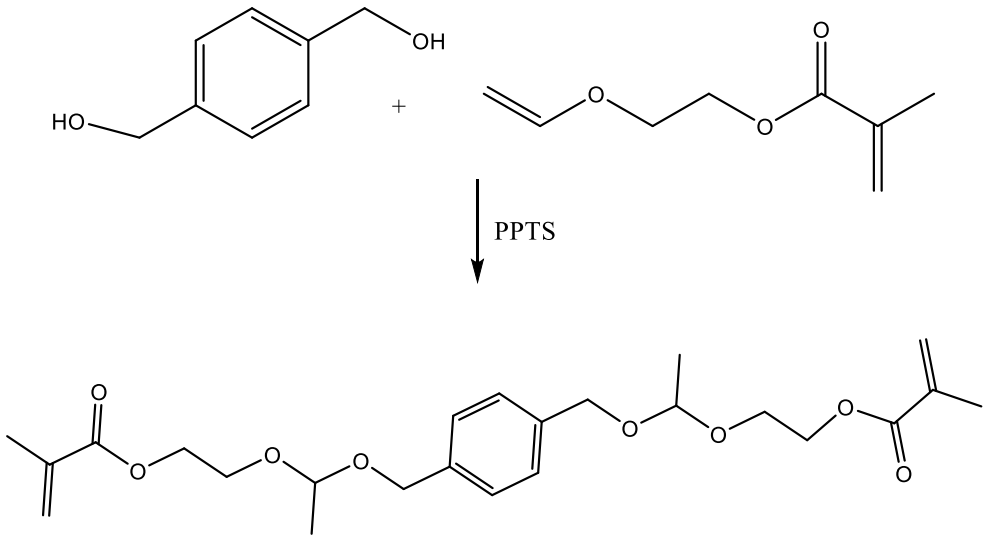

Figure 14 - Synthetic reaction where the acid- and photo-degradable cross-linker

2.3 Characterization of the synthesized cross-linkers

2.3.1 Nuclear magnetic resonance spectroscopy

Both cross-linkers were analysed by NMR spectroscopy to verify their successful synthesis and their final structure. A Bruker 500 MHz spectrometer was used to acquire the ^{1}H-NMR spectra of the cross-linkers. A sample of ~10 mg the compound to be analysed in each case was diluted in 1 ml of $CDCl_3$ and then transferred to the appropriate NMR tube in order for the measurement to be conducted.

2.4 Polymer synthesis

2.4.1 Materials

For the polymerization process 2-(dimethylamino)ethyl methacrylate (98%) was purchased from Aldrich and methyl methacrylate , 2,2-diphenyl-1-picrylhydrazyl was obtained from Sigma Aldrich, 1-methoxy-2-methyl-1-(trimethylsiloxy)propene (97%) was ordered from Alfa aesar, and tetrabutylammonium bibenzoate (TBABB) had been synthesized as reported earlier by Dicker et al [2].

For the precipitation and purification of the resulting polymers, n-hexane (reagent grade, 96%) was used obtained from Scharlau, as well as cyclohexane.

2.4.2 Group Transfer Polymerization

For the synthesis of the desired star polymers, GTP and an arm-first approach is employed [3]. The arms of all stars consist of block and random copolymers of poly-[2-(dimethylamino)ethyl methacrylate] (PDMAEMA) and poly-methyl methacrylate (PMMA) at different ratios, while the core differs depending on the cross-linker used in each case. All monomers need to be accordingly prepared prior to the polymerization, and the equipment to be used needs to be completely free of any possible impurities and moisture. The monomers were prepared the day before the polymerization by passing them through a basic aluminium oxide column to remove the inhibitor they contained along with any other acidic impurities and were then transferred in 250 ml round bottom flasks, followed by addition of calcium hydride in order to remove any traces of moisture and 2,2-diphenyl-1-picrylhydrazyl (DPPH, inhibitor) to prevent the polymerization of the monomers. The monomers are stirred for 3 hours at a minimum and are then stored in the fridge to be used the next day. The glass equipment used in the polymerization process or in the purification of the monomers, are sonicated in a basic aqueous solution for an hour, rinsed ten times with water to remove the base, then washed out with an acidic aqueous solution to remove any traces of the basic solution, washed again with water and finally, rinsed with acetone. The glassware is then placed in the oven at 160ºC to dry overnight before use.

For the polymerization, THF is distilled, along with the initiator (MTS) and the monomers (DMAEMA and MMA). The cross-linkers that have been synthesized cannot be distilled, so to be sufficiently dry they are placed under vacuum for at least 3 hours before being used and are then diluted with 2 ml freshly distilled THF to facilitate the addition of small amounts of cross-linker into the reaction flask of the polymerization.

Four different star polymers were synthesized, two for each synthesized cross-linker. The targeted molecular weight of the arms in all cases was 10000 g/mole and the ratio of PDMAEMA:PMMA 30:70. A block copolymer and a random copolymer was synthesized in each case. The preparation of the $PDMAEMA_{30} - b - PMMA_{70}$ – star, with the use of the acid-degradable crosslinker, is described in detail below.

The polymerization took place in a 40ml glass vial sealed with a rubber septum. The vial was taken out of the oven and while it was still hot (oven temperature 160˚C) the catalyst (TBABB) was added (~10mg, 20 μmol) and the vial was sealed. When it reached room temperature, the vial was purged under nitrogen and then 20 ml freshly distilled THF were added via a glass syringe. When the catalyst was completely dissolved in the solvent, 0.12 ml ($5.7*10^{-4}$ mol) initiator (MTS) were added with a glass syringe and a digital thermometer was fixed on the bottom of the vial in order for the temperature to be monitored during the polymerization. The initial temperature was noted and then the monomers were added in the reaction flask. In the case of the block copolymer arms, 1.9 ml (11.4 mmol) DMAEMA were added first with a glass syringe, and the temperature increased from 28.5ºC to 37.1ºC. The increase in the temperature

is indicative of the polymerization reaction that takes place, since it is an exothermic reaction. As long as the temperature still increases, there is still monomer in the flask that is able to react, while as it starts decreasing the reaction has concluded, and the 'living' PDMAEMA chains are obtained. When the temperature reached again RT, 4.5 ml (42 mmol) MMA were added, and the temperature increased from 31ºC to 59.5ºC. After the temperature reached RT, an aliquot of 0.1 ml was collected and analysed via size exclusion chromatography (SEC). The cross-linker was added, at a ratio of 4:1 moles with respect to the initiator, as it has been previously proven that this ratio is ideal for the synthesis of well-formed star polymers [4]. So, 1.5 ml of the cross-linker solution in THF (0.84 ml of pure cross-linker) was added, and the temperature rose from 31.6ºC to 33.1ºC. The star polymers were formed during this step. After the temperature reached RT once more, an aliquot of 0.1 ml was collected for SEC analysis, and the polymer was precipitated and purified. The reactions that take place during the synthesis of the star polymers, are presented below (Figures 15 and 16).

For the purification of the star polymers fractional precipitation was employed. The polymer solution was diluted further with THF until a total volume of 80 ml and was stirred while cyclohexane was added dropwise until the solution became turbid. The temperature of the solution was then raised to approximately 30ºC to check if the solution would become transparent again. Further addition of cyclohexane led to the precipitation of the polymer in the bottom of the beaker. The mixture was left to rest, and then the supernatant was transferred to a clean beaker, where the same process was repeated again, while the first fraction was placed in a vacuum oven to dry. All the collected fractions were finally placed in a vacuum oven to dry, and then a sample of each was analysed by SEC. The precipitation process was repeated until the polymers were sufficiently purified, even though free linear polymers were still present in some cases.

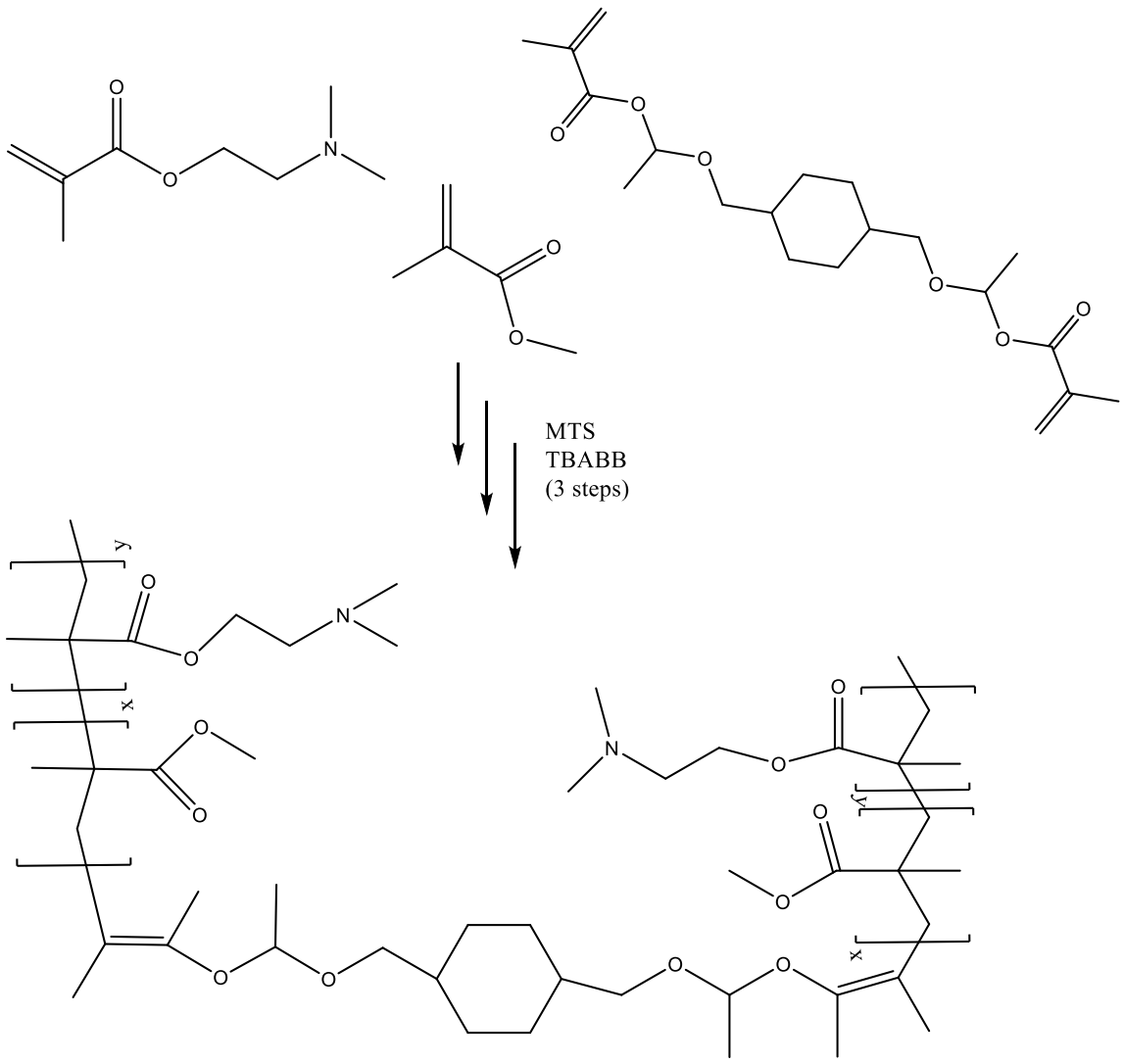

Figure 15 - Synthesis of the star polymers using an acid-degradable cross-linker

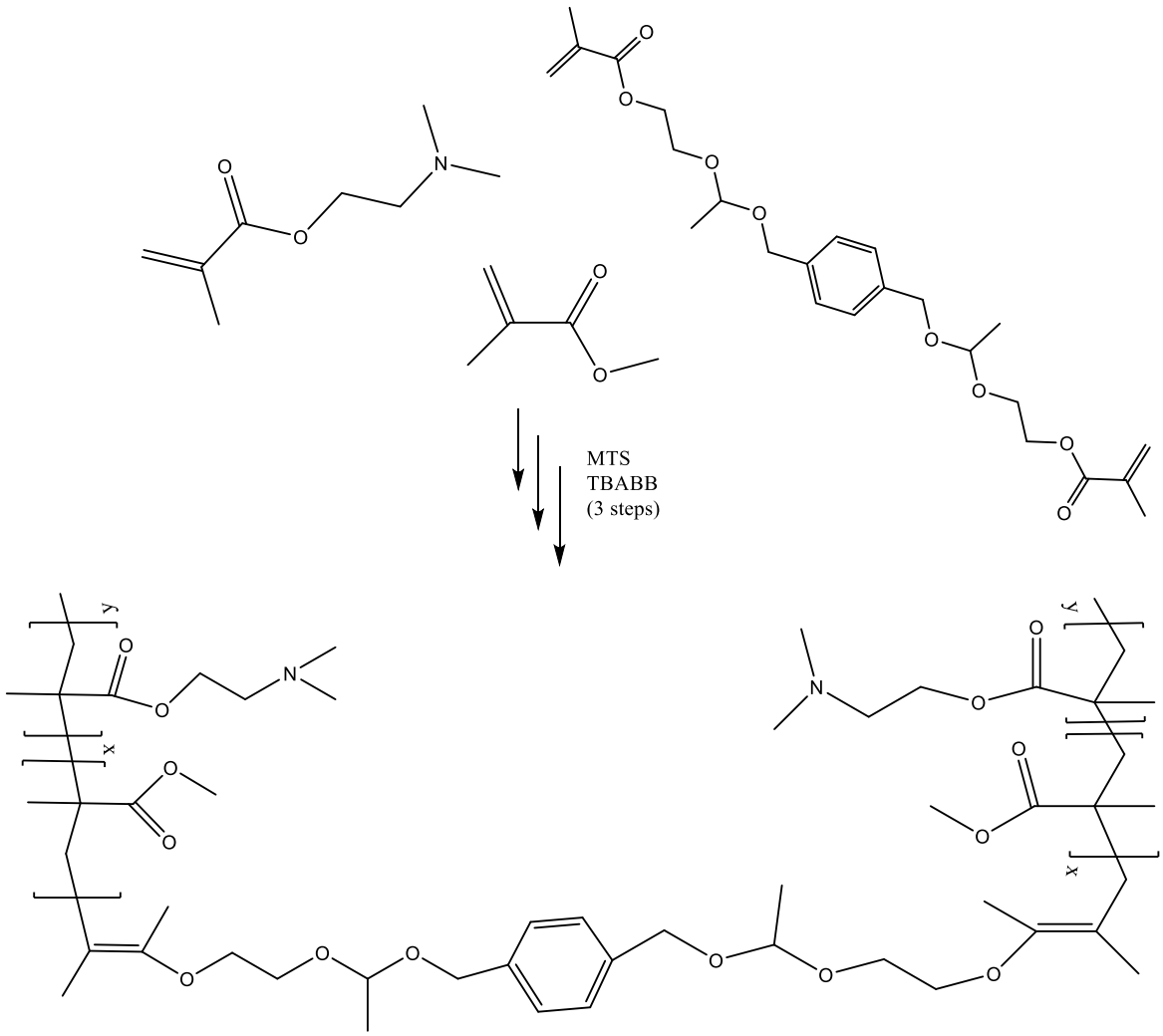

Figure 16 - Synthesis of the star polymers using the acid- and photo-degradable cross-linker

The targeted polymers, the amount of reagents used in each polymerization, along with the rise in temperature that was noted in each step, are presented in the following Table (Table 1).

Table 1 – Star polymers, quantities of reagents and temperature rise for the synthesis of all polymers prepared in this work

Polymer		**Reaction steps**	**Solvent (ml)**	**Initiator (ml)**	**DMAEMA (ml)**	**MMA (ml)**	**Cross-linker (ml)**	**$T_{initial}$ (ºC)**	**T_{final} (ºC)**
Block co-polymer	$PDMAEMA_{30}$	1	20	0.12	1.9	-	-	28.5	37.1
	$PDMAEMA_{30}$-b-$PMMA_{70}$	2	-	-	-	4.5	-	31	59.5
	$PDMAEMA_{30}$-b-$PMMA_{70}$-star	3	-	-	-	-	1.5	31.6	33.1
Random co-polymer	$PDMAEMA_{30}$-co-$PMMA_{70}$	1	20	0.12	1.9	4.5	-	28.6	60.7
	$PDMAEMA_{30}$-co-$PMMA_{70}$-star	2	-	-	-	-	1.5	33.1	34.2
Block co-polymer	$PDMAEMA_{30}$	1	20	0.12	1.9	-	-	26.5	34.9
	$PDMAEMA_{30}$-b-$PMMA_{70}$	2	-	-	-	4.5	-	29.3	60.6
	$PDMAEMA_{30}$-b-$PMMA_{70}$-photodegradable star	3	-	-	-	-	1.6	29.2	30.8
Random co-polymer	$PDMAEMA_{30}$-co-$PMMA_{70}$	1	20	0.12	1.9	4.5	-	26.6	57
	$PDMAEMA_{30}$-co-$PMMA_{70}$-photodegradable star	2	-	-	-	-	1.6	27.3	29.2

2.5 Characterization of the synthesized star polymers

2.5.1 Nuclear magnetic resonance spectroscopy

All synthesized star polymers were analysed using a Bruker 500 MHz spectrometer to verify their successful formation. A sample of ~10 mg of polymer was dissolved in 1 ml of $CDCl_3$ and then transferred to the appropriate NMR tube for the measurement to be conducted.

2.5.2 Size exclusion chromatography

To determine the molecular weights and the molecular weight distribution of the synthesized star polymers, SEC was employed using a Waters 515 isocratic pump equipped with two Polymer Laboratory columns, PL-mixed-D and PL-mixed-E, a Waters 2487 Dual Absorbance detector and a Waters 410 refractive index detector. THF with added 2% triethylamine was used as eluent at a flow rate of 1 ml/min. The universal calibration method, using poly(methyl methacrylate) as standards, was used to determine the molecular weight of the polymers. A ~20 mg sample of the polymer to be analyzed was dissolved in 1 ml of THF and filtered through 0.45 μm filter prior to the measurement.

2.5.3 Dynamic light scattering

For the DLS measurements, a Malvern Zetasizer NanoZS90 was employed. Contrary to the typical DLS systems, the Zetasizer only conducts measurements at 90º with no ability to change the angle of the measurement. The cuvettes used for the measurements were square quartz glass, transparent on all sides. Solutions of the star polymers of a 0.1% wt. concentration in THF were prepared, that were homogeneous and transparent, and prior to the measurement, were filtered through 0.45 μm filters. The data collected during the measurement were analysed using the Zetasizer® software and were directly depicted as a plot of intensity *vs* size or volume *vs* size.

2.5.4 Scanning electron microscopy

The morphology of the star polymers was observed using field emission scanning electron microscopy (FE-SEM, JEOL JSM-7000F). Solutions of 0.1% wt. concentration of the star polymers were prepared, followed by the deposition of a drop of the solution on a glass substrate for SEM. After the solvent had evaporated completely and before the samples were imaged by SEM, they were sputtered with gold.

2.6 Polymer hydrolysis

In order for the star copolymers containing the acid-degradable cross-linker to undergo hydrolysis, they must first be treated with an acidic solution. A 40 mg sample of the $PDMAEMA_{30}$-*b*-$PMMA_{70}$ star copolymer, as well as the random $PDMAEMA_{30}$-$PMMA_{70}$ star copolymer, were dissolved in 2 ml dry THF respectively and a 10-fold molar excess of hydrochloric acid was added (0.0152 mmol cross-linker in the sample, 0.152 mmol HCl 1M) and the mixture was passed through a 0.45 μm filter. After 2 hours had passed, a sample of each polymer was analyzed by SEC.

For SEM analysis, a drop of the prepared solution is deposited on a glass substrate and the solvent is evaporated prior to imaging.

Last, for ^{1}H NMR spectroscopy analysis, the solvent is evaporated under vacuum, the hydrolyzed products are subsequently dissolved in 1 ml $CDCl_3$ and the solution is transferred to the appropriate NMR tube.

The hydrolysis process followed is the same for polymers formed using either of the synthesized cross-linkers.

2.7 Polymer photo-degradation

To study the photodegradation of the $PDMAEMA_{30}$-*b*-$PMMA_{70}$-photodegradable star copolymer, a 40 mg sample of the star polymer was dissolved in 2 ml dry THF, passed through a 0.45 μm filter and placed in a quartz cuvette. A sample of the intact polymer was analyzed by SEC and the cuvette was then subjected to UV irradiation. The wavelength chosen for the degradation was 254 nm, since 1,4-benzenedimethanol absorbs at approximately 280 nm. After one hour of irradiation, a second sample of the solution was analyzed by SEC. This process was repeated until it was obvious by SEC that the population of the star polymers in the sample was significantly decreased or completely eradicated, and the differences between the chromatograms after successive irradiation was negligible.

The solution was diluted to a final volume of 5 ml and used to prepare the samples for SEM analysis, by depositing a drop of the solution on a glass substrate and evaporating the solvent.

For ^{1}H NMR spectroscopy analysis, a second sample was prepared. 20 mg of polymer were dissolved in 1 ml $CDCl_3$ and placed in the appropriate NMR tube. The initial spectrum was recorded, and the NMR tube was subjected to UV irradiation. After one hour of irradiation, a second NMR spectrum was recorded. The process was repeated until the differences between the recorded spectra were negligible.

2.8 Nuclear magnetic resonance spectroscopy [5]

Nuclear magnetic resonance spectroscopy is based on the principle of nuclei being positively charged spinning on an axis and forming a tiny magnetic field. The nuclear magnetic field can either align or oppose with an external magnetic field B_0.

The magnetic fields of the nuclei are randomly oriented when there is no external magnetic field. When a sample that contains these nuclei is placed between the magnetic poles of a strong magnet, the nuclei acquire specific orientation. A spinning ^{13}C or ^{1}H nucleus orient so that their weak magnetic field either aligns or opposes that of the external magnetic field. The two orientations do not require the same energy and so they do not have the same probability. Where the two fields align, the energy required is lower, so that state is preferable to that of the opposing fields.

If the oriented nuclei are irradiated with electromagnetic radiation of appropriate frequency, an energy absorption takes place and the state with the lower energy reverts to the state of highest energy (spin reversal). When this reversal takes place, we can say that the nuclei are resonating with the applied radiation. That is the reason why this technique is called “nuclear magnetic resonance”.

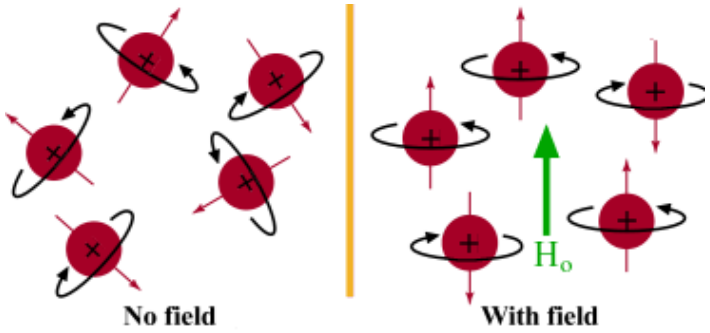

Figure 17 - Randomly oriented nuclear magnetic fields vs oriented nuclei under the influence of an external magnetic field

The specific frequency needed for resonance depends on the strength of the external magnetic field and on the type of the nucleus. If the magnetic field used is very strong, the energy difference between the two spin states is large, thus the radiation required is of higher frequency (higher energy) so that the spin reversal takes place. If the magnetic field used is weaker, the energy required for the reversal of spin to take place, is lower.

The H and C nuclei are not the only ones that manifest the phenomenon of nuclear magnetic resonance. All the nuclei with an odd number of protons (e.g. ^{1}H, ^{2}H, ^{14}N, ^{19}F, ^{31}P) and all the nuclei with an odd number of neutrons, such as ^{13}C, manifest magnetic properties. Only the nuclei with an even number of protons and neutrons (^{12}C, ^{16}O) do not cause such phenomena.

The absorption frequency is not the same for all the ^{1}H or ^{13}C nuclei. All the nuclei in molecules are surrounded by electrons. When an external magnetic field is exercised on a certain molecule, the electrons form their own microscopic local magnetic fields.

These magnetic fields act contrary to the exercised field, so the real field in the nucleus is smaller than the external.

H(real) = H (exercised) – H (local)

It can be said that the nuclei are protected by the full extent of the exercised field due to the electrons that surround them. Because of the fact that each molecule's nucleus exists in a different electronic environment, it is protected in a different extent, so that the real exercised magnetic field is not the same for each nucleus. If the device is sensitive, the minute differences between the real exercised field that each nucleus "feels" can be detected, so we get a different NMR signal for each distinct chemical carbon or hydrogen nucleus of a molecule. Thus, the NMR of an organic compound effectively "maps" the carbon-hydrogen connection network.

NMR signals are gathered in graphs that show the increase of the magnetic field from left to right. So, the left part of the graph is the downfield region, and the right part of the graph is the upfield region. To determine the absorption site, the NMR graph is graded, and a reference point is used.

The point in the graph that a nucleus absorbs, is called chemical shift. The NMR graphs are graded using an arbitrary scale that is called δελτα scale. One δελτα point equals one part per million (ppm) of the function frequency of the spectrometer.

The nuclei that are better protected by the electrons need stronger exercised field so that they can resonate, thus they absorb on the right side of the graph. The nuclei that are less protected, need weaker exercised field to resonate, thus they absorb on the left side of the spectrum.

The area that each peak encloses is proportionate to the number of electrons that cause the peak. By integrating the area of each peak it is possible to count the relative number of each distinct type of proton in a molecule.

A common occurrence is the splitting of the absorption of a proton into multiple peaks. The phenomenon of multiple peaks is caused by the interaction or coupling of the nuclear spin of nearby atoms. In other words, the microscopic magnetic field of a nucleus affects the magnetic field that the nearby nuclei "feel". The differences in the extent of the electronic protection are due to the differences in the chemical shift among nuclei. According to a general rule, called ν+1 rule, protons with ν equivalent nearby protons, show ν+1 peaks in the NMR spectrum. Chemically equivalent protons do not show spin splitting.

2.9 Gel permeation chromatography (GPC)/Size exclusion chromatography (SEC) [6, 7]

Chromatography is a separation technique mainly used for the separation of the different constituents of a mixture. The sample is dissolved in a solvent called the mobile phase, and then travels through a structure, usually a column, that is packed with another material, called the stationary phase. The separation of the different constituents is based on the different interactions that the constituents have with the mobile and stationary phases. Chromatography can be either preparative or analytical, but they are not mutually exclusive. In the case of preparative chromatography, the goal is to purify the components of the mixture for later use, while in the case of analytical chromatography, the target is to establish the presence of the different components of the mixture or to measure the relative proportions of each analyte in the mixture. There are many forms of chromatography, but Gas Chromatography (GC) and Liquid Chromatography (LC) are the two most commonly used techniques in the chemical analysis field.

GPC, also known as SEC, is a form of liquid chromatography. It employs a liquid mobile phase that carries the sample, and a stationary phase, typically chemically modified inorganic silica or polymeric beads, that is packed into a column. The mobile phase passes between the beads and through the pores of the stationary phase that resides inside the columns, carrying along with it the sample of the mixture that needs to be separated (Figure 18). The separation of the different constituents relies exclusively on the size of the polymer molecules in the solution, hence the name "size exclusion chromatography". What is interesting about synthetic polymers, is that no matter the length of their chain, they can still be recognized as the same polymer. In practice, that means that every polymer sample contains polymer chains of different molecular weights. Via GPC/SEC the distribution of molecular weights in the sample can be determined (polydispersity index).

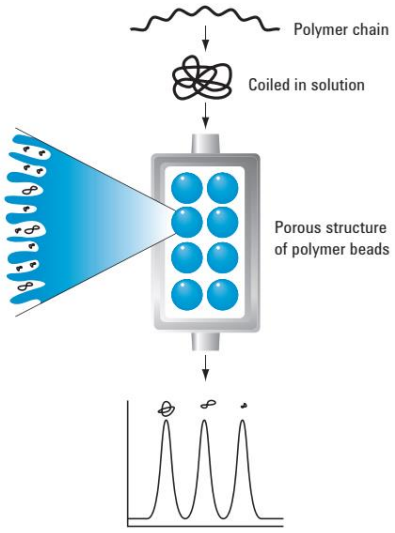

Figure 18 - Schematic representation of the way SEC separated molecules of different sizes [6]

A GPC/SEC instrument typically consists of a container for the solvent (mobile phase), a pump that pushes the solvent into the instrument, an injection port that facilitates the introduction of the sample into the columns that hold the stationary phase, one or more detectors to detect the components of the mixture being analyzed as they exit the column, and a suitable software to control the different parts and parameters of the instrument, as well as process and display the data received from the detectors.

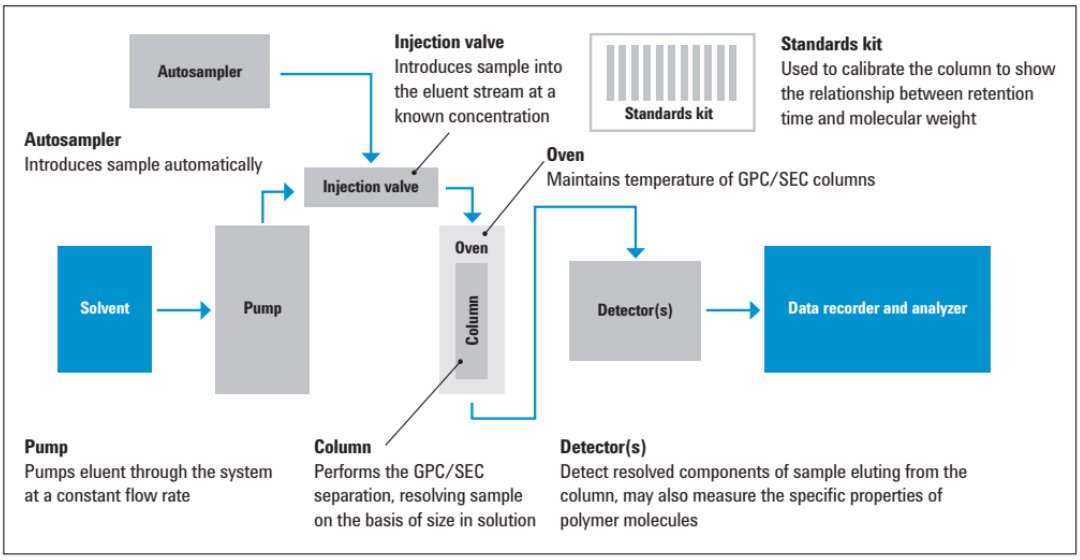

Figure 19 - Main components of SEC systems [6]

The data collected from the detectors are depicted in a graph, also called chromatogram. This graph shows the amount of material exiting the column at any one time, with the chains with high molecular weight exiting first, followed by chains with successively lower molecular weight. The time it takes for a group of chains with the same size to exit the column is referred to as retention time, since the molecules are retained inside the column during their analysis. The data collected from the graph is then compared to a calibration curve (Figure 19) that shows the retention time of a set of polymers with known molecular weight. That way, the molecular weight distribution of the analyzed sample can be calculated. The typically calculated value for the molecular weight is actually the number average molecular weight, M_n. M_w is the most quoted value for the molecular weight of the polymer, it greatly influences the physical properties of the material, and it can also be calculated this way, but since it is sensitive to the size of the molecules, its value is always greater than M_n. This is always the case with only exception that of the polymer being completely monodisperse. The ratio of M_w to M_n is used to calculate the polydispersity index (PDI) of the polymer, that constitutes an indication of the distribution of molecular weights in the sample. The broader the sample of molecular weights, the large the PDI value.

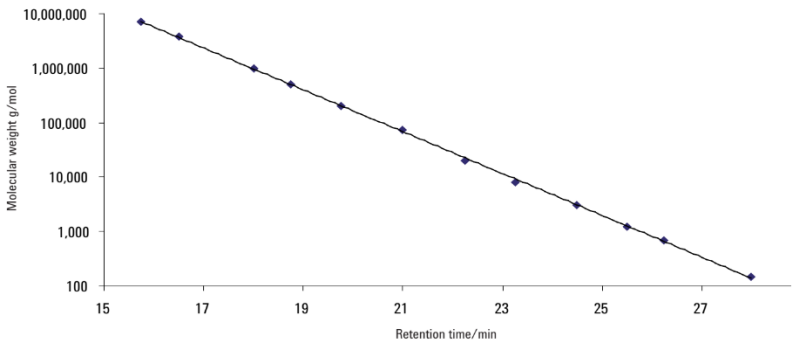

Figure 20 - Calibration curve [6]

There are a few criteria that need to be met in order to choose a certain solvent for the GPC set-up. The solvent must be able to dissolve the sample, and it must not either interact in any way with the stationary phase or induce any interactions between the sample and the stationary phase, so that the separation can be completely dependent on the size of each polymeric molecule. The separation takes place inside the column that, as was previously mentioned, is packed with porous beads of different sizes that consist of either polymer or silica, that are specifically designed to have pores of a specific size. The columns vary in length from 50 to 300 mm and they can have an internal diameter of 4.6 to 25 mm. The type of beads used in each column and their size is chosen for different molecular weight ranges, and the length and the internal diameter of the column depend on the intended use of the column. The pump has to be able to maintain a constant flow rate so that the acquired results can be comparable between different analyses, and it also has to be smooth so as not to send pulses into the column.

2.10 Dynamic light scattering

Dynamic light scattering (DLS), also known as photon correlation spectroscopy (PCS) or quasi-elastic light scattering (QLS), is a spectroscopic method, mainly used to determine the size distribution of particles (polymers, colloids, nanoparticles etc.) in solution or suspension [8, 9]. What DLS measures, is the Brownian motion of the particles in the solution due to the constant collisions between them and the molecules of the solvent, and it relates that motion to the size of the particles. Generally, the larger the particle, the slower the Brownian motion, while smaller particles are further displaced after the collision with the solvent molecules and so move more rapidly. The velocity of the Brownian motion in each case is expressed by the translational diffusion coefficient, D. The translational diffusion coefficient is part of the Stokes-Einstein equation that calculates the size of the particle as follows:

$$d(H) = \frac{kT}{3\pi\eta D}$$

Where d(H) is the hydrodynamic diameter of the particle, D is the translational diffusion coefficient, k is Boltzmann's constant, T is the absolute temperature and η is the viscosity. The diameter that is calculated by this function is the diameter of a sphere that is characterized by the same translational diffusion coefficient as the particle being measured. The translational diffusion coefficient depends on a number of factors: i) the size of the "core" of the particle, ii) the ionic strength of the medium (low conductivity media generate an extended layer of ions around the particle, thus reducing the diffusion speed and lead to an apparently larger hydrodynamic diameter) and iii) the surface structure (any change in the surface of the particles that can have an effect on the speed of the particles' diffusion, will lead to a corresponding change in the apparent hydrodynamic size of the particles).

When the particles that are going to be measured are small compared to the laser that is used during the measurement (typically around $\lambda/_{10}$), the scattering from the particles is of the same energy as the incident light (elastic scattering) and is not angle-dependent (Rayleigh scattering) [10]. When the size of the particles exceeds that threshold though, Rayleigh scattering is replaced by Mie scattering, that is anisotropic, so the scattered light is of unequal energy in relation to the incident light (inelastic scattering) as well as angle dependent (the scattered light is more intense in the direction of the incident light, and bigger particles exhibit higher angle-dependence).

During a dynamic light scattering measurement, the speed of the diffusing, due to Brownian motion, particles is measured. The measurement is essentially the rate at which the intensity of the scattering light fluctuates and is detected by a suitable detector. This measurement is reflected by a speckle pattern, in which the position of each speckle constantly changes, since the system is in constant Brownian motion. The rate at which the intensity fluctuates depends on the size of the particles, for example small particles lead to more fluctuations in the measured intensity.

The frequencies of the intensity fluctuations are recorded by a digital autocorrelator. An autocorrelator is essentially a signal comparator that, in the case of DLS, compares one signal with itself at various time intervals. By comparing the intensity of the signal at time equal to t to the intensity of the signal at a very short time after that (t+δt), the relationship between the two signals, or else their correlation, will be very strong. The same process is repeated for longer amounts of time and it is noted that the correlation reduces with time. The correlation is also dependent on the size of the particles, as large particles do not exhibit quick changes in their intensity fluctuations, so the correlation can persist for a longer amount of time in comparison to smaller particles, that move rapidly and cause high fluctuations in their intensity, so their correlation exhibits a quicker reduction. The correlation function of the scattered intensity created by the correlator is the following:

$$G(\tau) = < I(t)I(t+\tau) >$$

Where τ is the time difference of the correlator.

When the correlation function refers to a large number of monodisperse particles that are in Brownian motion, it is an exponential decaying function of the correlator time delay τ:

$$G(\tau) = A[1 + B\exp(-2\Gamma\tau)]$$

Where A is the baseline of the correlation function and B the intercept of the correlation function. Γ is given by the equation $\Gamma = Dq^2$. D is the translational diffusion coefficient, and the wavevector q is expressed as $q = 4\pi\left(\frac{n}{\lambda_0}\right)\sin(\frac{\theta}{2})$, where n is the refractive index of the dispersant, λ is the wavelength of the laser and θ is the scattering angle.

In the correlogram that derives from a measurement, the time at which the correlation starts to decay in a significant amount gives an indication of the mean size of the particles in the sample. More monodisperse samples generate steeper decaying, while mono polydisperse samples lead to extended decay times. The size can be obtained from the correlation function with the use of various algorithms. The size distribution that derives from them is a plot of the relative intensity of the scattered light by the various sized particles in the sample and is known as the intensity size distribution. If it is a single smooth peak, there is no need for converting it to a volume distribution using the Mie theory.

A typical DLS instrument consists of three components: the laser, the sample and the light detector. The instrument used for the measurements during this Master Thesis, was a Malvern Zetasizer ZS90, that carries a laser of 632.8 nm that provides the beam of coherent monochromatic light that is then scattered by the sample [11]. The cuvettes used for the measurements were square quartz glass, transparent on all sides, and all the samples were homogeneous and transparent before the measurement and were then filtered through 0.45 μm filters. The instrument's detector is at a 90º angle and Zetasizer® was the software used for the measurements. The data collected during the measurement, were directly depicted as a plot of intensity *vs* size or volume *vs* size.

2.11 Scanning electron microscopy (SEM)

SEM is a type of electron microscopy [12]. It uses a focused high-energy electron beam (energy values can vary between 0.2 keV to 40 keV) that scans the surface of the sample and interacts with its atoms/molecules in various depths in order to generate various signals that can ultimately provide crucial information for the analyzed sample. The types of signals that can be produced [13] are numerous, including secondary electrons (SE), reflected or back-scattered electrons (BSE), characteristic X-rays and light (cathodoluminescence, CL) [14], and each of them require a specified detector. Most SEMs use secondary electron detectors as standard equipment, and even though it is rare for an instrument to be equipped with detectors for all possible signals, it can be done. The type of signal generated can provide different information about the analyzed sample. For example, secondary electrons produce SEM images that show the morphology of the samples, while backscattered and diffracted backscattered electrons are used to determine crystalline structure and characteristic X-rays are mainly used for elemental analysis.

The scanning electron microscope consists of an electron gun that produces a beam of monochromatic electrons. This stream of electrons passes through a set of condenser lenses that focuses the electrons into a thin, tight and coherent, high-energy beam. Lastly, the beam passes through the objective lens that focuses it on the specified spot on the sample. When the incident beam reaches the sample, it interacts with it and

produces various signals, that can be detected by a number of different detectors depending on the nature of the signal. The signal is then amplified and finally displayed on the computer monitor.

In the case of secondary electron imaging (SEI), the secondary electrons are emitted from very small depths in the sample. When the incident electron beam reaches the sample, it transfers its energy to the spot that the beam is focused. The electrons in the beam are also known as primary electrons and manage to dislodge electrons form the surface of the sample, that are called secondary electrons. The secondary electrons are then collected, and the signal is amplified by electronic amplifiers and displayed on a computer monitor as variations in brightness. The higher the number of secondary electrons, the brighter the image will be. So, the final image can be described as a distribution map of the intensity of the emitted signal from each area of the sample.

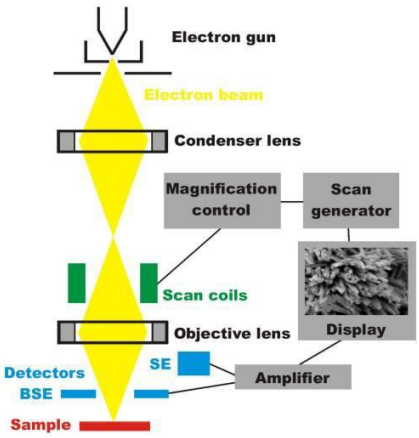

Figure 21 - Schematic represenation of SEM components

The magnification that can be achieved by SEM ranges from about ×10 to ×500.000 times. Its spatial resolution is also not standard, and depends on the size of the electron spot, and so on the system that produces the electron beam and on the wavelength of the electrons. Since the spot size and the interaction volume are a comparatively large area, the resolution SEM can achieve is not high enough so that individual atoms can be displayed, but it has quite a few compensating features. First of all, its breadth of applications in the study of materials is unique, and its contribution to the characterization of solid materials is significant. It provides the opportunity to image a relatively large area of the analyzed sample as well as the ability to image bulk materials and not only thin films. Also, depending on the signals produced and detected, it provides a wide variety of analytical modes to determine the composition, as well as the properties of the sample that is being analyzed. Despite these strengths SEM has a number of limitations also. The analyzed samples must be solid, dry, and small enough in order to fit into the analysis chamber. They also have to be stable in the high vacuum that is needed for the system to function. Additionally, for conventional SEM imaging, the samples need to be electrically conductive, at least on the surface, as well as electrically grounded, to prevent the accumulation of electrostatic charge. So, non-conductive samples need to be coated with an ultrathin layer of conductive material that is usually deposited on the surface of the sample by low vacuum sputter coating. The most commonly used materials for sputtering is gold, gold/palladium alloys, iridium etc.

SEM can be utilized in a number of different research fields, such as geology, biology, and materials science. SEM has been used for the characterization of polymeric materials in different studies, but in the case of star polymers it's use is not that simple. Star polymers as a general rule are small and compact molecules, a characteristic that

makes them difficult to observe via microscopy techniques such as Atomic Force Microscopy (AFM) as well as SEM. Typically, they are below the resolution limits, or if not, they usually appear as collapsed globular structures that manage to obscure the structural details of their complex architectures, so arm resolution is extremely rare, but information about the molecular size in the dry state can still be collected [15]. For the purposes of this Master Thesis, SEM was used to confirm visually the degradation of the star polymers, both after hydrolysis and light irradiation [16].

2.12 References

[1] Nithyanandan K., Kannan P., Kumar K.S., Ramamurthy P., *Journal of Polymer Science Part A: Polymer Chemistry*, Vol. 49, 1138-1146 (2011)

[2] Dicker, I. B., Cohen, G. M., Farnham, W. B., Hertler, W. R., Laganis, E. D., & Sogah, D. Y. (1990). Oxyanions catalyze group-transfer polymerization to give living polymers. Macromolecules, 23(18), 4034–4041. doi:10.1021/ma00220a002

[3] Georgiou T.K., Vamvakaki M., Patrickios C.S., *Biomacromolecules* 2004, 5, 2221-2229

[4] Simmons, M. R., Yamasaki, E. N., & Patrickios, C. S. (2000). Cationic homopolymer model networks and star polymers: synthesis by group transfer polymerization and characterization of the aqueous degree of swelling. Polymer, 41(24), 8523–8529. doi:10.1016/s0032-3861(00)00201-9

[5] John E. McMurry, Organic Chemistry, Cengage Learning; 8th edition (2012), ISBN-13**:** 978-1133152118

[6] An introduction to Gel Permeation Chromatography and Size Exclusion Chromatography, Agilent Technologies Inc., 2015

[7] Kostanski, L. K., Keller, D. M., & Hamielec, A. E. (2004). Size-exclusion chromatography—a review of calibration methodologies. Journal of Biochemical and Biophysical Methods, 58(2), 159–186. doi:10.1016/j.jbbm.2003.10.001

[8] Light Scattering from Polymer Solutions and Nanoparticle Dispersions, W. Schärtl, Springer, ISBN 3-540-71950-4

[9] Dynamic Light Scattering with applications to Chemistry, Biology, and Physics, Bruce J. Berne, Robert Pecora, Dover Publications, Inc. ISBN 0486411559, 9780486411552

[10] Sourav Bhattacharjee, DLS and zeta potential – What they are and what they are not?, *Journal of Controlled Release*, 2016, doi: 10.1016/j.jconrel.2016.06.017

[11] Zetasizer Nano Series, User Manual, Malvern Instruments Ltd., 2013

[12] Stokes, Debbie J. (2008), *Principles and Practice of Variable Pressure Environmental Scanning Electron Microscopy (VP-ESEM)*. Chichester: John Wiley & Sons. ISBN 978-0470758748.

[13] Goldstein, G. I.; Newbury, D. E.; Echlin, P.; Joy, D. C.; Fiori, C.; Lifshin, E. (1981), *Scanning electron microscopy and x-ray microanalysis*. New York: Plenum Press. ISBN 0-306-40768-X.

[14] Deborah L. Vezie, Edwin L. Thomas, W. Wade Adams, *Polymer*, Vol.36, No. 9, pp. 1761-1779, 1995

[15] Jing M. Ren, Thomas G. McKenzie, Qiang Fu, Edgar H. H. Wong, Jiangtao Xu, Zesheng An, Sivaprakash Shanmugam, Thomas P. Davis, Cyrille Boyer, Greg G. Qiao, *Chem. Rev.* 2016, 116, 6743-6836

[16] Jenny Liu, Alan O. Burts, Yongjun Li, Aleksandr V. Zhukhovitskiy, Maria Francesca Ottaviani, Nicholas J Turro, and Jeremiah A. Johnson, *J. Am. Chem. Soc.*, DOI: 10.1021/ja3067176

3. Results and Discussion

3.1 Characterization of the synthesized cross-linkers

3.1.1 Acid – degradable cross-linker

The successful synthesis, the final structure and the adequate purification of the synthesized cross-linkers were verified by ^{1}H NMR spectroscopy.

For the acid-degradable cross-linker the ^{1}H NMR spectrum is presented below (Figure 22), along with its analysis.

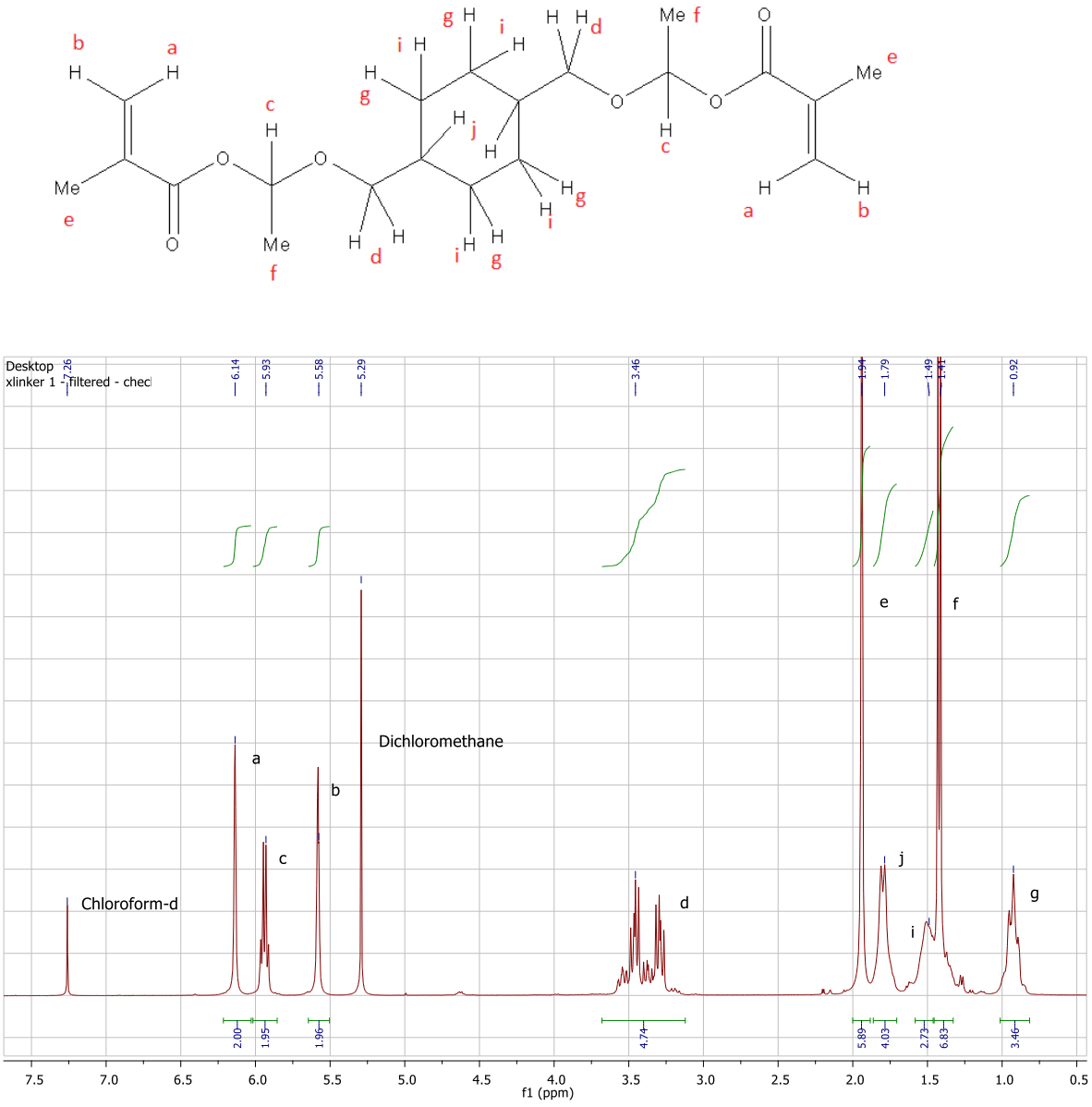

Figure 22 – ^{1}H NMR spectrum and structure of the acid-degradable cross-linker

Peak assignment ($CDCl_3$): 0.92ppm [equatorial H of cyclohexane, 4H], 1.41ppm [2(CH_3), 6H], 1.49ppm [axial H of cyclohexane, 4H], 1.79ppm [2(CH), 2H], 1.94ppm [2(CH_3), 6H], 3.46ppm [2(CH_2), 4H], 5.58ppm [olefinic H trans to CO_2 2H], 5.93ppm [2(CH), 2H], and lastly 6.14ppm [olefinic H cis to CO_2, 2H].

The peak at 5.93 ppm confirmed the formation of the desired acetal-bond between the reactants during the synthesis of the cross-linker. The proton peaks at 5.58 ppm and 6.14 ppm also verify that the resulting molecule does indeed have double bonds at each end, an essential characteristic of a molecule to be used as a cross-linker during polymerization.

3.1.2 Acid- and photo-degradable cross-linker

In order to proceed to the synthesis of the cross-linker, the required vinyl ether was synthesized first. Its structure and purity were verified by ^1H – NMR spectroscopy and the acquired spectrum is presented below (Figure 23).

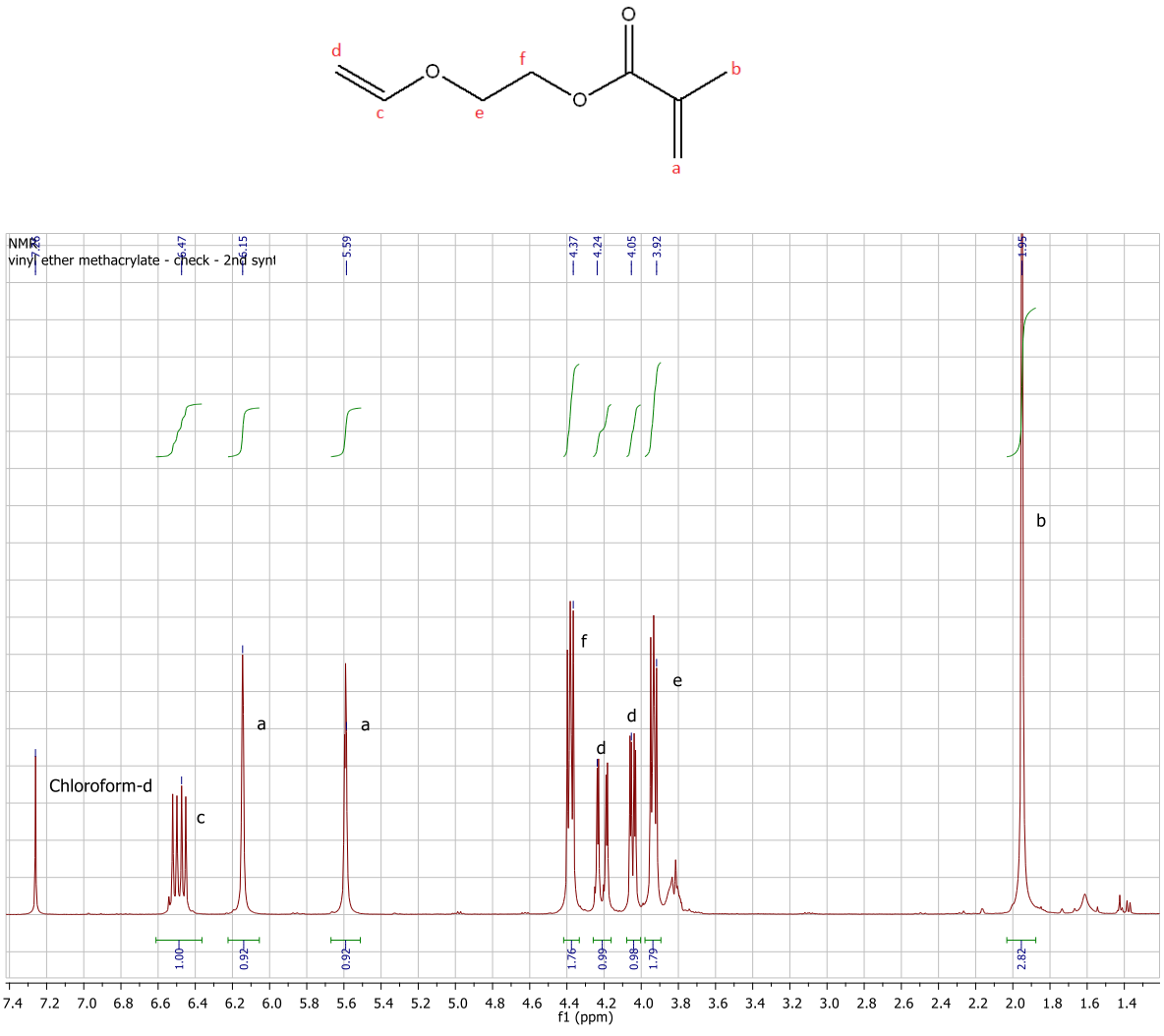

Figure 23 – ^1H NMR spectrum and molecular structure of vinyl ether methacrylate

Peak assignment ($CDCl_3$): 1.95ppm [(CH_3), 3H], 3.92ppm [(CH_2), 2H], 4.05ppm and 4.24ppm [(CH_2), 1H for each peak], 4.37ppm [(CH_2), 2H], 5.59ppm and 6.15ppm [(CH_2), 1H for each peak], and last 6.47ppm [(CH), 1H]. The double bonds on each end of the molecule allow the formation of the cross-linker, and provide the methacrylate double bonds that enable its polymerization.

The synthesis and purity of the cross-linker was also verified via ^1H NMR spectroscopy (Figure 24).

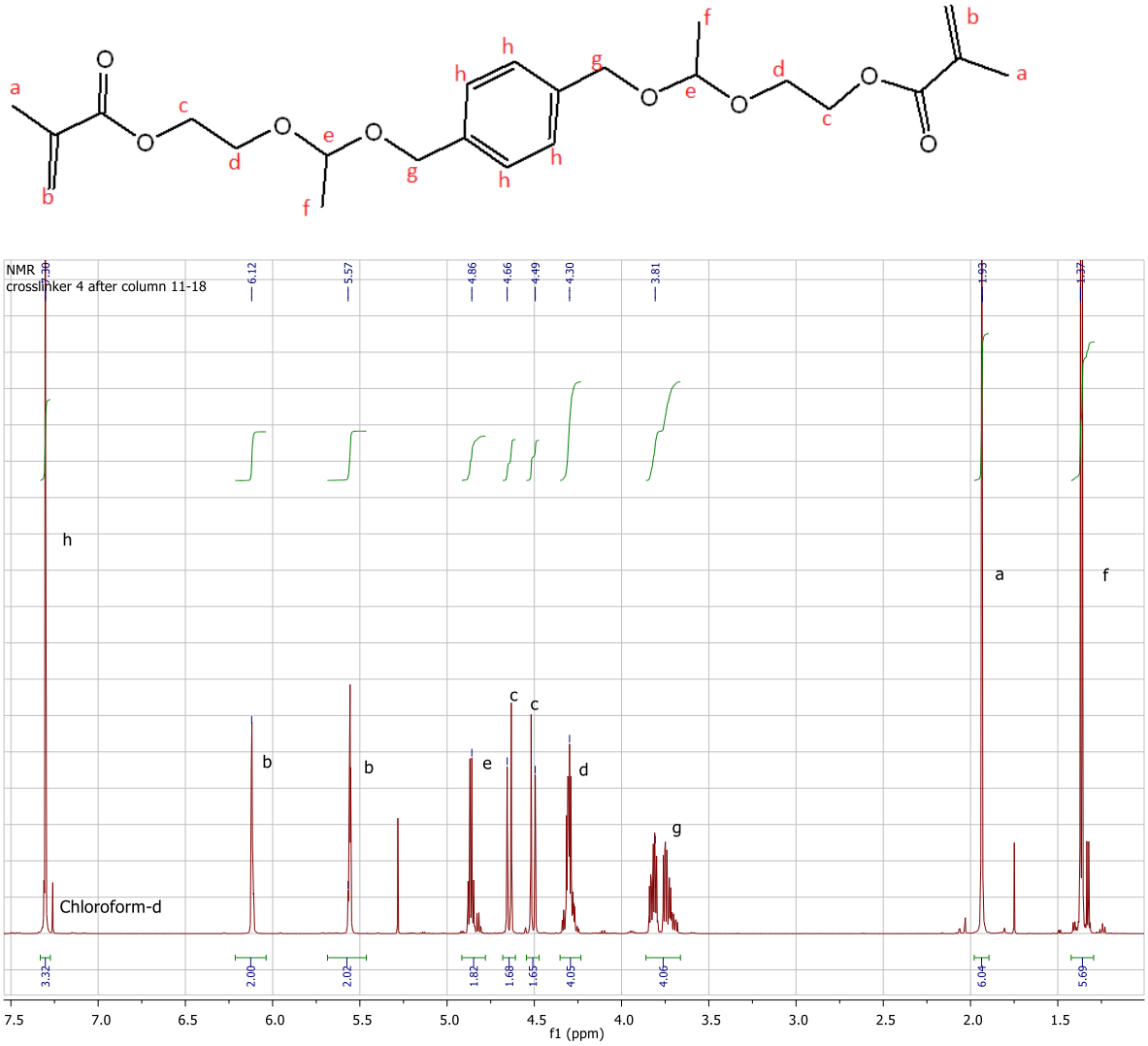

Figure 2417 – ^1H NMR spectrum and molecular structure of the acid- and photo-degradable cross-linker

Peak assignment ($CDCl_3$): 1.37ppm [2(CH_3), 6H], 1.93ppm [2(CH_3), 6H], 3.81ppm [2(CH_2), 4H], 4.30ppm [2(CH_2), 4H], 4.49ppm and 4.66ppm [2(CH_2), 4H], 4.86ppm [2(CH), 2H], 5.57ppm and 6.12ppm [2(CH_2), 4H], and last at 7.30ppm [aromatic protons, 4H].

As is the case of the acid-degradable cross-linker, the peak at 4.86 ppm confirms the formation of the acetal bond, and the successful synthesis of the cross-linker.

3.2 Characterization of the star polymers synthesized using the acid-degradable cross-linker

3.2.1 Size exclusion chromatography

To characterize the synthesized star polymers, samples of the final purified polymers were analysed using different characterization techniques.

First, the aliquots collected during the polymerization process were analysed by SEC to determine the average molecular weight of the synthesized polymers, as well as the polydispersity index. The data collected was compared against a calibration curve that was generated by analysing standard polymer samples of known molecular weight. In this case, the standard samples used were linear PMMA, that give a quite accurate value of the molecular weight of the linear precursor chains. It should be noted though that the molecular weight values for the star polymers that arise from SEC are effective values, because during the calibration of the system, linear standards were used. Consequently, the obtained values for M_n, M_w, and M_p are lower than the real values for the star polymers due to their compact nature in comparison to the linear polymer standards [1,2].

In the picture below (Figure 25), the chromatographs of the PDMAEMA$_{30}$-*b*-PMMA$_{70}$ linear precursor, along with the chromatograph of the corresponding star can be seen.

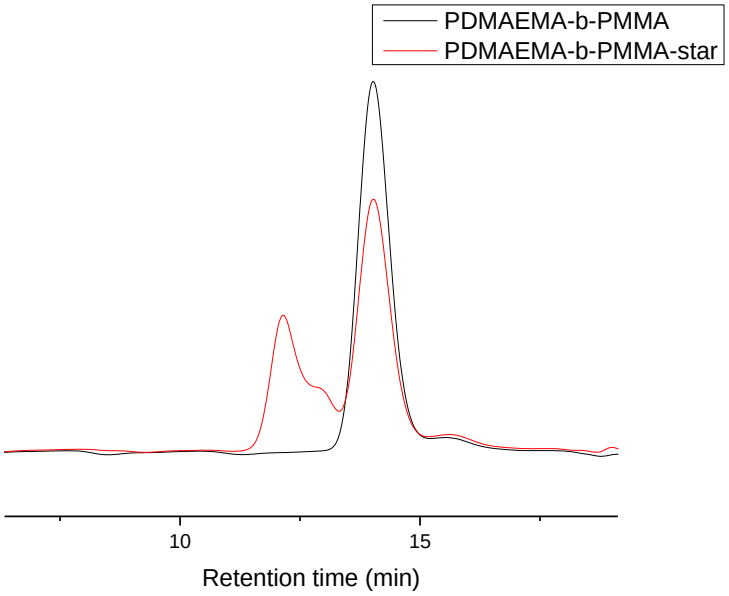

Figure 25 - SEC chromatographs of the block copolymer arms and the acid-degradable star polymer

The single narrow peak of the PDMAEMA$_{30}$-*b*-PMMA$_{70}$ copolymer indicates that, due to the living polymerization method employed for its synthesis, the polymer has a quite narrow molecular weight distribution. In the case of the star polymer, two peaks can be seen, one at lower elution times that corresponds to the star polymer, and one at higher elution times that corresponds to the free linear polymer chains. The peak of the star polymer is wider than that of the linear polymer and that is attributed to the wide distribution of molecular weights in each star (the 'random' way that each star is formed is responsible for the uncertainty concerning the number of arms in each star and thus the wide distribution of molecular weights). The peak of the free linear polymer that is seen in the chromatograph of the star, can be attributed to the fact that some of the living chains could not react to form a star due to their length and steric hindrance.

By purifying the polymer via fractional precipitation, the removal of the majority of the free linear polymers is possible, and the chromatograph of the resulting purified product is presented below (Figure 26).

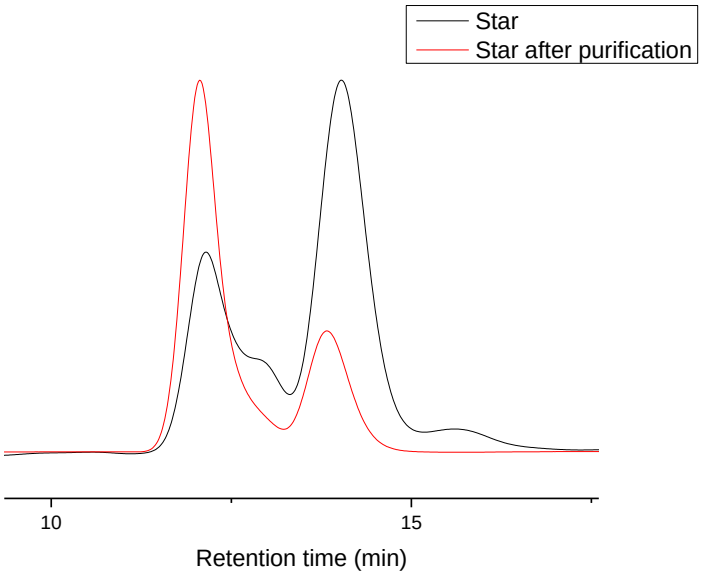

Figure 26 – SEC chromatographs of the acid-degradable star polymer before and after purification

The random PDMAEMA$_{30}$-PMMA$_{70}$-star was also analyzed with SEC. In the figure below (Figure 27), the chromatographs of the linear precursor polymer, along with that of the star polymer is shown.

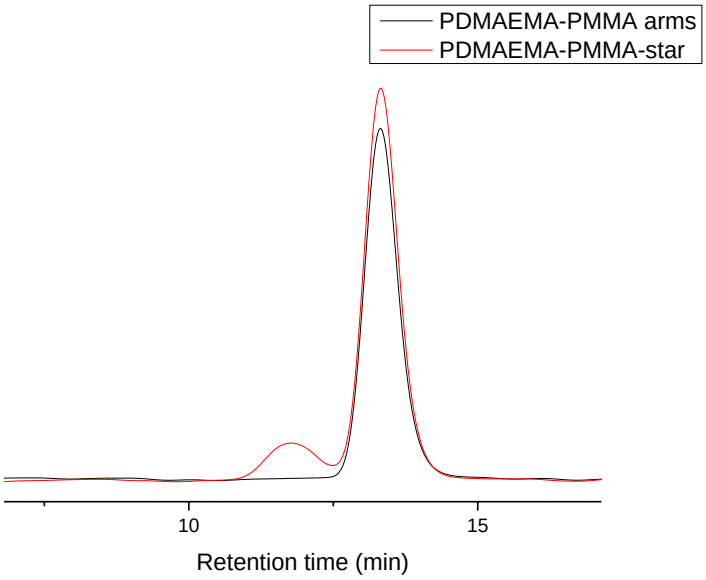

Figure 27 - SEC chromatographs of the random copolymer arms and the acid-degradable star polymer

In the chromatograph of the random PDMAEMA-PMMA copolymer, a single narrow peak can be seen, indicating a low polydispersity index, which is expected of polymers synthesized via a living polymerization method such as GTP. In the chromatograph of the star polymer two peaks can be seen: the first peak at lower elution times corresponds to the star polymer and the second peak corresponds to unattached linear precursors. The peak of the star polymers is quite broad as expected, but its low intensity indicates that in this case the cross-linker was not very effective in reacting with the linear arms to form the star polymer. That can be attributed to the length of the arms which was large and so the steric hindrance was high, and the arms could not easily react to lead to the formation of stars.

The final polymer was purified via fractional precipitation to remove some of the unattached arms. The chromatograph of the resulting purified polymer is presented below (Figure 28).

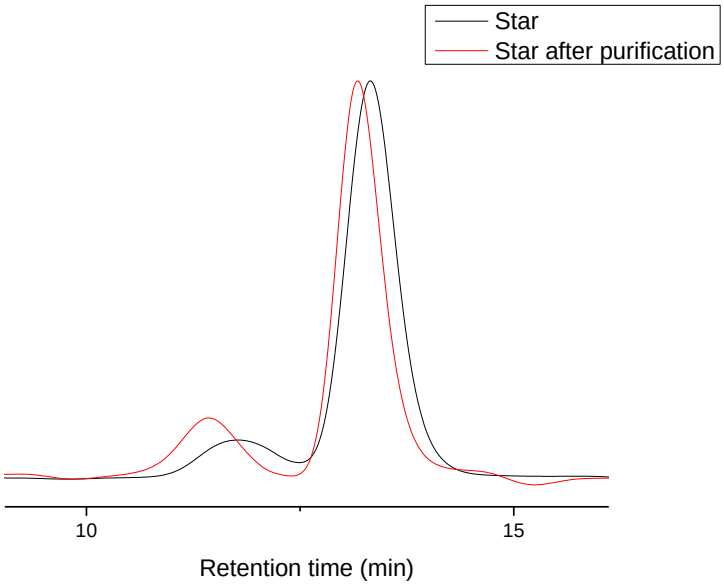

Figure 28 - SEC chromatographs of the acid-degradable star polymer before and after purification

After a number of attempts to purify the polymer, no further difference was noted.

The results acquired via SEC for both synthesized stars using the acid-degradable cross-linker can be seen in the table below (Table 2).

Table 2 – Theoretical molecular weights and number average and weight average molecular weights of the star polymers measured by SEC

Polymers		**Theoretical Molecular Weight**	**SEC Results**			
			M_w	**M_n**	**M_p**	**M_w/M_n**
Block co-polymer	PDMAEMA$_{30}$-*b*-PMMA$_{70}$	11700	10300	9600	10300	1.08
	PDMAEMA$_{30}$-*b*-PMMA$_{70}$-star	-	57000	51000	62000	1.12
Random co-polymer	PDMAEMA$_{30}$-PMMA$_{70}$	11700	20000	18000	20000	1.07
	PDMAEMA$_{30}$-PMMA$_{70}$-star	-	98000	90000	95000	1.08

3.2.2. ^{1}H – Nuclear magnetic resonance spectroscopy

The two different star polymers were also characterized via ^{1}H nuclear magnetic resonance spectroscopy.

The spectrum of the acid-degradable block copolymer star is presented below (Figure 29).

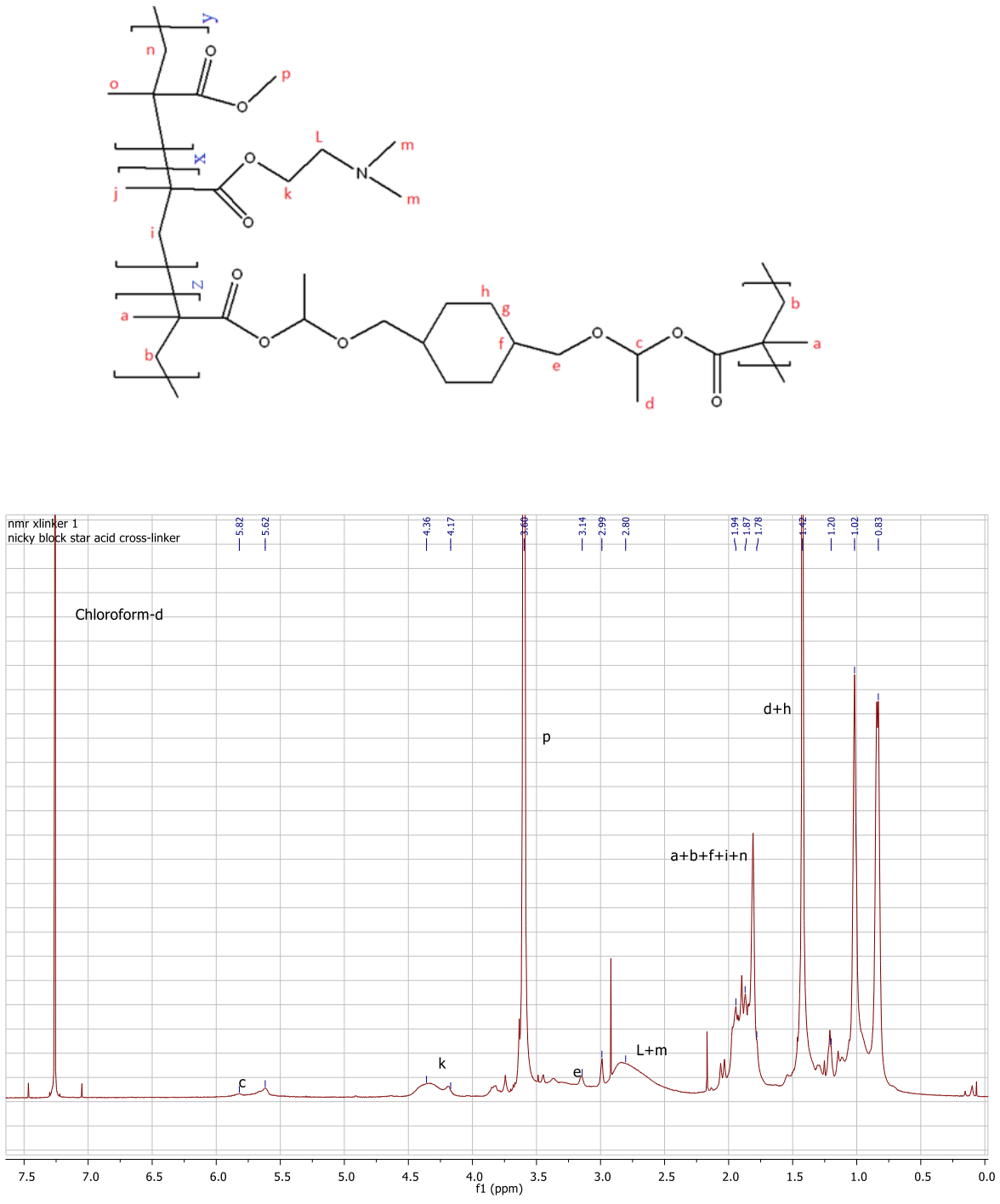

Figure 29 – ^{1}H NMR spectrum and molecular structure of the acid-degradable block copolymer star

By analysing the spectrum of the PDMAEMA$_{30}$-*b*-PMMA$_{70}$-star polymer, it is noted that all the expected peaks are accounted for: 1.94ppm [2(CH_3), 6H], 1.87ppm [2(CH_2), 4H], 5.82ppm [acetal proton, 2H], 1.43ppm [2(CH_3), 6H], 3.14ppm [2(CH_2), 4H], 1.79ppm [2(CH), 2H], 1.02ppm [equatorial protons of cyclohexane, 4H], 1.42ppm [axial protons of cyclohexane, 4H], 0.83ppm and 1.02ppm [(CH_3), 3H], 1.94ppm [(CH_2), 2H], 4.1ppm [(CH_2), 2H], 2.8ppm [(CH_2), 2H], 2.5-2.8ppm [2(CH_3), 6H]. Lastly, for the PMMA: 1.78-1.94ppm [(CH_2), 2H], 0.83-1.02ppm [(CH_3), 3H] and 3.6ppm [(CH_3), 3H].

While the nature of the polymer inhibits the precise integration of the peaks since the majority of them overlap, the presence of PDMAEMA, PMMA and cross-linker in the polymer is verified.

In the case of the random PDMAEMA$_{30}$-PMMA$_{70}$-star copolymer, the spectrum is presented below (Figure 30). Even though the arms of the star polymer are random copolymers, no change is expected to be seen in the NMR spectrum in comparison to that of the star with the block-copolymer arms, since the structure of the DMAEMA and MMA repeat and the two polymers are chemically identical.

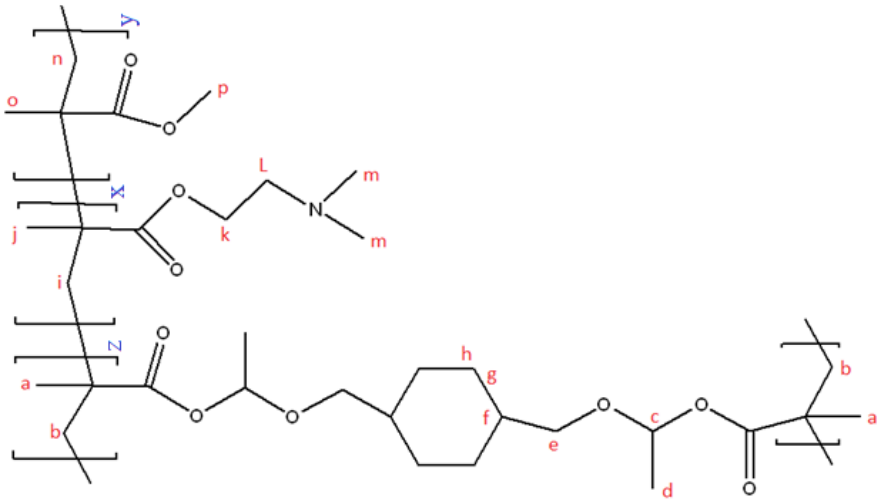

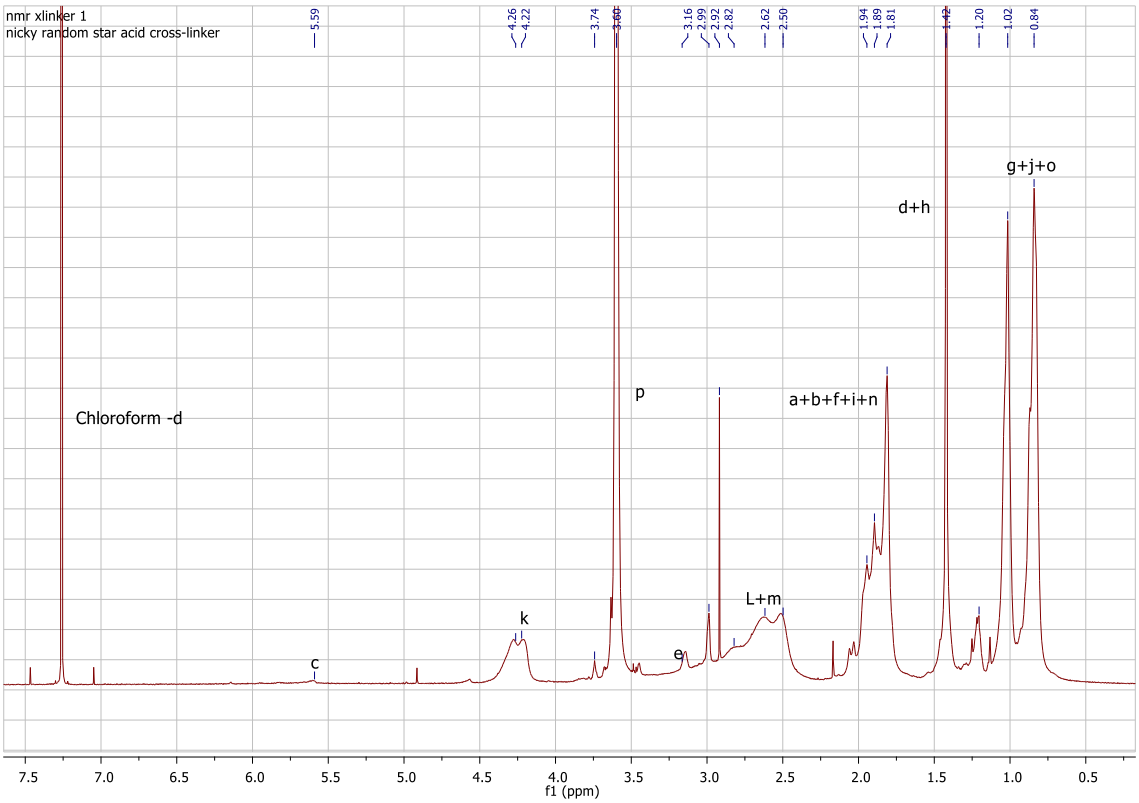

Figure 18 – ^{1}H NMR spectrum and molecular structure of the acid-degradable random copolymer star

The peak assignment in the ^{1}H NMR spectrum of the random copolymer is: 1.94ppm [2(CH_3), 6H], 1.81ppm [2(CH_2), 4H], 5.59ppm [acetal protons, 2H], 1.42ppm [2(CH_3), 6H], 3.16ppm [2(CH_2), 4H], 1.81ppm [2(CH), 2H], 1.02ppm [equatorial protons of cyclohexane, 4H], 1.42ppm [axial protons of cyclohexane, 4H], 0.84ppm and 10.2ppm [2(CH_3), 6H], 1.94ppm [2(CH_2), 4H], 2.82ppm [2(CH_2), 4H], 4.22ppm [2(CH_2), 4H] and last 2.5-2.8ppm [2(CH_3), 6H]. Lastly, for the PMMA: 0.84ppm and 1.02ppm [2(CH_3), 6H], 1.81-1.94ppm [2(CH_2), 4H] and 3.60ppm [(CH_3), 3H].

3.2.3 Dynamic light scattering

The hydrodynamic diameter of the PDMAEMA$_{30}$-*b*-PMMA$_{70}$-star polymer in a 0.1% wt. solution in THF was measured. The graph below (Figure 31) shows the size distribution of the polymers.

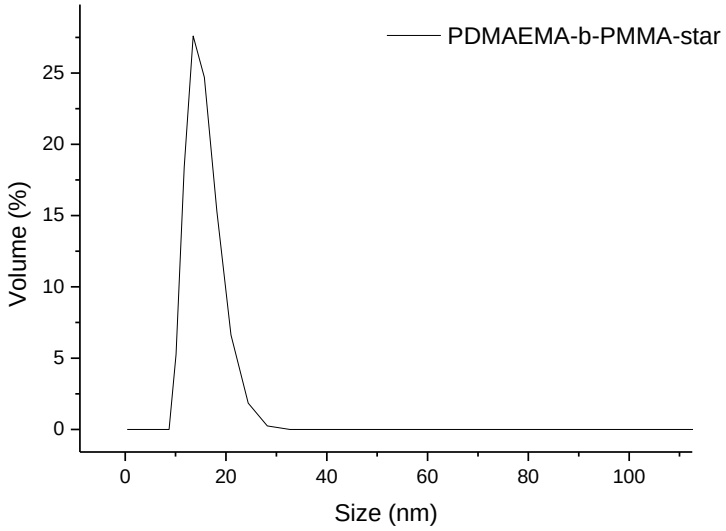

Figure 31 - Hydrodynamic diameter of the acid-degradable block copolymer star

The hydrodynamic diameter of the random $PDMAEMA_{30}$-$PMMA_{70}$-star copolymer in THF is presented below (Figure 32).

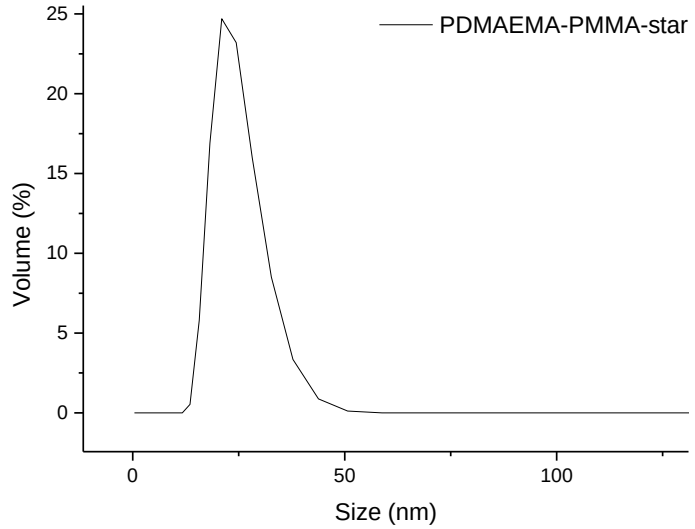

Figure 32 - Hydrodynamic diameter of the acid-degradable random copolymer star

The measured hydrodynamic diameters of the star polymers are shown in the table below (Table 3).

Table 3 – Hydrodynamic diameters of the synthesized star polymers using the acid-degradable cross-linker

Polymer	**Size (nm)**
PDMAEMA$_{30}$-*b*-PMMA$_{70}$-star	14
PDMAEMA$_{30}$-PMMA$_{70}$-star	21

3.2.4 Scanning electron microscopy

The images of the PDMAEMA$_{30}$-*b*-PMMA$_{70}$-star copolymers at different magnifications (Figure 33), are presented below.

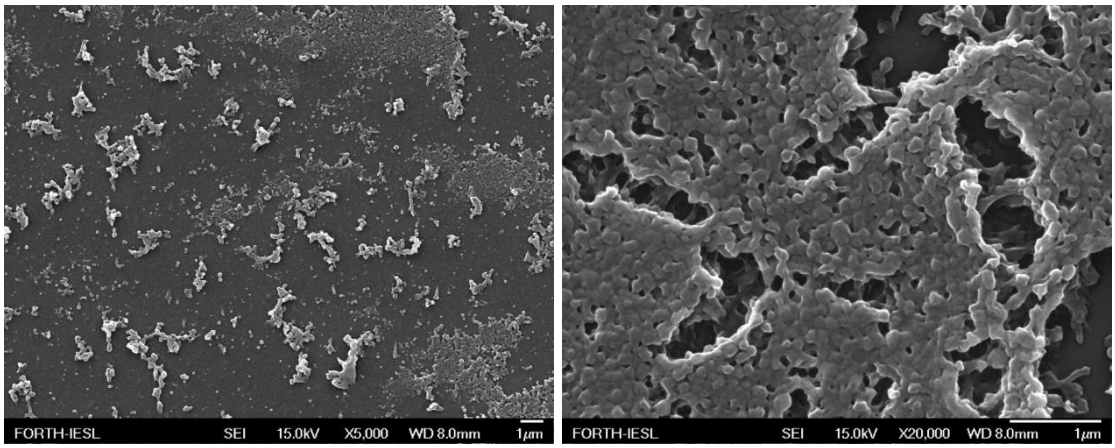

Figure 33 - SEM image of the acid-degradable block copolymer star

The images acquired for the acid-degradable block copolymer stars show the formation of either a network of star polymers or the formation of aggregates of distinct star polymers which appear as spherical structures in SEM. The length of the arms of the stars was chosen to be around 10000 g/mole (SEC approximated the M_n of the block co-polymer arms at 9600 g/mole) to avoid the inter-crosslinking of the stars. However, upon drying the stars are organized in a network-like structure as seen in the SEM images.

Images of the acid-degradable random PDMAEMA$_{30}$-PMMA$_{70}$-star copolymers were also acquired and are presented below (Figure 34).

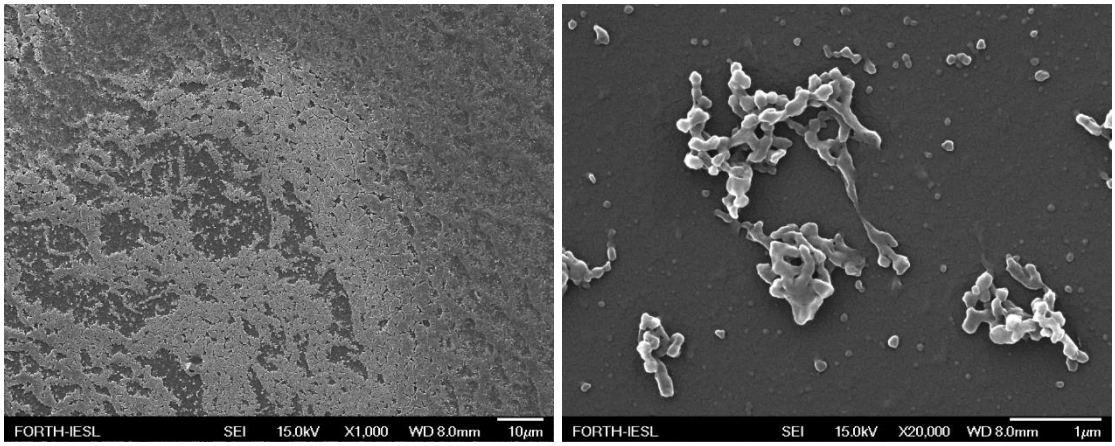

Figure 34 - SEM image of the acid-degradable random copolymer star

By observing the images acquired for the acid-degradable random copolymer stars, we can see that they have formed aggregates, as in the case of the acid-degradable block copolymer stars, that were attributed to the tendency of the star polymers to aggregate upon drying for SEM imaging. These aggregates either form a continuous film or smaller aggregates.

3.3 Characterization of the star copolymers synthesized using the acid- and photo-degradable cross-linker

3.3.1 Size exclusion chromatography

The samples of the free linear arms as well as the samples of the star polymers, were analyzed with SEC to acquire an estimation of the molecular weight and the polydispersity index of the polymers which were synthesized.

In Figure 35 below, the chromatographs for the linear PDMAEMA$_{30}$-*b*-PMMA$_{70}$ copolymer and its corresponding star polymer can be seen.

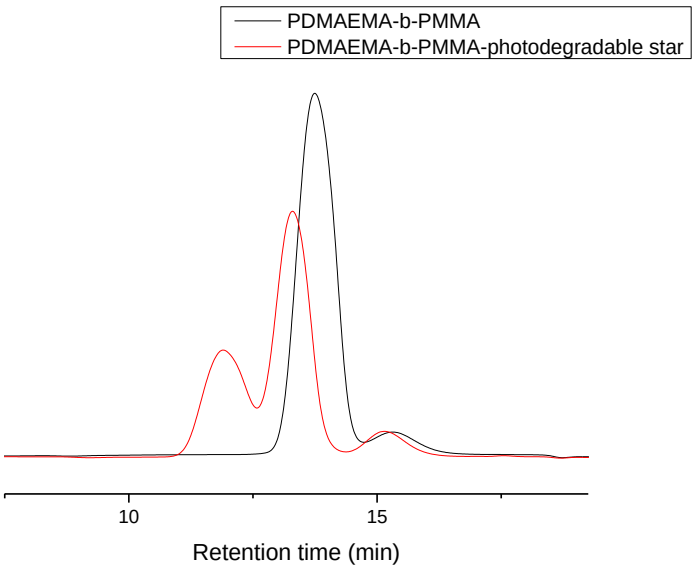

Figure 35 - SEC chromatographs of the block copolymer arms and the star copolymer containing the acid- and photo-degradable cross-linker

The chromatograph of the precursor linear polymer is a narrow peak, as expected, indicating once more that the polymerization led to a polymer with narrow molecular weight distribution. A smaller peak is also noted at lower molecular weights which is attributed to polymer chains of smaller length that have been already terminated. The chromatograph of the star polymers shows two peaks, the first of which, at lower elution times, corresponds to higher molecular weights and is attributed to the star polymers, while the peak of the linear precursor is still quite prominent and corresponds to linear polymeric chains that did not take part in the formation of the stars.

The final polymer was purified via fractional precipitation in cyclohexane to remove the remaining linear precursors of the star. The chromatograph of the final purified polymer can be seen below (Figure 36). The reason that the free linear precursors could not be removed was perhaps because they are block copolymers and form micelles which are stabilized in the solvent medium.

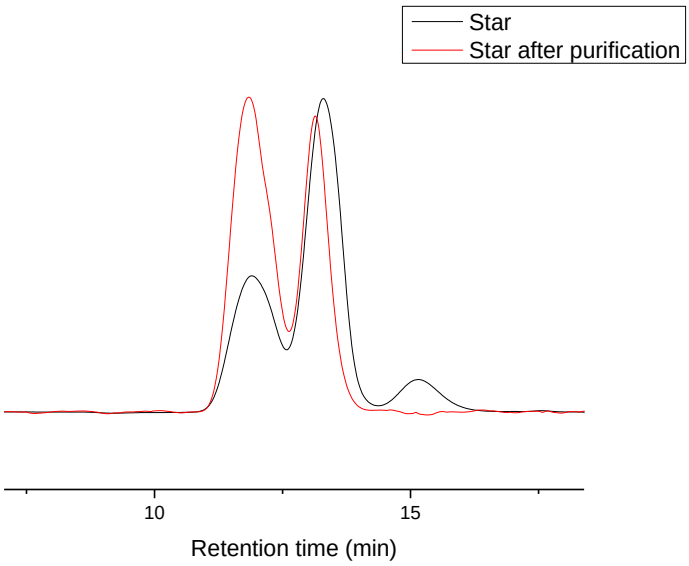

Figure 36 - – SEC chromatographs of the acid- and photo-degradable star polymer before and after purification

The samples of the random PDMAEMA$_{30}$-PMMA$_{70}$ star copolymer were also analyzed with SEC. The chromatographs of the linear precursors and the corresponding star are presented below (Figure 37).

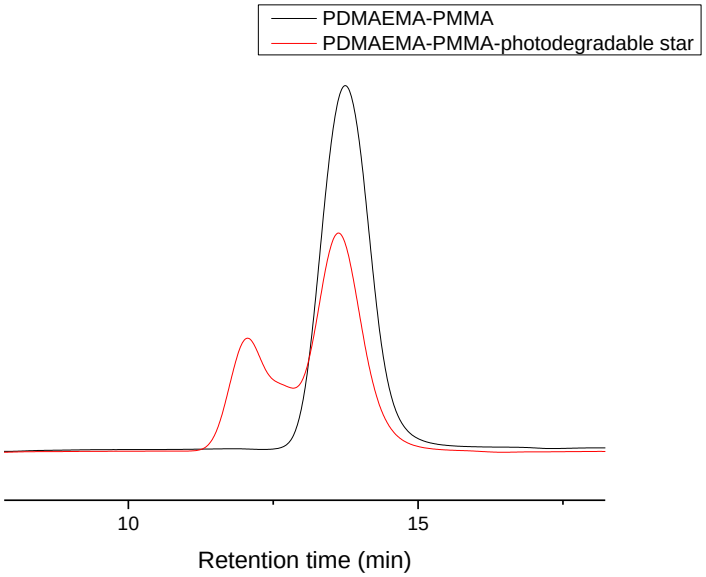

Figure 37 - SEC chromatographs of the precursor random copolymer and the star copolymer containing the acid- and photo-degradable cross-linker

The linear precursor shows a single narrow peak which corresponds to the arms of the stars and indicates that the polydispersity of the synthesized linear polymer is low, typical for polymers synthesized via living polymerization method. The chromatograph of the star shows two peaks. The first peak at lower elution times corresponds to the

newly formed star polymers, while the second peak corresponds to the linear precursor that remained unattached and did not take part in the formation of the star polymer.

The resulting polymer was purified via fractional polymerization in cyclohexane to remove the unattached polymer chains. The chromatograph of the purified polymer is shown below (Figure 38).

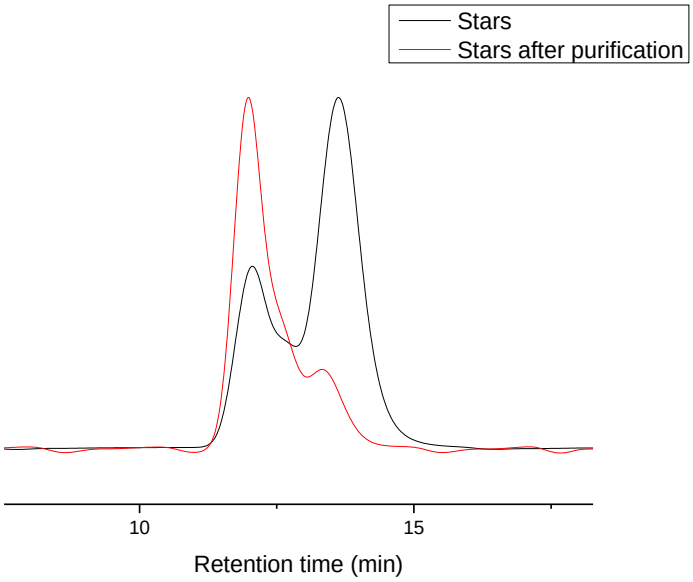

Figure 38 - SEC chromatographs of the acid- and photo-degradable random copolymer star before and after purification

The results acquired from SEC for both stars synthesized with the acid- and photo-degradable cross-linker can be seen in the table below (Table 4).

Table 4 – Theoretical molecular weights and number and weight average molecular weights of the star polymers measured by SEC

Polymers		**Theoretical Molecular Weight**	**SEC Results**			
			M_w	**M_n**	**M_p**	**M_w/M_n**
Block copolymer	$PDMAEMA_{30}$-*b*-$PMMA_{70}$	11700	14000	12000	13000	1.09
	$PDMAEMA_{30}$-*b*-$PMMA_{70}$-photodegradable star	-	86000	80000	83000	1.08
Random copolymer	$PDMAEMA_{30}$-$PMMA_{70}$	11700	14000	12000	13000	1.12
	$PDMAEMA_{30}$-$PMMA_{70}$-photodegradable star	-	70000	65000	70000	1.06

By comparing the theoretical molecular weight of the linear precursors, which was calculated by multiplying the degree of polymerization with the molecular weight of the monomer repeat unit, with the molecular weight determined via SEC, a good agreement was obtained, given the use of linear PMMA standards, verifying the good control of the polymerization reaction.

3.3.2 ^{1}H Nuclear magnetic resonance spectroscopy

The star polymers synthesized using the acid- and photo-degradable cross-linker were also analyzed by ^{1}H NMR spectroscopy. The ^{1}H NMR spectrum of the PDMAEMA$_{30}$-*b*-PMMA$_{70}$-photodegradable star copolymer, is presented below (Figure 39)

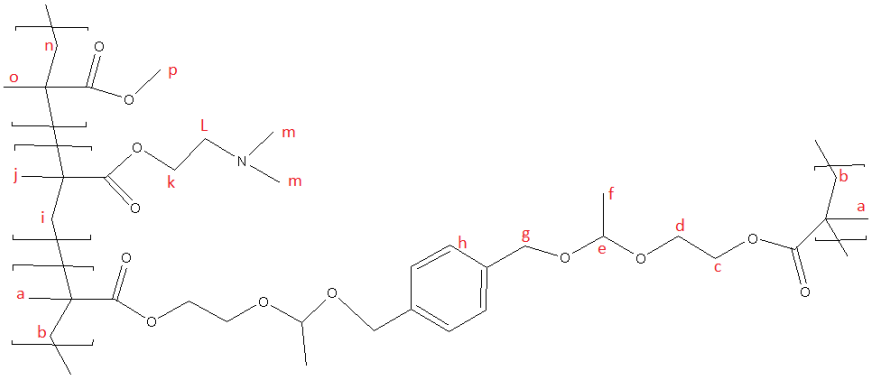

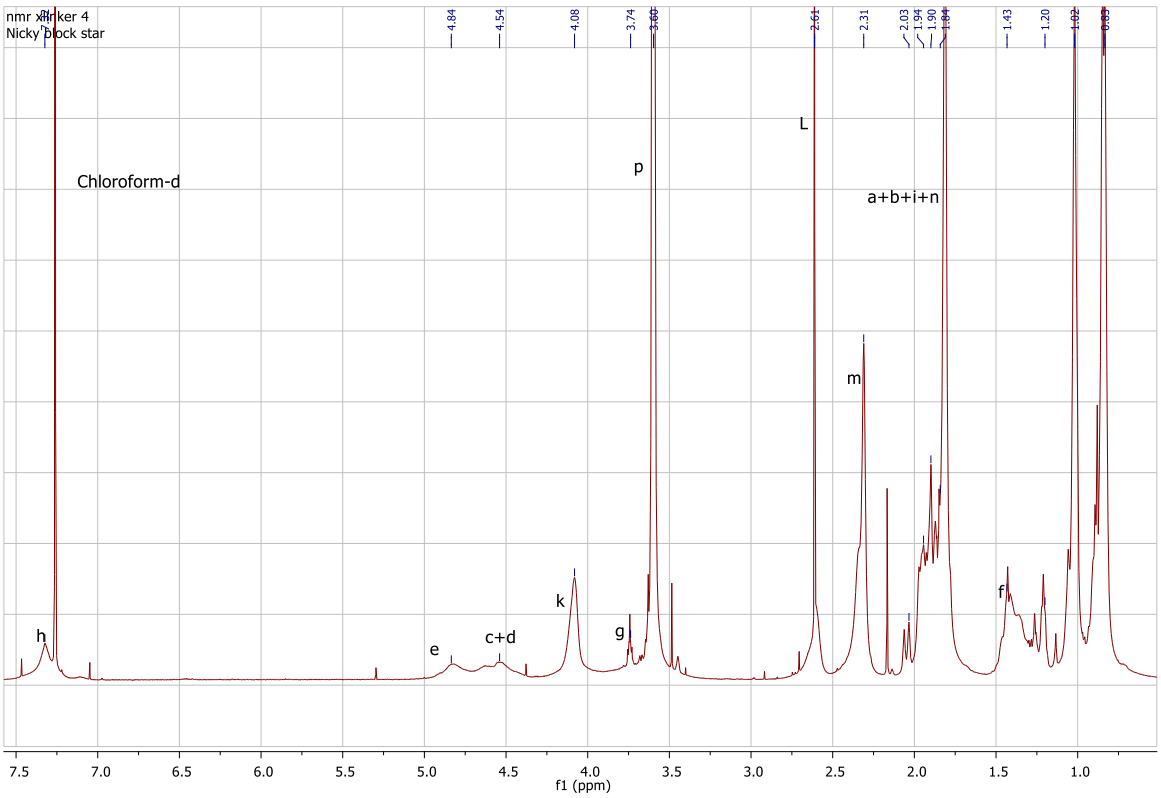

Figure 39– ^{1}H NMR spectrum and molecular structure of the acid- and photo-degradable block copolymer star

The ^{1}H NMR spectrum of the copolymer exhibits all peaks due to the two monomers used and the cross-linker verifying the molecular structure of the copolymer. However, due to the overlap of the peaks the precise copolymer composition could not be determined.

The peak assignment is as follows:7.32ppm [aromatic protons of benzyl ring, 4H], 4.84ppm [acetal protons, 2H], 4.54ppm [2(CH_2), 4H], 3.74ppm [2(CH_2), 4H], 1.90ppm [2(CH_3), 6H], and lastly 1.43ppm [2(CH_3), 6H]. The peaks corresponding to the PDMAEMA are the following: 0.83ppm and 1.02ppm [(CH_3), 3H], 1.90ppm [(CH_2), 2H], 2.31ppm [2(CH_3), 6H], 2.61ppm [(CH_2), 2H] and 4.08ppm [(CH_2), 2H]. Lastly, the protons peaks of PMMA are the following: 0.83ppm and 1.02ppm [(CH_3), 3H], 1.84-1.94ppm [(CH_2), 2H] and 3.60ppm [(CH_3), 3H].

The ^{1}H NMR spectrum of the random $PDMAEMA_{30}$-$PMMA_{70}$-photodegradable star copolymer can be seen below (Figure 40).

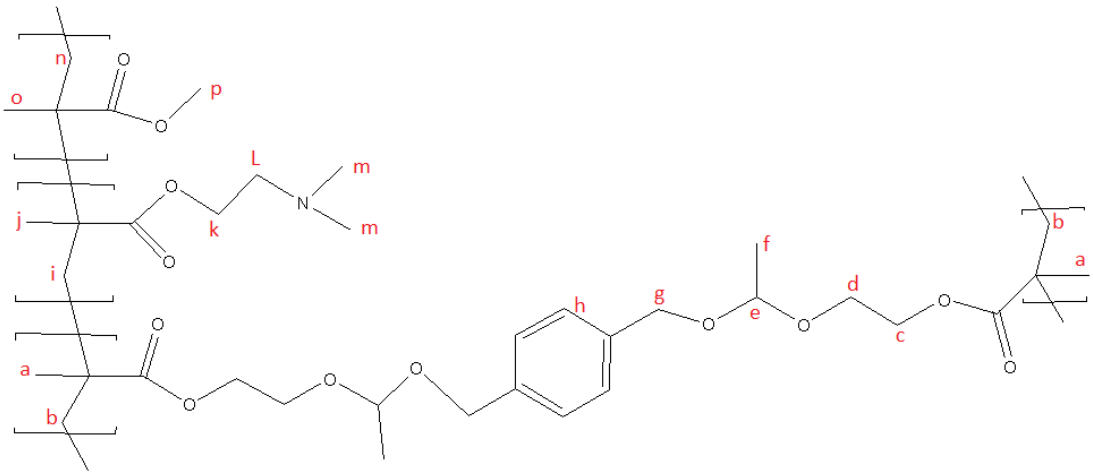

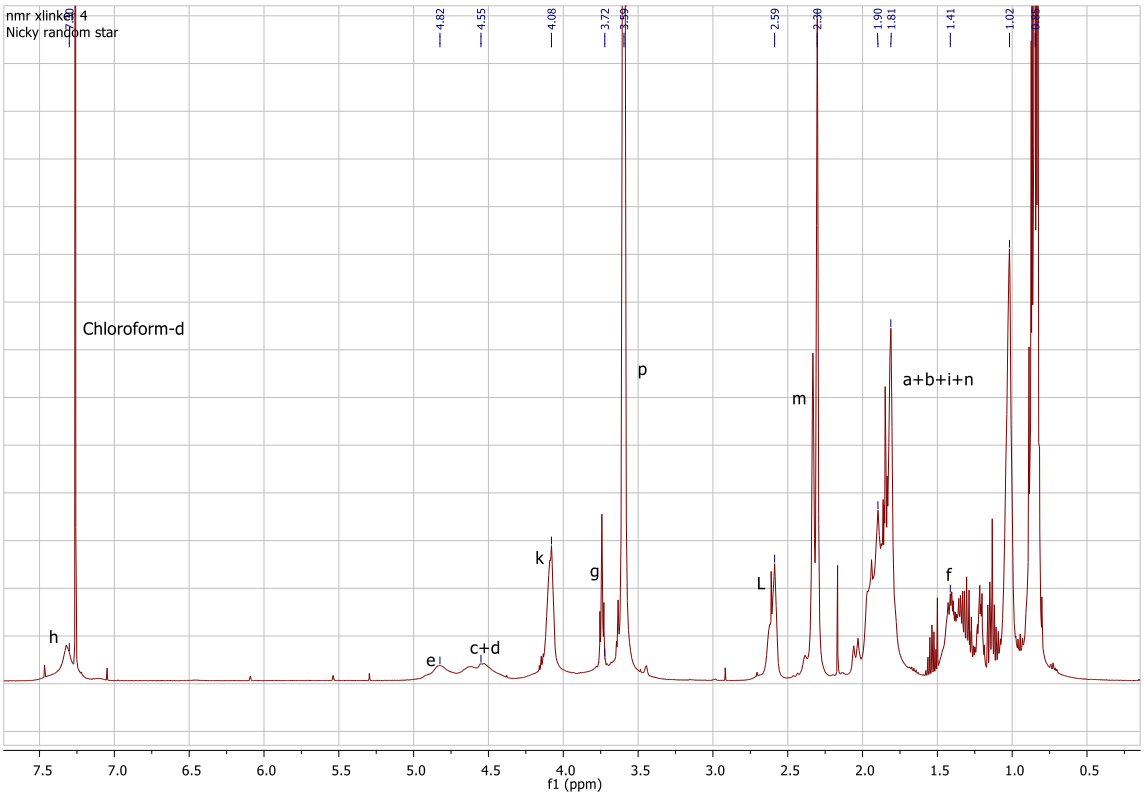

Figure 40 – ^{1}H NMR spectrum and molecular structure of the random acid- and photo-degradable copolymer star

The peak assignment is as follows: 7.32ppm [aromatic protons of the benzyl ring, 4H], 4.82ppm [acetal protons, 2H], 4.55ppm [2(CH_2), 4H], 3.72ppm [2(CH_2), 4H], 1.84ppm [2(CH_3), 6H] and 1.39ppm [2(CH_3), 6H]. The PDMAEMA part of the polymers gives the following peaks: 0.85ppm and 1.02ppm [(CH_3), 3H], 1.90ppm [(CH_2), 2H], 2.30ppm [2(CH_3), 6H], 2.60ppm [(CH_2), 2H] and 4.08ppm [(CH_2), 2H]. The proton peaks of the PMMA are: 0.85ppm and 1.02ppm [(CH_3), 3H], 1.8-1.9ppm [(CH_2), 2H] and 3.59ppm [(CH_3), 3H].

3.3.3 Dynamic light scattering

DLS measurements for the two different star polymers were conducted using a 0.1% wt. solution in THF.

The size distribution of the PDMAEMA$_{30}$-*b*-PMMA$_{70}$-photodegradable star can be seen below (Figure 41).

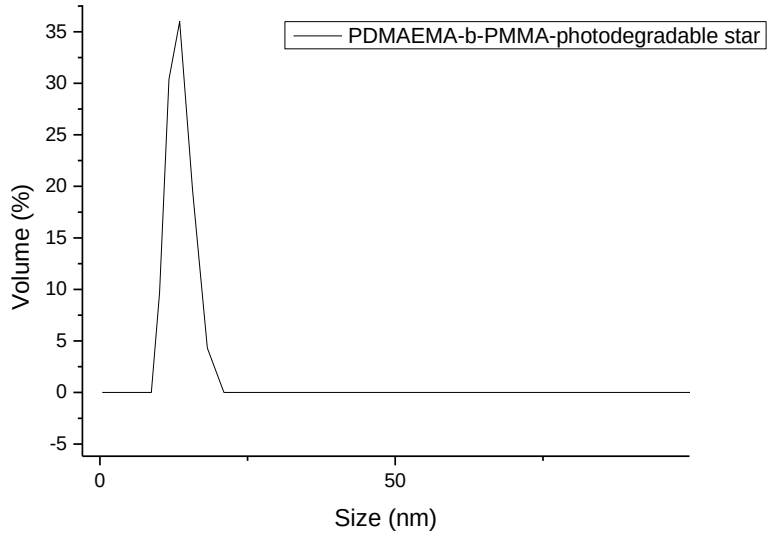

Figure 41 - Hydrodynamic diameter of the acid- and photo-degradable block copolymer star

The size distribution of the random $PDMAEMA_{30}$-$PMMA_{70}$-photodegradable star is as follows:

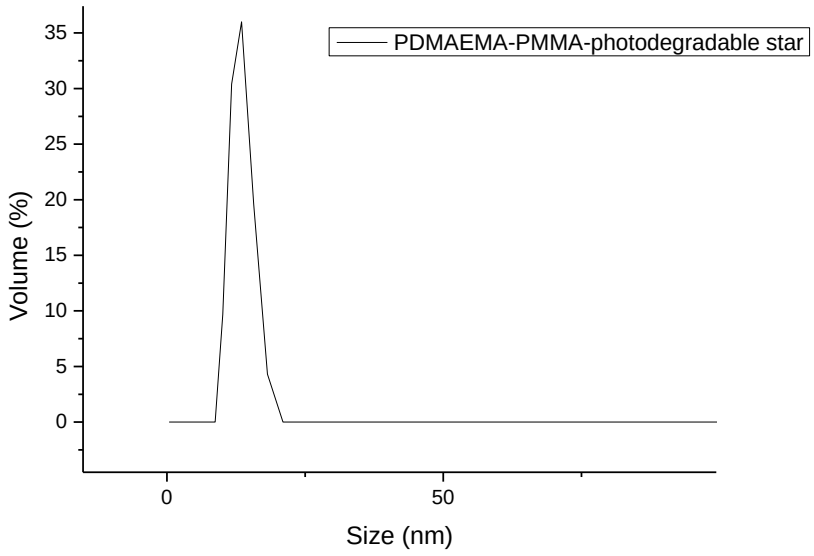

Figure 42- Hydrodynamic diameter of the acid- and photo-degradable random copolymer star

The sizes of the star polymers as measured by DLS can be seen in the following table (Table 5).

Table 5 - Hydrodynamic diameters of the star copolymers synthesized using the acid- and photo-degradable cross-linker

Polymer	Size (nm)
PDMAEMA$_{30}$-*b*-PMMA$_{70}$-photodegradable star	14
PDMAEMA$_{30}$-PMMA$_{70}$-photodegradable star	13

3.3.4 Scanning electron microscopy

The acid- and photo-degradable star polymers were also observed by SEM. The images for the PDMAEMA$_{30}$-*b*-PMMA$_{70}$-photodegradable star are shown below (Figure 43).

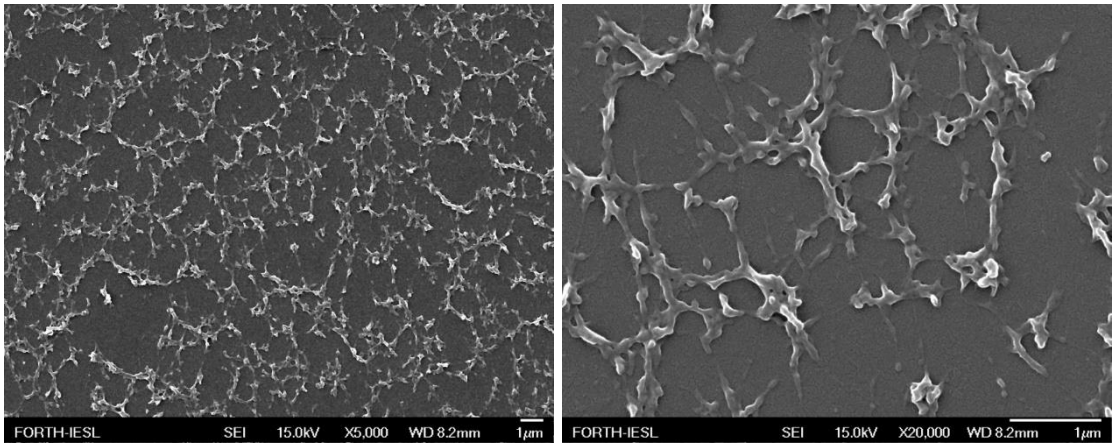

Figure 43 - SEM image of the acid- and photo-degradable block copolymer star

The SEM images acquired for the PDMAEMA$_{30}$-*b*-PMMA$_{70}$-photodegradable star copolymer show aggregated stars on the substrate. While the length of the arms (M_n= 12.000 g/mole measured by SEC) should prevent core-crosslinking, the interaction between the star polymers leads to their assembly upon drying.

The images for the random PDMAEMA$_{30}$-PMMA$_{70}$-photodegradable star copolymer are presented below (Figure 44).

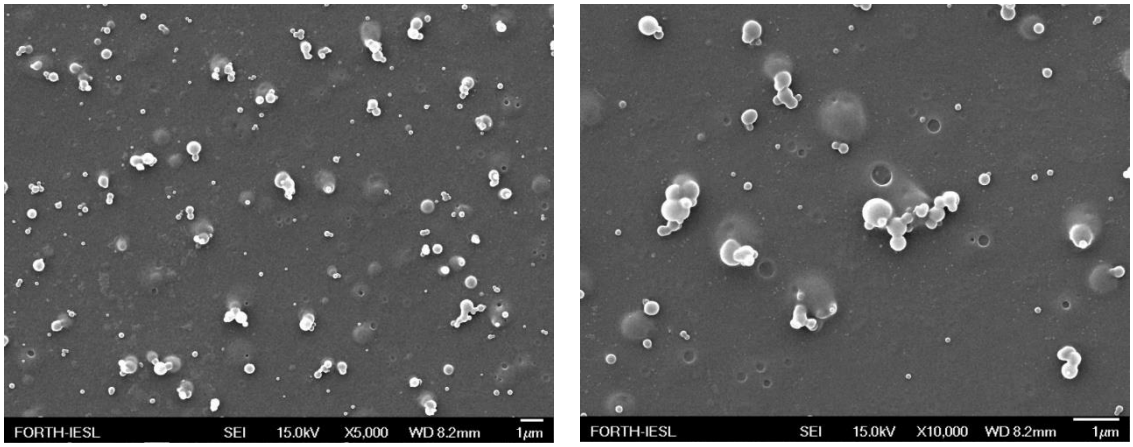

Image 44 - SEM image of the acid- and photo-degradable random copolymer star

While spherical structures were more likely to occur in the instance of the star polymers with block copolymer arms, in this case the random $PDMAEMA_{30}$-$PMMA_{70}$-photodegradable star is organized. Distinct polymer spheres can be seen, as well as a number of aggregated spheres.

3.4 Hydrolysis of the star copolymers containing the acid-degradable cross-linker

The two different cross-linkers and, ultimately, the star polymers synthesized, could degrade under low pH or light irradiation.

First, the two star copolymers containing the acid-degradable cross-linker were hydrolysed in THF in the presence of hydrochloric acid, at room temperature.

The target of this study is to quantitatively prove that the polymers can undergo degradation and not to study in detail the kinetics of the degradation process. A 10-fold molar excess of hydrochloric acid with respect to the amount of cross-linker present in the sample was added in the solution [4]. After 2 h a sample was withdrawn and analyzed by SEC. Next, the samples were dried in a vacuum oven their analysis by ^1H NMR in $CDCl_3$ and the spectra were compared to those prior to hydrolysis. The hydrolyzed samples were also analyzed by SEM.

3.4.1 Size exclusion chromatography

The SEC chromatograms of the PDMAEMA$_{30}$-*b*-PMMA$_{70}$-star copolymer before and after hydrolysis are shown below (Figure 45).

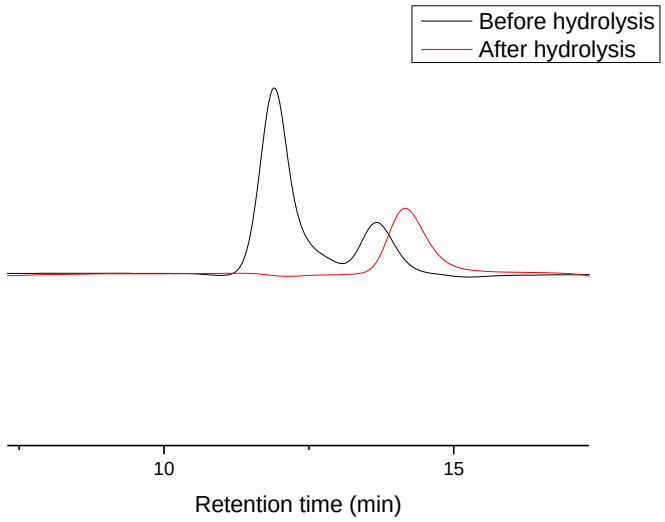

Figure 45 - SEC chromatograms of the acid-degradable block copolymer star before and after hydrolysis

From the above chromatograms the complete degradation of the star copolymer is confirmed.

A similar process was followed for the degradation of the random PDMAEMA$_{30}$-PMMA$_{70}$-star and the SEC chromatograms of the precursor and the degraded sample are presented below (Figure 46).

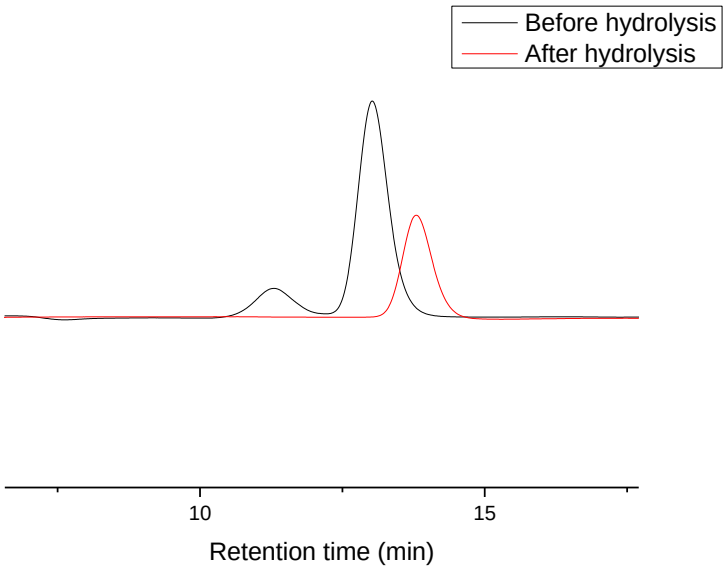

Figure 46 - SEC chromatograms of the acid-degradable copolymer star before and after hydrolysis

The slight difference observed between the peaks of the remaining arms in the chromatograph of the star before hydrolysis and the peak of the linear chains after hydrolysis for both polymers, is attributed to a change of the solubility of the arms after the degradation of the polymers.

The hydrolysis mechanism for the two polymers is similar despite the difference in the polymer type of the linear precursors. The hydrolysis reaction is depicted below.

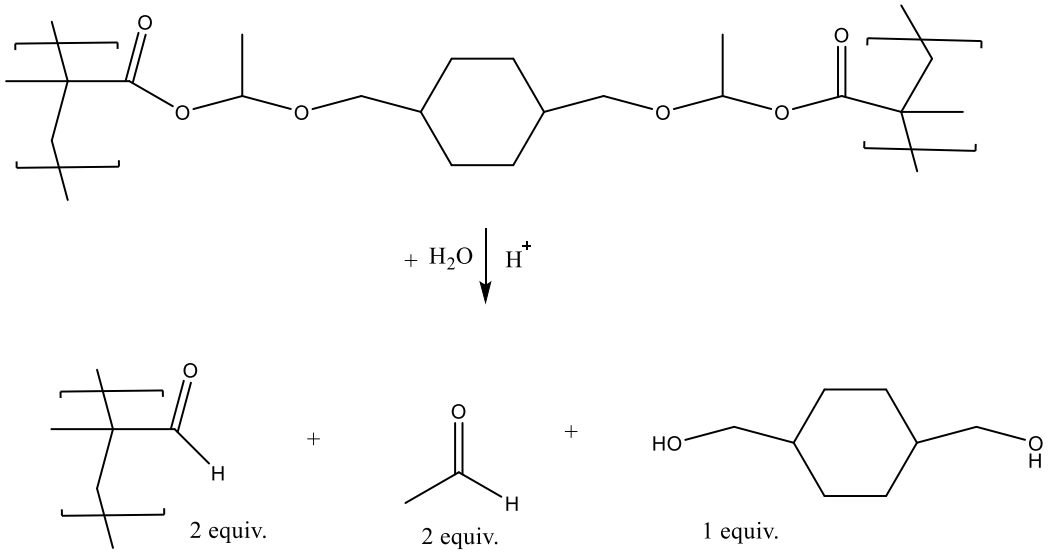

Figure 47 - Acid hydrolysis of the acid-degradable cross-linker [6,7]

The table below (Table 6) shows the molecular weight values for the polymers before degradation and their hydrolysis products as determined by SEC.

Table 6 – Number, and Weight average molecular weights and peak molecular weight of the star polymers before and after hydrolysis

Polymers	**Before hydrolysis**				**After hydrolysis**			
	M_w	**M_n**	**M_p**	**M_w/M_n**	**M_w**	**M_n**	**M_p**	**M_w/M_n**
PDMAEMA$_{30}$-*b*-PMMA$_{70}$-star	78000	72000	79000	1.07	12000	11500	12700	1.07
PDMAEMA$_{30}$-PMMA$_{70}$-star	130000	125000	142000	1.04	18000	17000	18000	1.04

3.4.2 ^{1}H – Nuclear magnetic resonance spectroscopy

The degradation of the polymers was also verified via ^{1}H NMR spectroscopy.

The NMR spectrum of the hydrolyzed PDMAEMA$_{30}$-*b*-PMMA$_{70}$-star can be seen below (Figure 48).

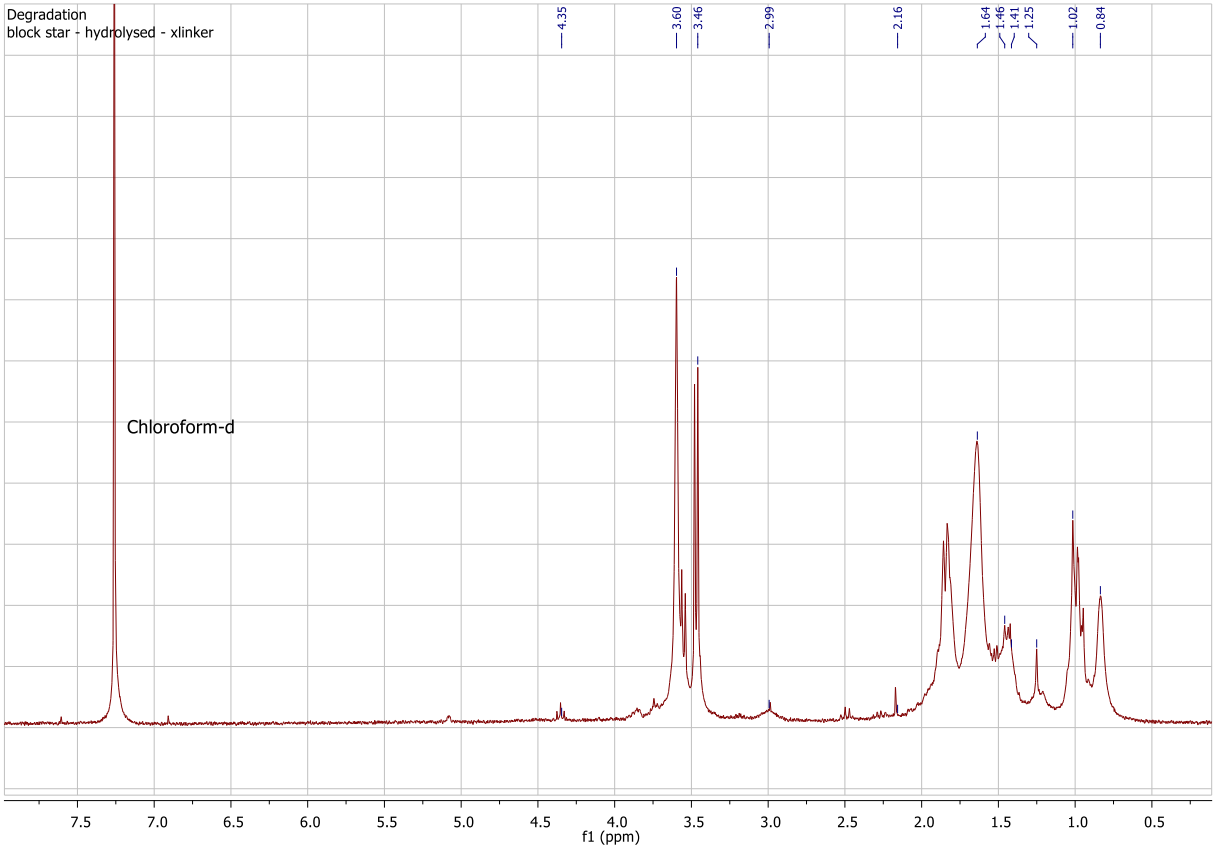

Figure 48 – ^{1}H NMR spectrum of the acid-degradable block copolymer star after hydrolysis

Peak assignment is as follows: 4.34ppm [2(OH), 2H], 3.45ppm [2(CH_2), 2H], 2.16ppm [(CH_3), 3H], 1.64ppm [axial protons of cyclohexane, 4H], 1.41ppm [equatorial protons of cyclohexane, 4H], 1.46ppm 1.45ppm [2(CH), 2H] and at 1.02ppm and 0.84ppm [(CH_3), 3H]. The lack of an acetal proton peak at 5.82 ppm verifies the degradation of the star copolymer. Upon degradation of the cross-linker, one 1,4-cyclohexanedimethanol molecule, two acetaldehyde molecules are produced. Since the ends of the cross-linker are still attached to their respective arms though, no free methacrylic acid is produced in the solution, instead arms with a carboxylic acid end-group are obtained.

The spectrum for the random PDMAEMA$_{30}$-PMMA$_{70}$-star copolymer after degradation, is shown below (Figure 49).

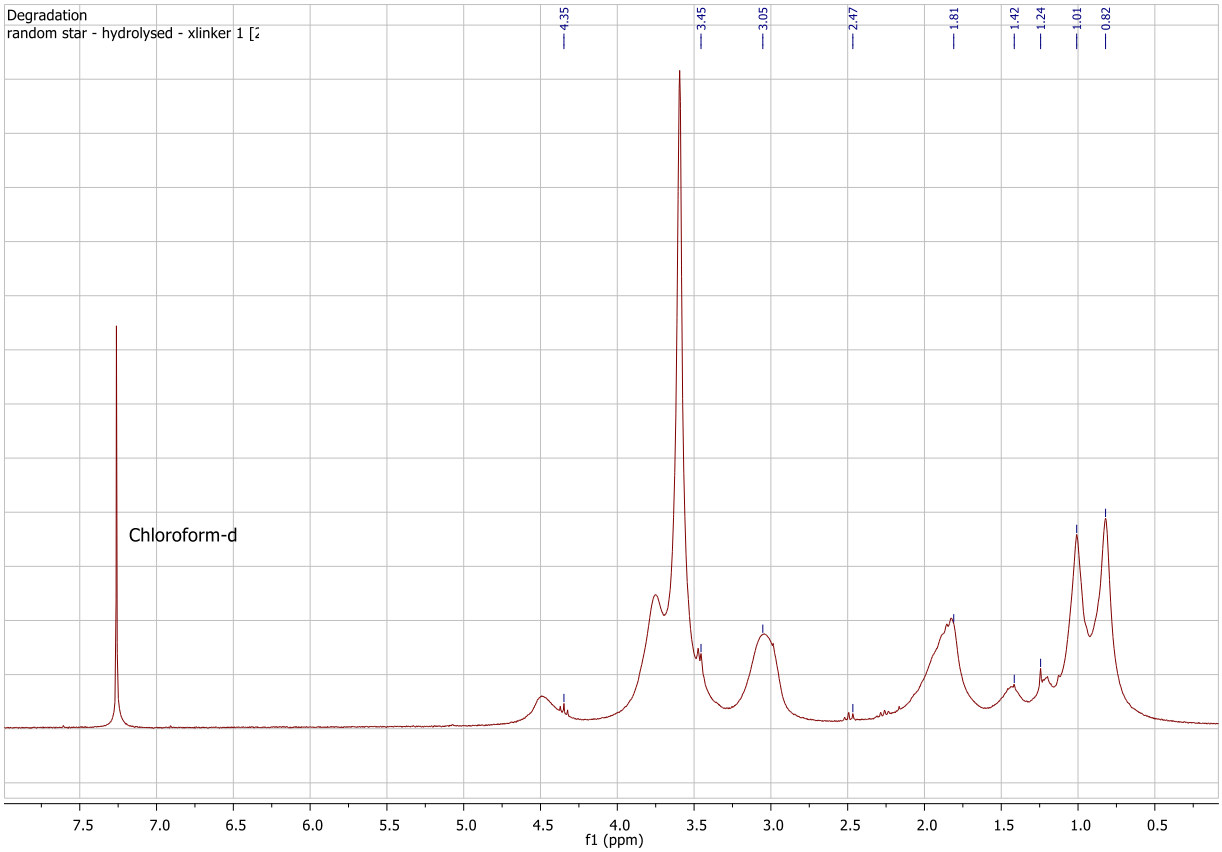

Figure 49 – ^{1}H NMR spectrum of the acid-degradable random copolymer star after hydrolysis

Peak assignment is as follows: 4.35ppm [2(OH), 2H], 3.45ppm [(CH_2), 2H], 2.47ppm [(CH_3), 3H], 1.81ppm [axial protons of cyclohexane, 4H], 1.42ppm [equatorial protons of cyclohexane, 4H], 1.24ppm [(CH_2), 2H], and at 1.01ppm and 0.82ppm [(CH_3), 3H]. Once more, the lack of a proton peak at the expected chemical shift for the acetal proton, is an indication that the cross-linker, and therefore the star polymer, is degraded.

3.4.3 Scanning electron microscopy

The SEM image for the hydrolyzed PDMAEMA$_{30}$-*b*-PMMA$_{70}$-star copolymer is shown below (Figure 50).

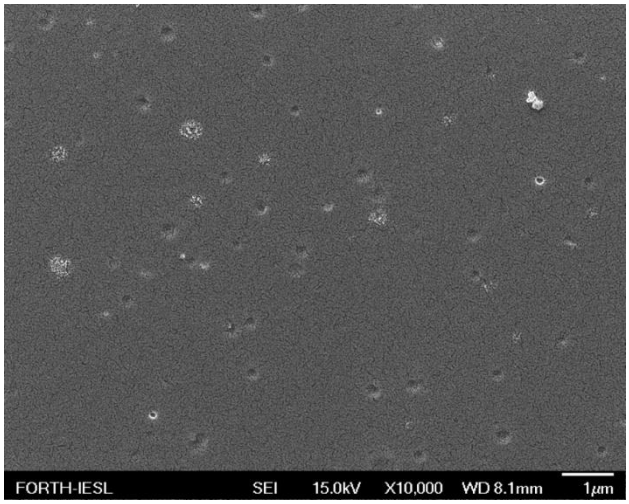

Figure 50 - SEM image of the acid-degradable block copolymer star after hydrolysis

By comparing the images of the precursor PDMAEMA$_{30}$-*b*-PMMA$_{70}$-star to those of the hydrolyzed star, distinct differences are observed. No polymeric structures can be seen, either in the form of spherical particles or as particulate aggregates observed above for the star polymers before degradation. Instead, a polymer film is observed suggesting the degradation of the star polymer to its constituent chains.

A SEM image of the hydrolyzed random PDMAEMA$_{30}$-PMMA$_{70}$-star is presented below (Figure 51). As expected, no distinct polymeric structures can be seen. The solution of the hydrolyzed polymer formed a film after the evaporation of the solvent and the roughness observed on the surface of the film is attributed to the layer of gold that was sputtered on the polymeric film.

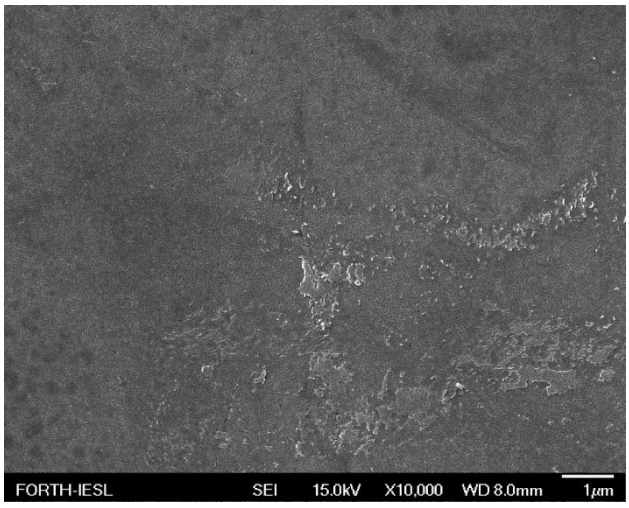

Figure 51 - SEM image of the acid-degradable random copolymer star after hydrolysis

3.5 Hydrolysis of the star polymers with the acid- and photo-degradable cross-linker

The two star polymers synthesized using the acid- and photo-degradable cross-linker were successfully hydrolyzed in THF in the presence of hydrochloric acid, at room temperature. The protocol used for their degradation was similar to that employed for the degradation of the star polymers synthesized with the acid-degradable cross-linker.

3.5.1 Size exclusion chromatography

The chromatogram of the PDMAEMA$_{30}$-*b*-PMMA$_{70}$-photodegradable star is shown below (Figure 52). By comparing the chromatograms of the star copolymer before and after hydrolysis, the complete degradation of the star polymer to its constituent chains is verified.

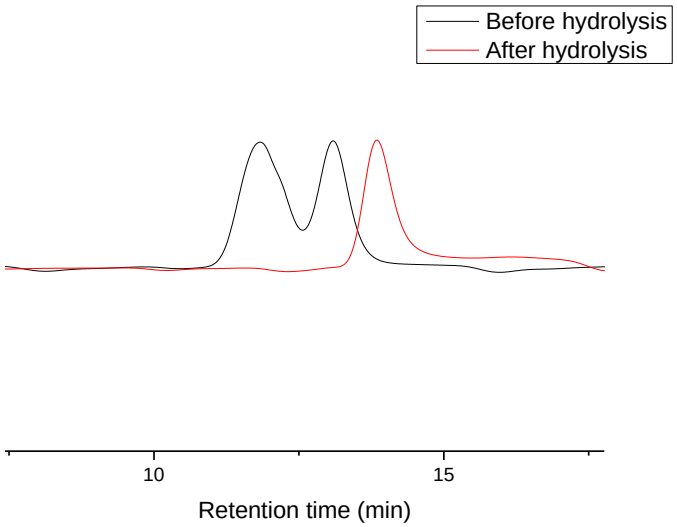

Figure 52 - SEC chromatograms of the acid- and photo-degradable block copolymer star before and after hydrolysis

A similar process was followed for the degradation of the random PDMAEMA$_{30}$-PMMA$_{70}$-photodegradable star and the SEC results are shown below (Figure 53). Again, complete hydrolysis of the star copolymer is confirmed by SEC.

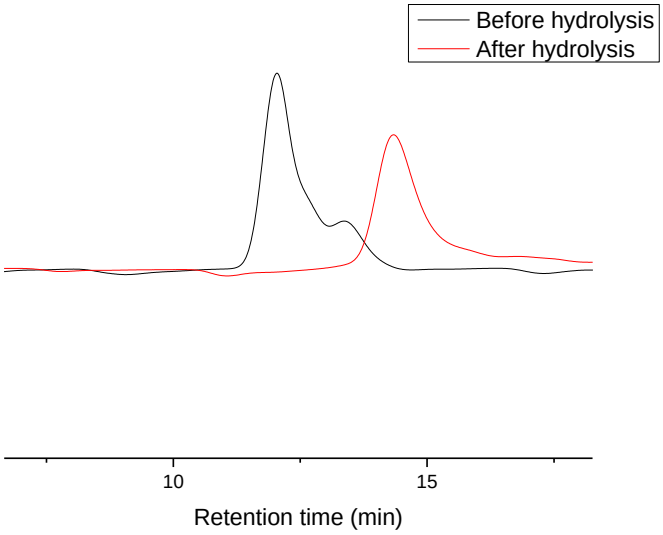

Figure 53 - SEC chromatograms of the acid- and photo-degradable random copolymer star before and after hydrolysis

The shift noted for the peak that corresponds to the arms of the star to higher elution times is attributed to the change in the solubility of the polymer after the hydrolysis, which changes the polymer conformation in the solution and thus, its hydrodynamic volume.

The hydrolysis mechanism for the two star polymers is similar to that shown above for the acid hydrolyzable cross-linker and is shown below:

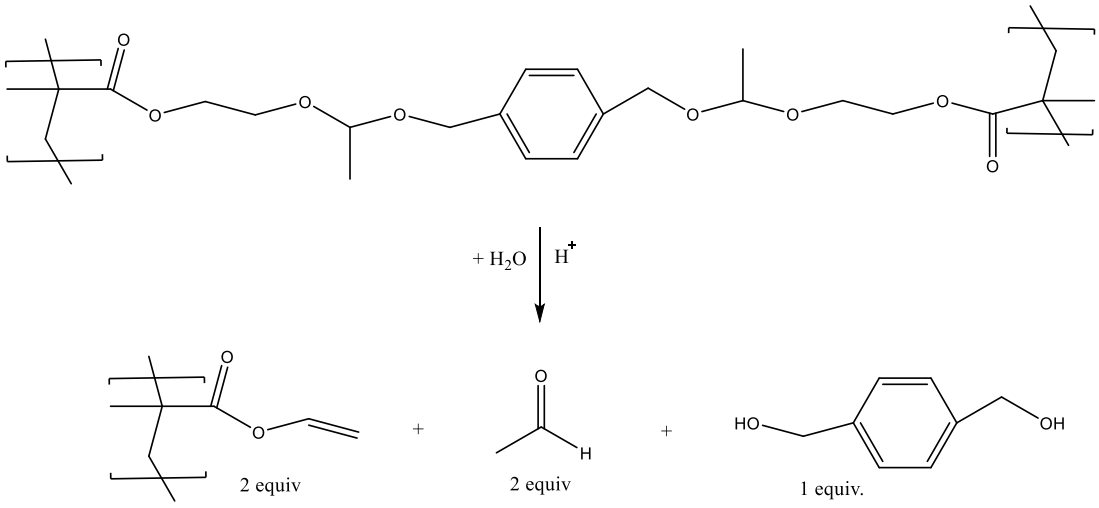

Figure 54 - Acid hydrolysis of the acid- and photo-degradable crosslinker [6,7]

In the following table (Table 7) the molecular weights along with the polydispersity indices for the two stars before degradation and their hydrolysis products after degradation are presented.

Table 7 – Number and Weight average molecular weights, and peak molecular weight of the star polymers before and after hydrolysis

Polymers	**Before hydrolysis**				**After hydrolysis**			
	M_w	**M_n**	**M_p**	**M_w/M_n**	**M_w**	**M_n**	**M_p**	**M_w/M_n**
PDMAEMA$_{30}$-*b*-PMMA$_{70}$-photodegradable star	90000	83000	85000	1.07	23000	22000	24000	1.05
PDMAEMA$_{30}$-PMMA$_{70}$-photodegradable star	68000	62000	70000	1.08	16000	14000	16000	1.12

3.5.2 ^{1}H Nuclear magnetic resonance spectroscopy

The hydrolysis of the star polymers was also verified via ^{1}H NMR spectroscopy. The spectrum of the hydrolyzed PDMAEMA$_{30}$-*b*-PMMA$_{70}$-photodegradable star is shown below (Figure 55).

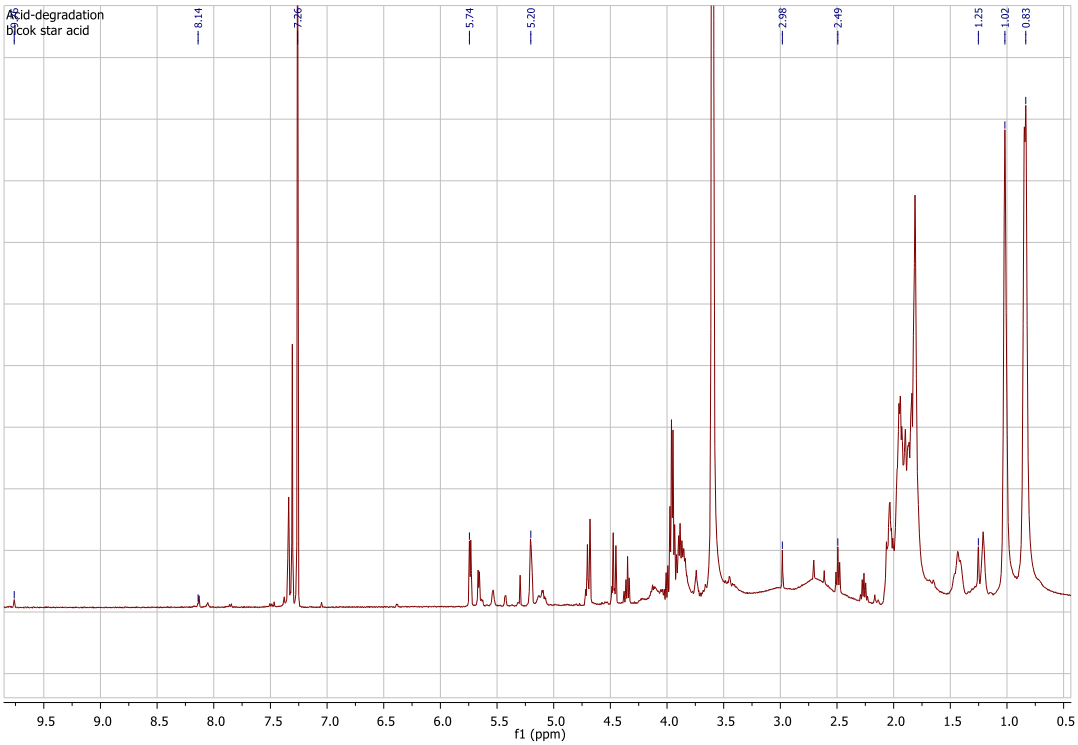

Figure 55 – ^{1}H NMR spectrum of the acid- and photo-degradable block copolymer star after hydrolysis

The peak assignment is as follows: 9.76ppm [2(CHO), 2H], at 8.13ppm [aromatic protons of 1,4-benzedimethanol, 4H], at 5.74ppm and 5.20ppm [(CH) and (CH_2) respectively of the double bond in vinyl methacrylate, 2H and 1H], 2.98ppm [benzyl protons of 1,4-benzenedimethanol, 2(CH_2), 2H], 2.6ppm [(C-OH), 2H] 1.21ppm [acetaldehyde's (CH_3) group, 3H], and last the methyl group of the methacrylate backbone appears at 1.02ppm and 0.83ppm [(CH_3), 3H]. The absence of the acetal proton of the cross-linker at 4.82ppm is noticeable and leads to the conclusion that the cross-linker has successfully degraded. Additionally, a few new proton peaks appear in the spectrum attributed to the degradation products of the cross-linker, while the peaks attributed to PDMAEMA have disappeared. That can be attributed to the fact that PDMAEMA, having a pK_a value of approximately 7.5 [5], gets protonated before hydrolysis occurs, and given the fact that protonated PDMAEMA is not soluble in chloroform, the peaks that would normally correspond to its protons, are not visible in the spectrum.

In the case of the random $PDMAEMA_{30}$-$PMMA_{70}$-photodegradable star, the ^1H NMR spectrum after hydrolysis, is shown below (Figure 56).

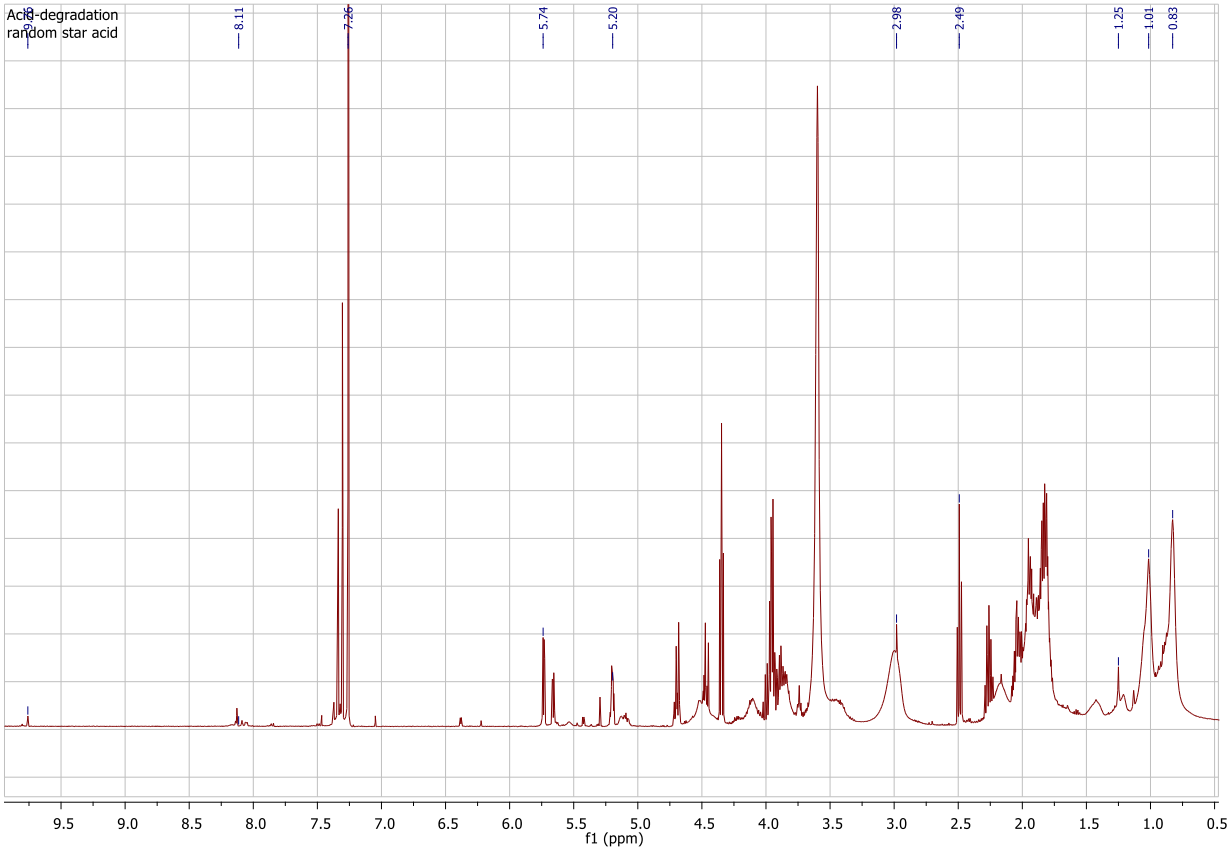

Figure 56 – ^1H NMR spectrum of the acid- and photo=degradable random copolymer star after hydrolysis

The peak assignment is as follows: 9.76ppm [2(CHO), 2H], 8.12ppm [aromatic protons of 1,4-benzedimethanol, 4H], 5.74ppm and 5.21ppm [(CH) and (CH_2) respectively, 1H and 2H], 2.98ppm [2(CH_2), 4H], 2.47ppm [(C-OH), 2H], 1.25ppm [(CH_3), 3H], and 1.02ppm and 0.83ppm the methyl group of the vinyl methacrylate backbone [(CH_3), 3H].

The degradation products for the random copolymer star are similar to those for the PDMAEMA$_{30}$-*b*-PMMA$_{70}$-photodegradable star. The proton peaks attributed to PDMAEMA are again absent due to its protonation. The lack of the acetal bond peak at 4.85ppm signifies again the breakage of the acetal bond and indicates the degradation of the star.

3.5.3 Dynamic light scattering

The hydrolyzed star polymers were also measured by DLS in order to determine the mean diameter of the degradation polymers.

For the PDMAEMA$_{30}$-*b*-PMMA$_{70}$-photodegradable star the size distribution in solution is depicted in the graph below (Figure 57).

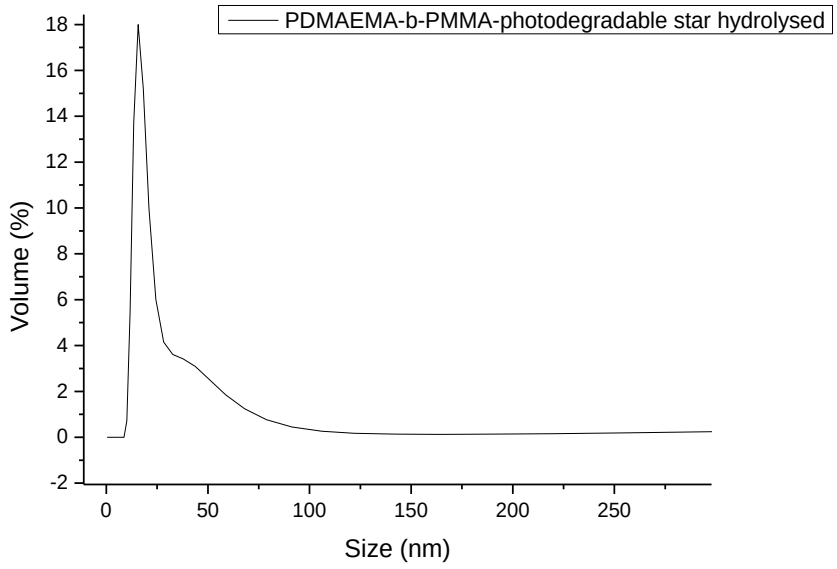

Figure 57 – Size distribution of the acid- and photo-degradable block copolymer star after hydrolysis

A solution of the random PDMAEMA$_{30}$-PMMA$_{70}$-photodegradable star at the same concentration after hydrolysis was also measured. The size distribution of the hydrolyzed polymer is shown below (Figure 58).

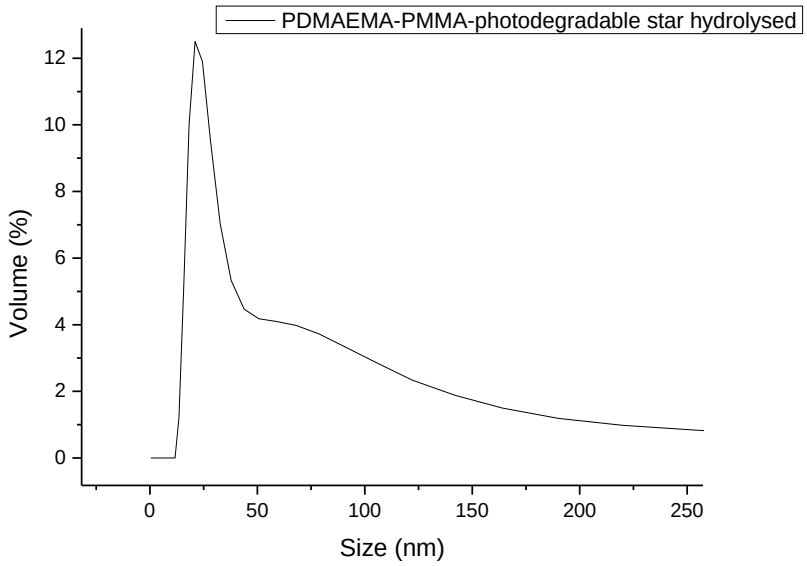

Figure 58 – Size distribution of the acid- and photo-degradable random copolymer star after hydrolysis

The mean hydrodynamic size for the two degraded polymers as measured by DLS, is presented in the table below (Table 8).

Table 8 – Hydrodynamic diameter for the hydrolyzed acid- and photo-degradable stars

Polymer	**Size (nm)**
PDMAEMA$_{30}$-*b*-PMMA$_{70}$-photodegradable star	15
PDMAEMA$_{30}$-PMMA$_{70}$-photodegradable star	20

The difference in the values of the mean diameter of the particles in the solution of the hydrolyzed PDMAEMA$_{30}$-*b*-PMMA$_{70}$-photodegradable star and the precursor star before hydrolysis is very small, but the difference in the distribution is quite prominent as the peak that depicts the approximate size of the hydrolyzed stars broadens significantly.

In the case of the random PDMAEMA$_{30}$-PMMA$_{70}$-photodegradable star though, the difference in the approximate size of the polymer before and after hydrolysis is quite significant, since the mean size increases from 13nm to 20nm that could indicate the formation of aggregates in the solution. This change is once again accompanied by a broadening of the distribution peak, which indicates an increase in the particle size and therefore polymer aggregation.

3.5.4 Scanning electron microscopy

Samples of the star polymers after hydrolysis were also prepared and observed by SEM.

For the PDMAEMA$_{30}$-*b*-PMMA$_{70}$-photodegradable star, the image is shown below (Figure 59).

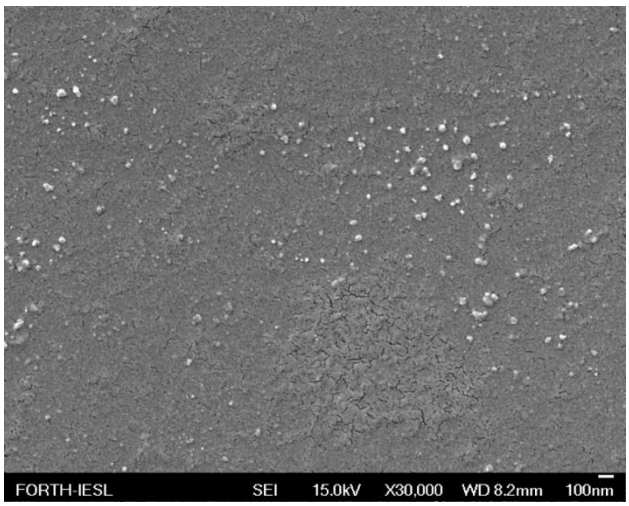

Figure 59 - SEM image of the acid- and photo-degradable block copolymer star after hydrolysis

When comparing the images of the star copolymer before and after hydrolysis, the difference is notable. Even though the difference in size is almost negligible (14 nm prior to hydrolysis and 15 nm after hydrolysis), in the case of the hydrolyzed polymer, aggregates are observed, but they do not resemble the polymer structures prior to hydrolysis.

In the case of the random PDMAEMA$_{30}$-PMMA$_{70}$-photodegradable star, the SEM after hydrolysis is shown below (Figure 60).

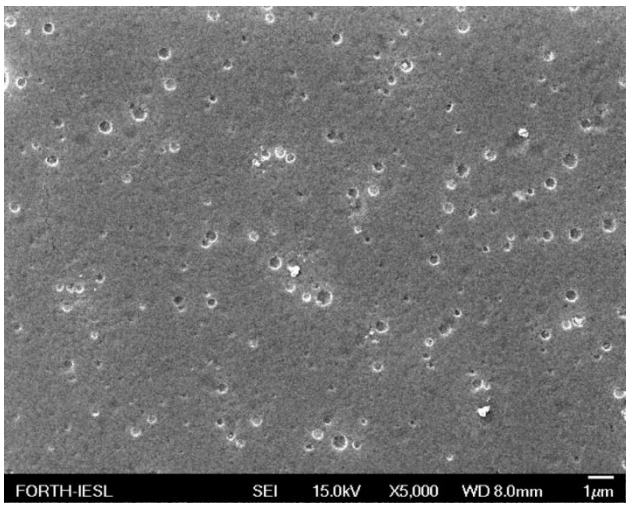

Figure 60 - SEM image of the acid- and photo-degradable random copolymer star after hydrolysis

Again, no distinct polymer structures in the form of spherical particles are observed that would resemble the polymer prior to hydrolysis. Instead, a polymer film is formed after complete evaporation of the solvent, suggesting the degradation of the star copolymer to its constituent chains, as well as a number of aggregates. The imperfections that can be observed on the surface of the sample, are attributed to the gold that was sputtered on the sample prior to its imaging and not on the products of hydrolysis.

3.6 Photo-degradation of the star copolymers containing the acid- and photo-degradable cross-linker

The star polymers synthesized in this work were tailored to degrade under the influence of certain external stimuli. It was proven above that all the synthesized stars, regardless of the cross-linker used for their synthesis, were successfully hydrolyzed in the presence of hydrochloric acid. The stars synthesized with the use of the aromatic cross-linker though, can also be degraded under irradiation with UV light as the aromatic ring, absorbs the light and transfers the energy to the neighboring acetal bond. Next, the photodegradation of the star copolymers was explored.

3.6.1 Size exclusion chromatography

The photo-degradation of the star polymers was monitored by SEC. For the PDMAEMA$_{30}$-*b*-PMMA$_{70}$-photodegradable star, after 12h of irradiation, the polymer was deemed completely degraded. The collective SEC results of the irradiated samples are presented below (Figure 61).

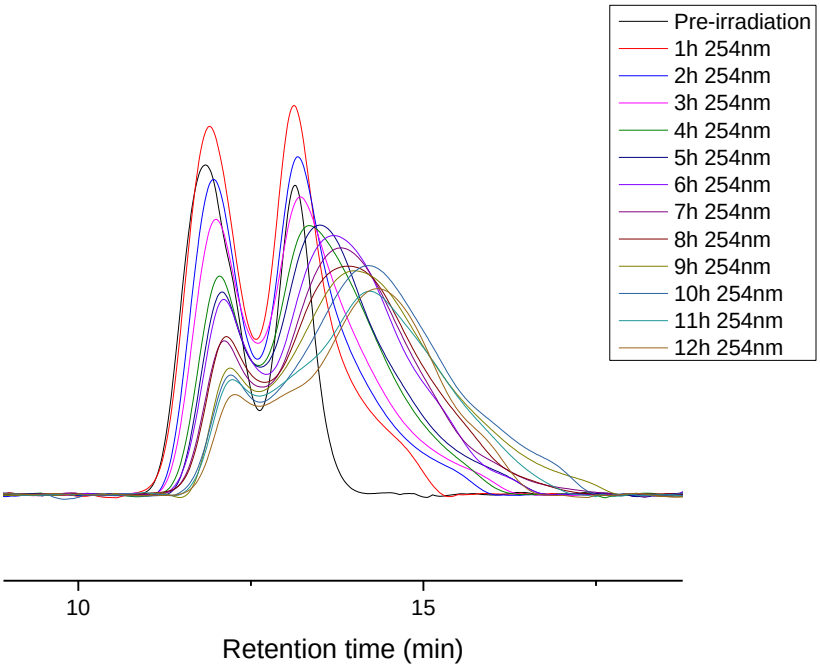

Figure 61 - SEC chromatograms of the UV irradiated acid- and photo-degradable block copolymer star as a function of irradiation time

A gradual decrease of the peak attributed to the star copolymer is observed, suggesting the destruction of the stars upon irradiation. At the same time, the peak of the degraded polymer seems to broaden and shift to higher elution times. Since it is not expected that the arms degrade under these conditions, the broadening of the peak and its shift is attributed to a change in the solubility of the polymer, and therefore to conformational changes, which alter its hydrodynamic size and elution time.

In the case of the random PDMAEMA$_{30}$-PMMA$_{70}$-photodegradable star, the degradation process was again monitored for 12h, at which point the SEC results verified that the star polymer was degraded. The SEC chromatographs of the degradation process are depicted below (Figure 62).

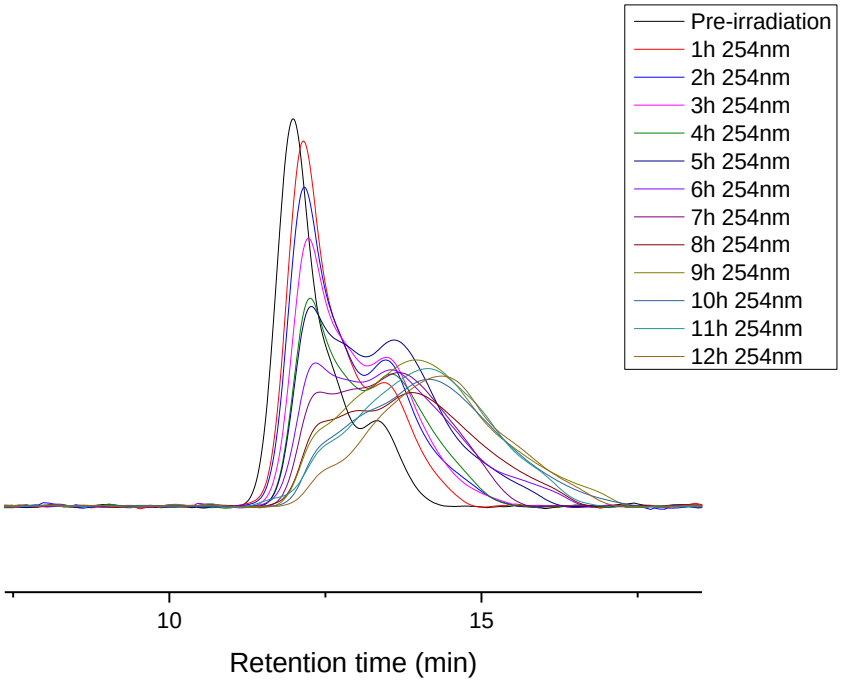

Figure 62 - SEC chromatographs of the acid- and photo-degradable random copolymer star upon UV irradiation

The gradual decrease of the star peak is noted, along with the increase of the intensity of the arms peak. As discussed above, as the degradation process proceeds, the solubility of the polymer and the chain conformation in the solution change, a fact that is reflected via the broadening of the SEC peak.

Summarizing, the star polymers prepared using the acid- and photo-degradable cross-linker can be degraded upon irradiation. The proposed mechanism of the photodegradation process is the following (Figure 63).

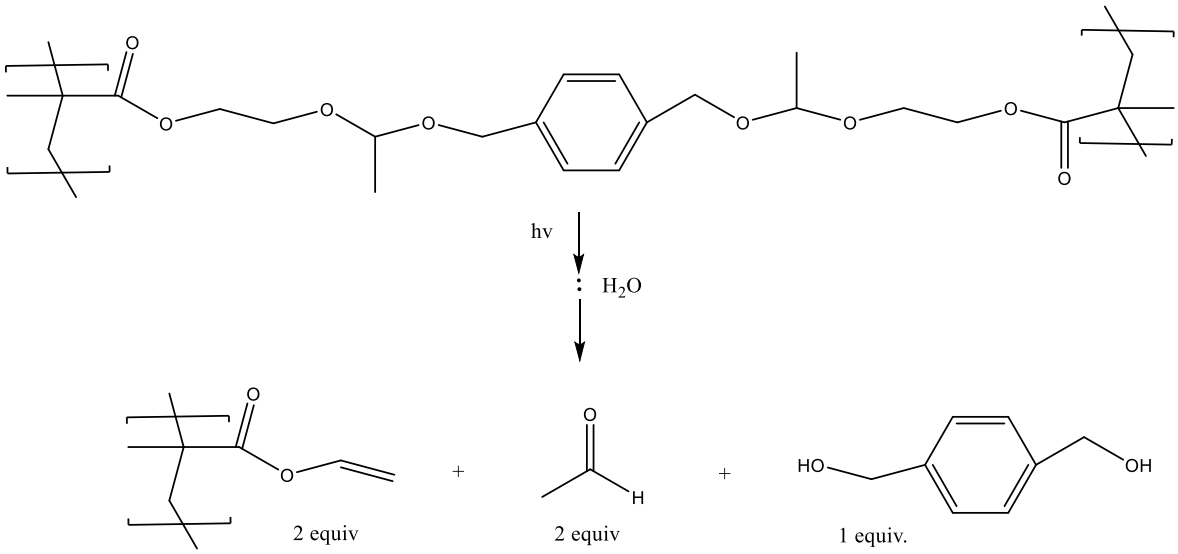

Figure 63 - Photo-degradation reaction of the acetal-based cross-linker [6,7,8,9]

3.6.2 ^{1}H – Nuclear magnetic resonance spectroscopy

The photodegradation process of the star polymers was also monitored by ^{1}H NMR spectroscopy. A 20 mg polymer sample was dissolved in 1ml of $CDCl_3$ and placed in the appropriate NMR tube. The spectrum was recorded, and then the tube was placed under UV irradiation. An NMR measurement was carried out every hour until there were no discernible changes in the proton peaks, in agreement with the SEC results discussed above. Twelve measurements were made in total for 12h irradiation time. Indicatively, four of the spectra received during the photodegradation process of the $PDMAEMA_{30}$-*b*-$PMMA_{70}$-photodegradable star copolymer (3h, 6h, 9h, 12h) are presented below (Figures 64 - 67).

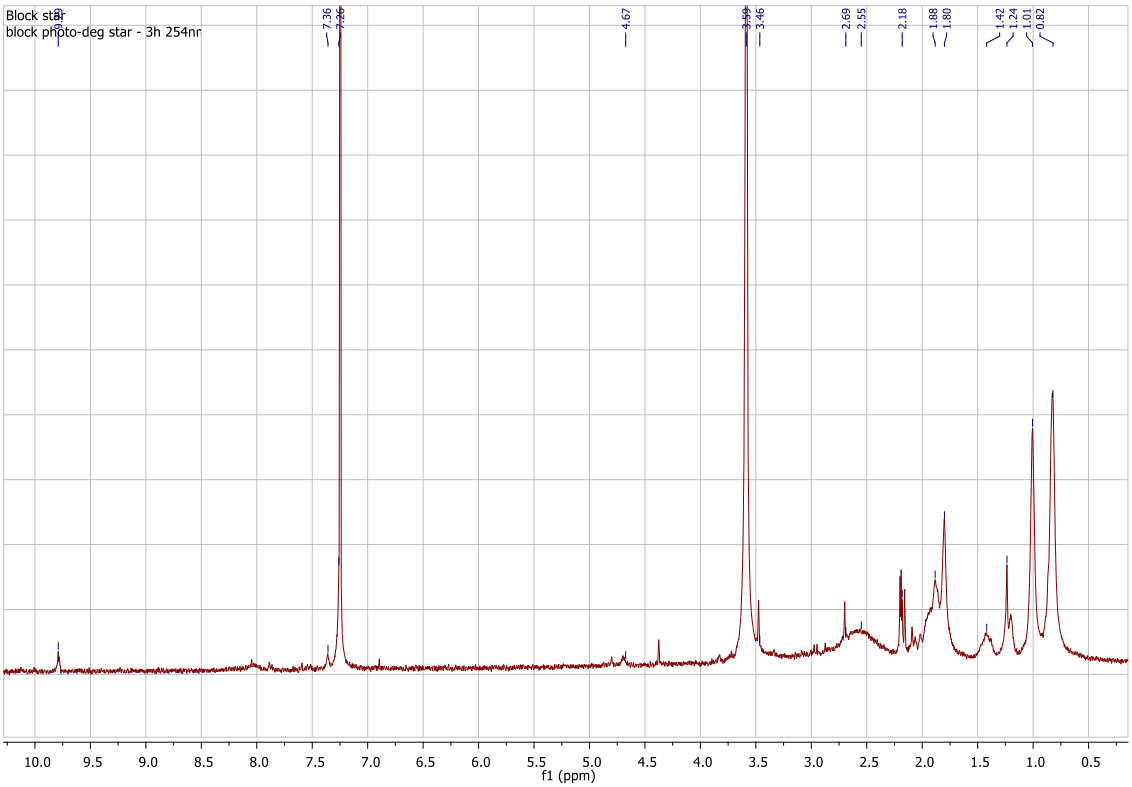

Figure 64 – ^{1}H NMR spectrum of the acid- and photo-degradable block copolymer star after 3h UV irradiation

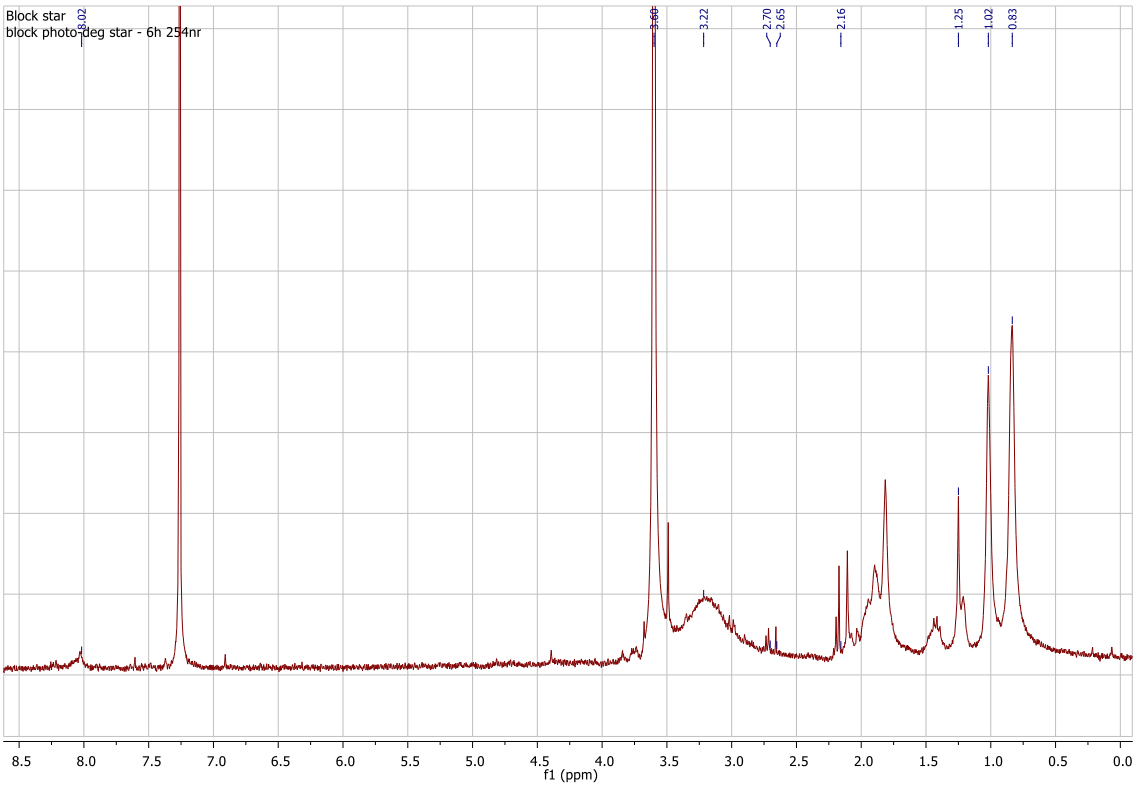

Figure 65 – ^{1}H NMR spectrum of the acid- and photo-degradable block copolymer star after 6h UV irradiation

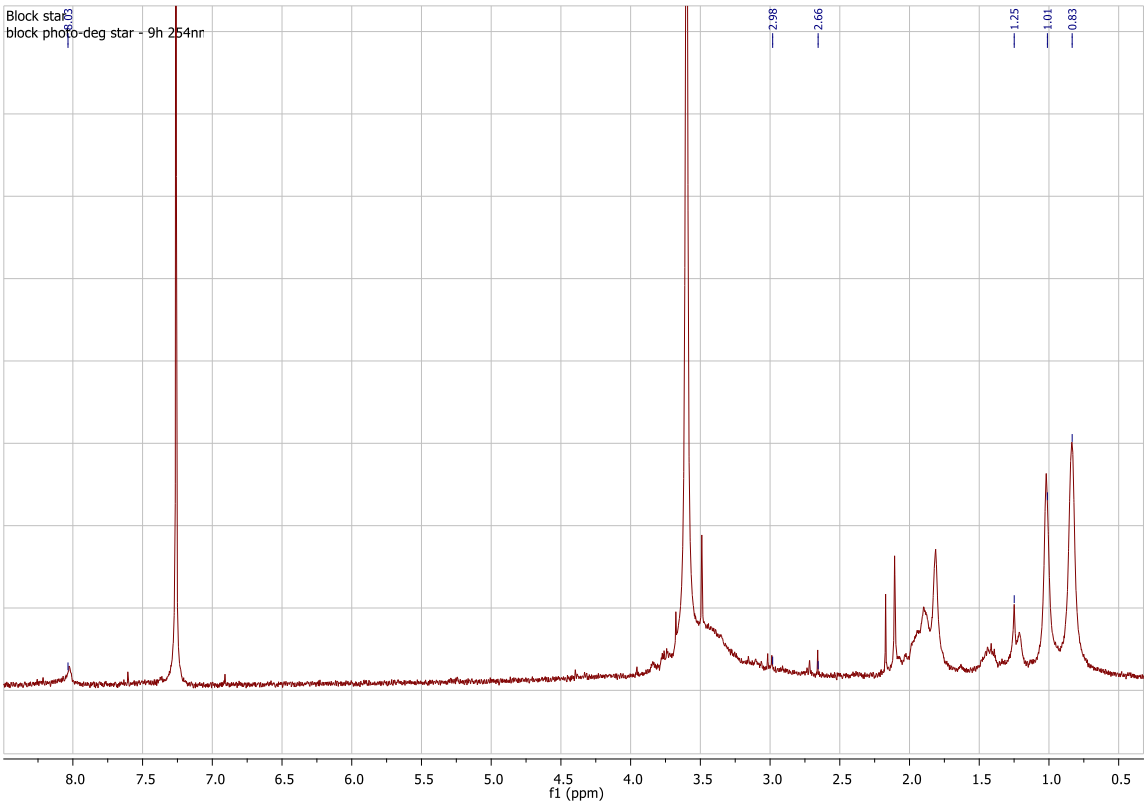

Figure 66 – ^{1}H NMR spectrum of the acid- and photo-degradable block copolymer star after 9h UV irradiation

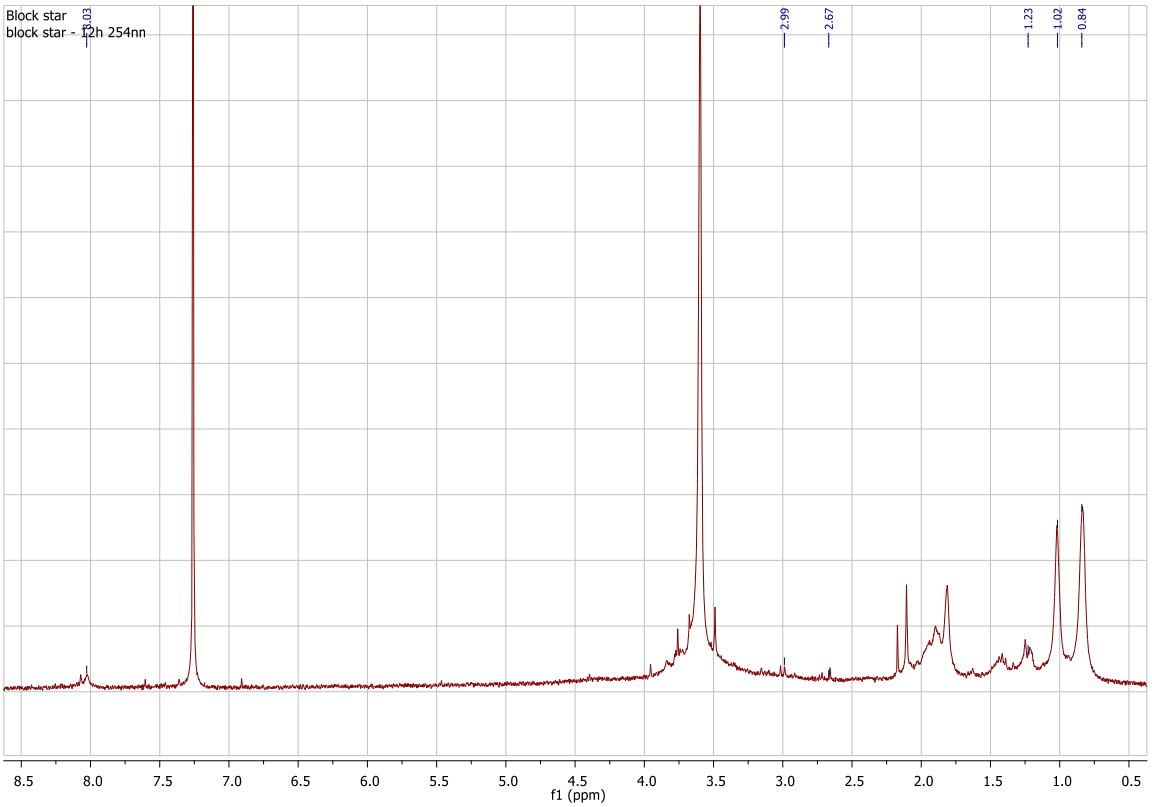

Figure 67 – ^{1}H NMR spectrum of the acid- and photo-degradable block copolymer star after 12h UV irradiation

The peak assignment is as follows: 9.76ppm [(CHO), H], 8.12ppm [aromatic protons of 1,4-benzenedimethanol, 4H], 4.67ppm [(CH) and (CH_2), 1H and 2H respectively], 2.98ppm [(CH_2), 2H], 2.47ppm [2(OH), 2H], 1.25ppm [(CH_3), 3H], and lastly 1.02ppm and 0.83ppm [(CH_3), 3H]. By analyzing the above spectra, the absence of the acetal proton peak at 4.84ppm indicates the degradation of the cross-linker, and thus the degradation of the polymer. Upon prolonged irradiation, the peaks of the degradation products that do not overlap with the peaks of the polymers, appear to be more distinct, as the cross-linker continues to degrade.

It is worth noting that the peaks corresponding to the DMAEMA repeat units are completely absent from the spectrum. A side experiment was then conducted to further explore this phenomenon, since PDMAEMA should not photo-degrade and thus, should not change upon irradiation. PDMAEMA was dissolved in both $CDCl_3$ and D_2O and its NMR spectra were recorded before and after irradiation with UV light. The spectra recorded for the PDMAEMA before (Figures 68, 70) and after irradiation (Figures 69, 71) in both solvents, are shown below.

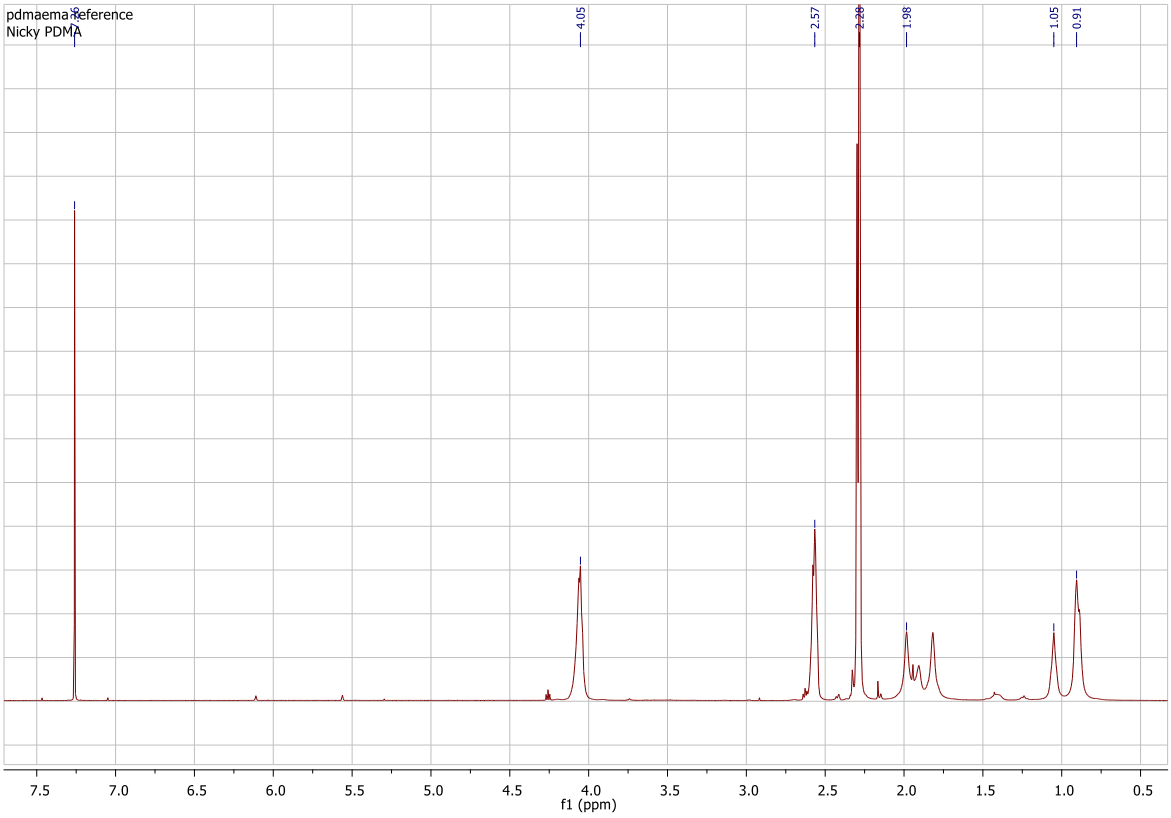

Figure 68 - PDMAEMA in deuterated chloroform

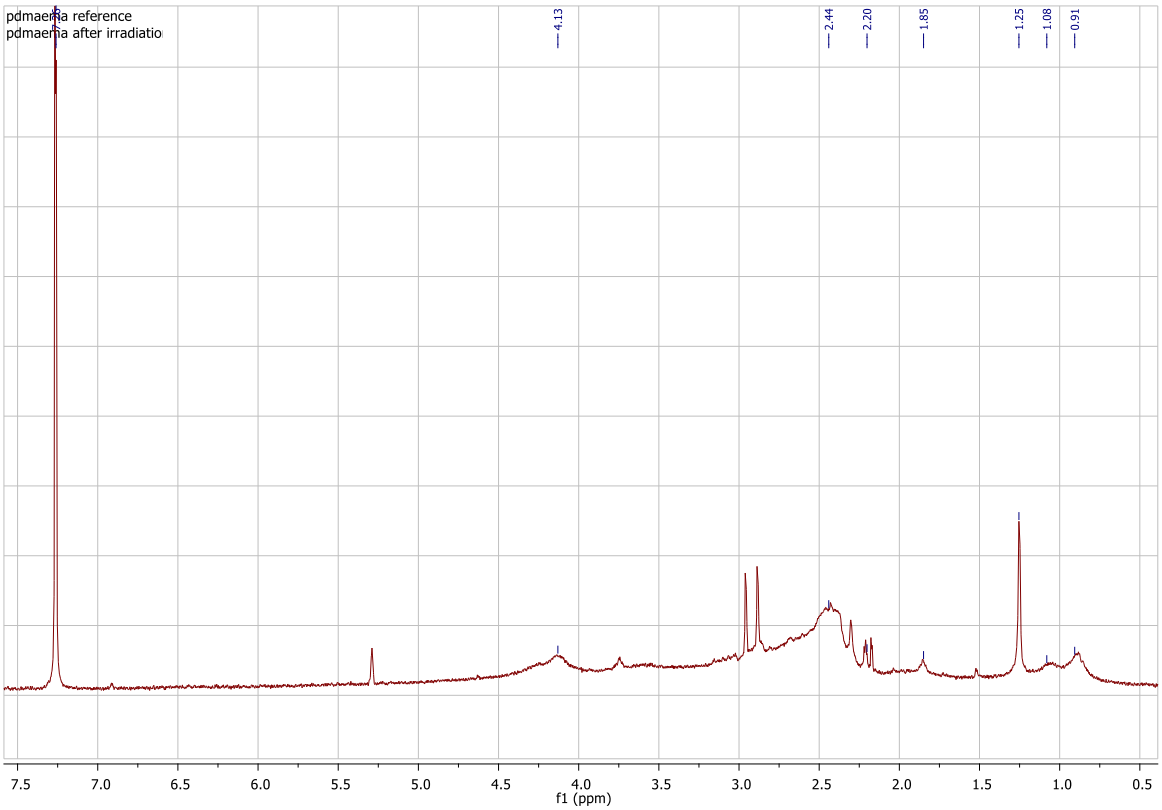

Figure 69 - PDMAEMA in deuterated chloroform after irradiation

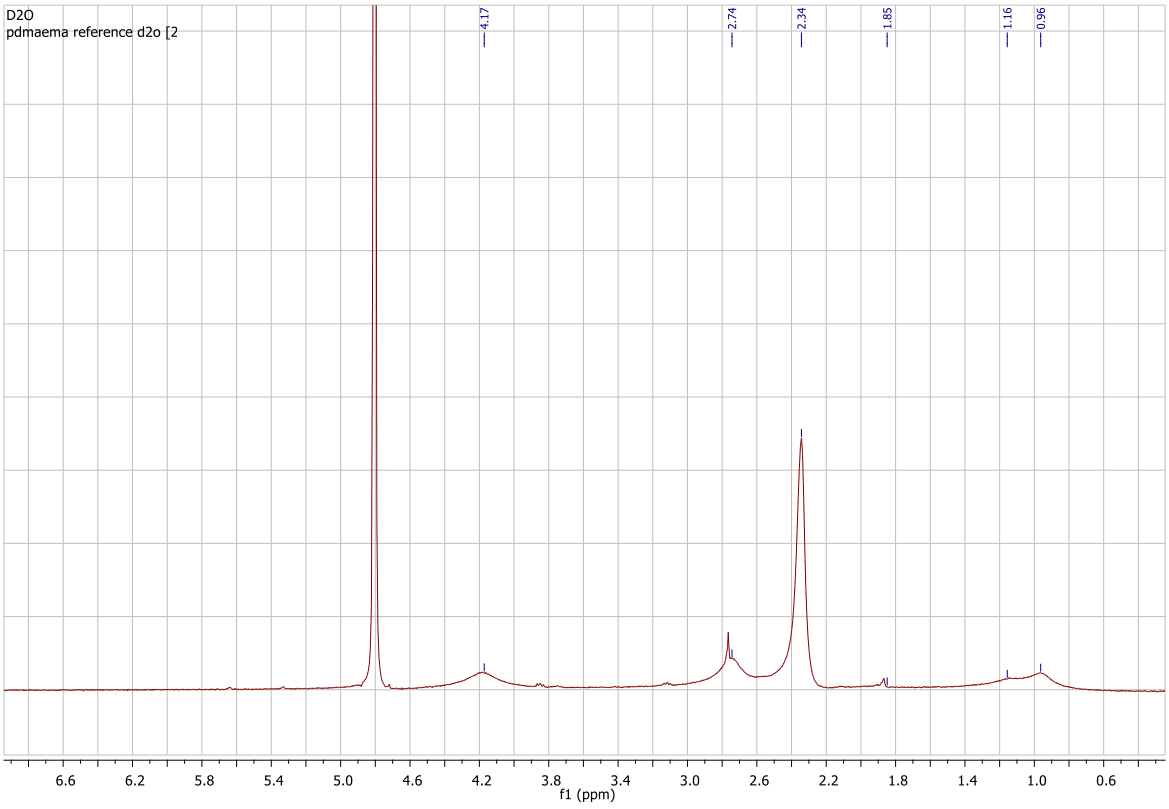

Figure 70 - PDMAEMA in deuterium oxide

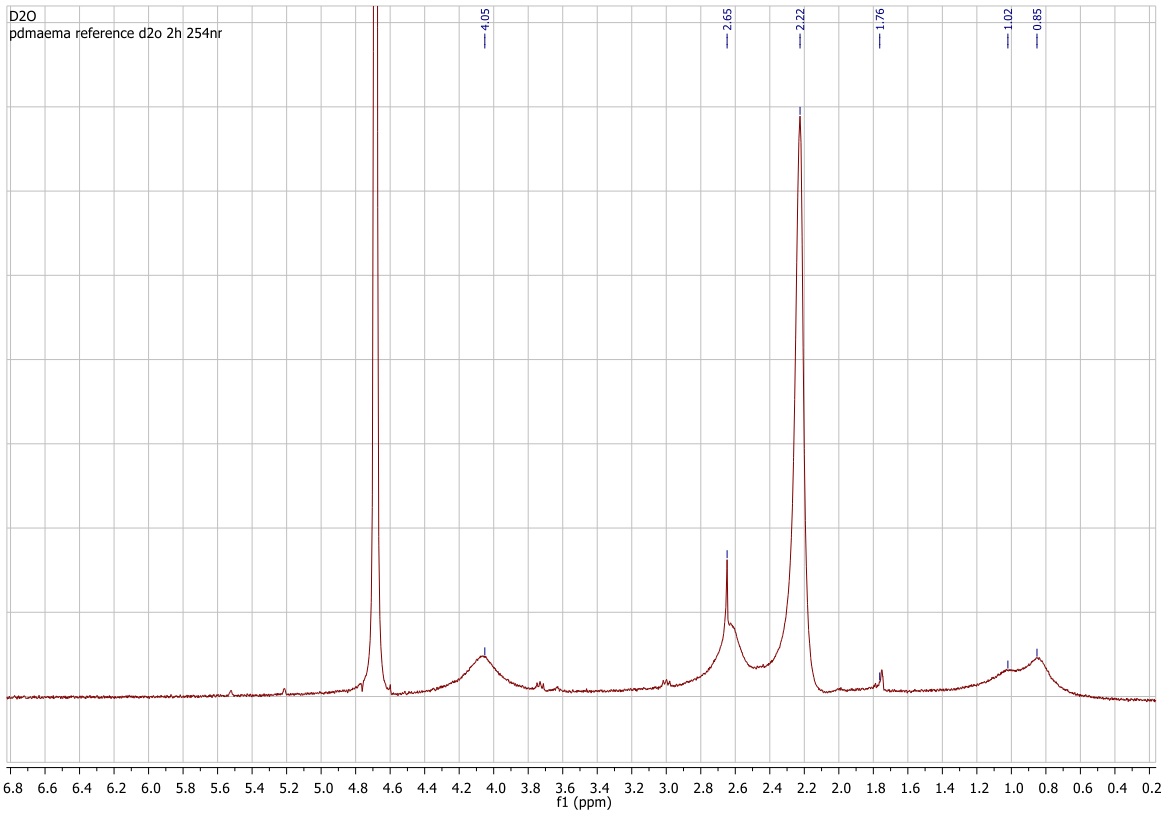

Figure 71 - PDMAEMA in deuterium oxide after irradiation

As seen in Figure 69, the ^{1}H NMR spectrum of PDMAEMA in chloroform changes substantially following UV irradiation, signifying the disappearance of the peaks and therefore a change in the solubility of the polymer in $CDCl_3$. On the other hand, the PDMAEMA spectrum in D_2O remains unchanged following UV irradiation of the sample. It is believed that DCl is produced in $CDCl_3$ upon irradiation which protonates the PDMAEMA units and render the polymer insoluble in the organic medium, which also explains the above results for the star copolymers.

Resuming the degradation experiments, a sample of the random $PDMAEMA_{30}$-$PMMA_{70}$-photodegradable star was prepared and photodegraded following a similar process. Four of the ^{1}H NMR spectra recorded during the photodegradation process (3h, 6h, 9h and 12h irradiation) are shown below (Figures 72 - 75).

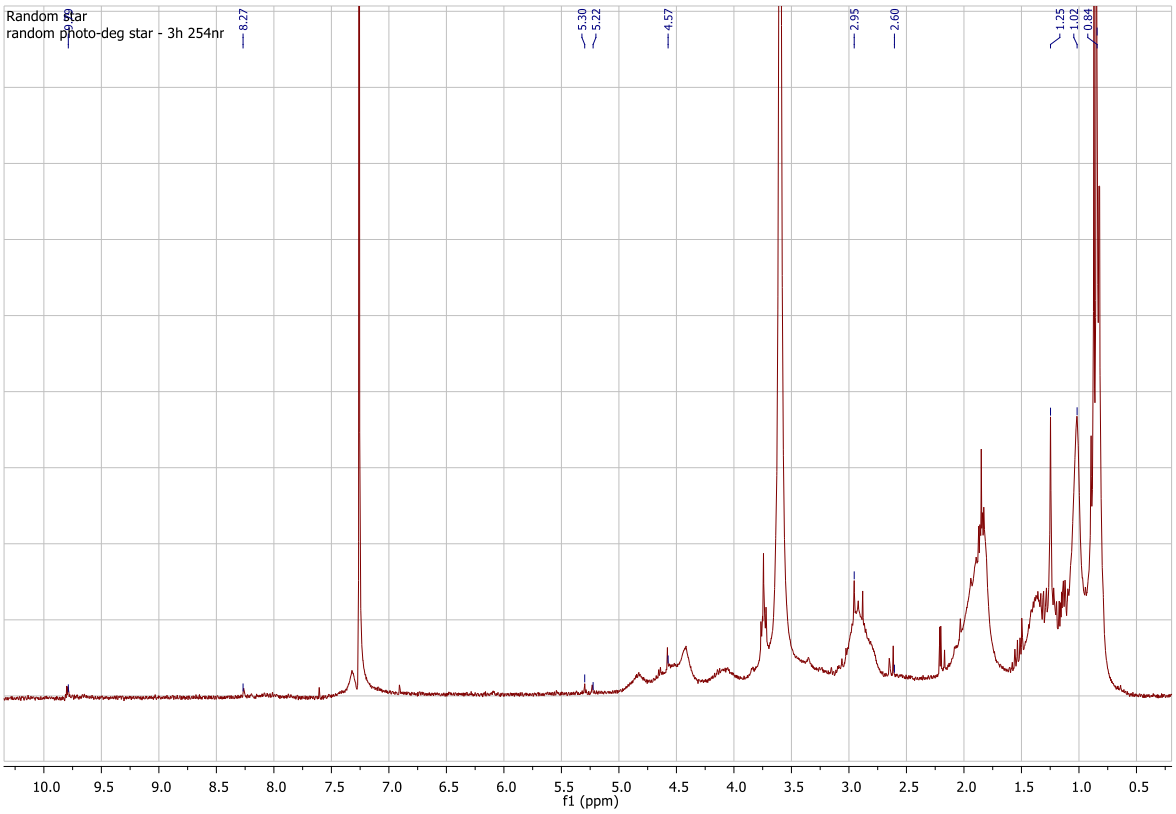

Figure 72 – ^{1}H NMR spectrum of the acid- and photo-degradable random copolymer star after 3h UV irradiation

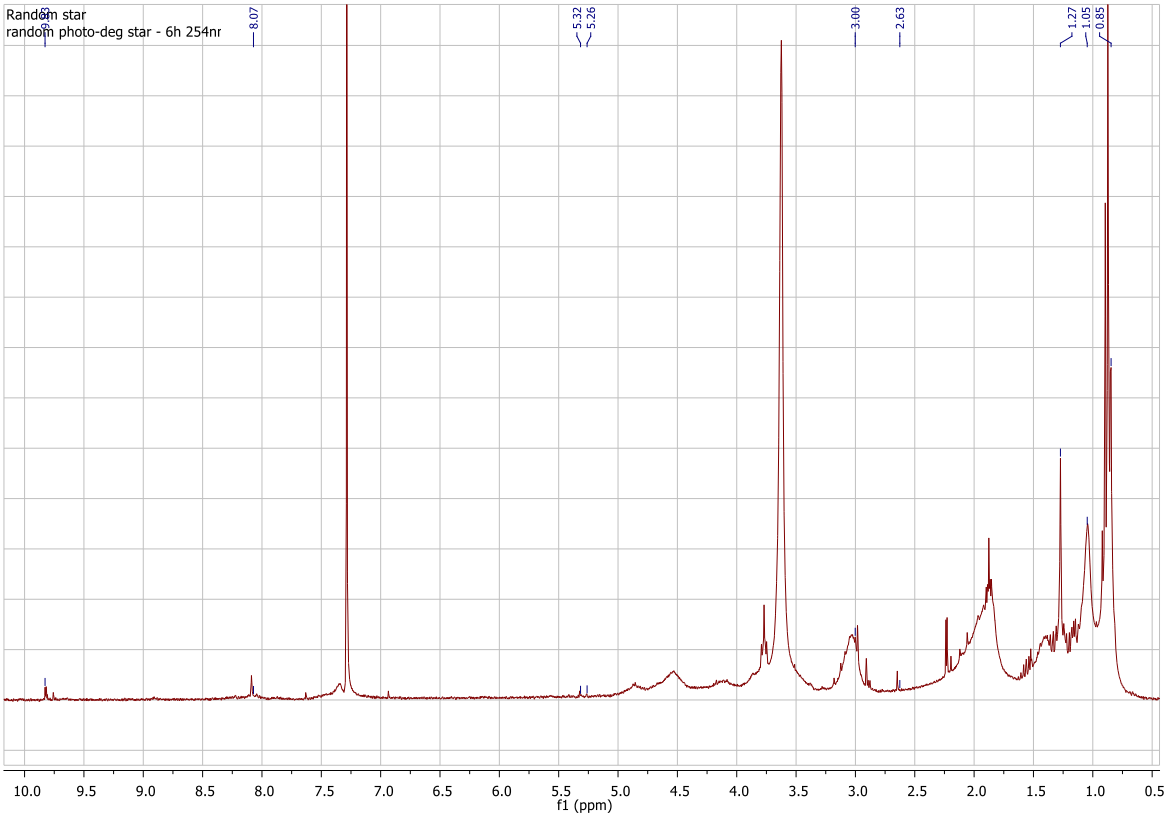

Figure 73 - ^{1}H NMR spectrum of the acid- and photo-degradable random copolymer star after 6h UV irradiation

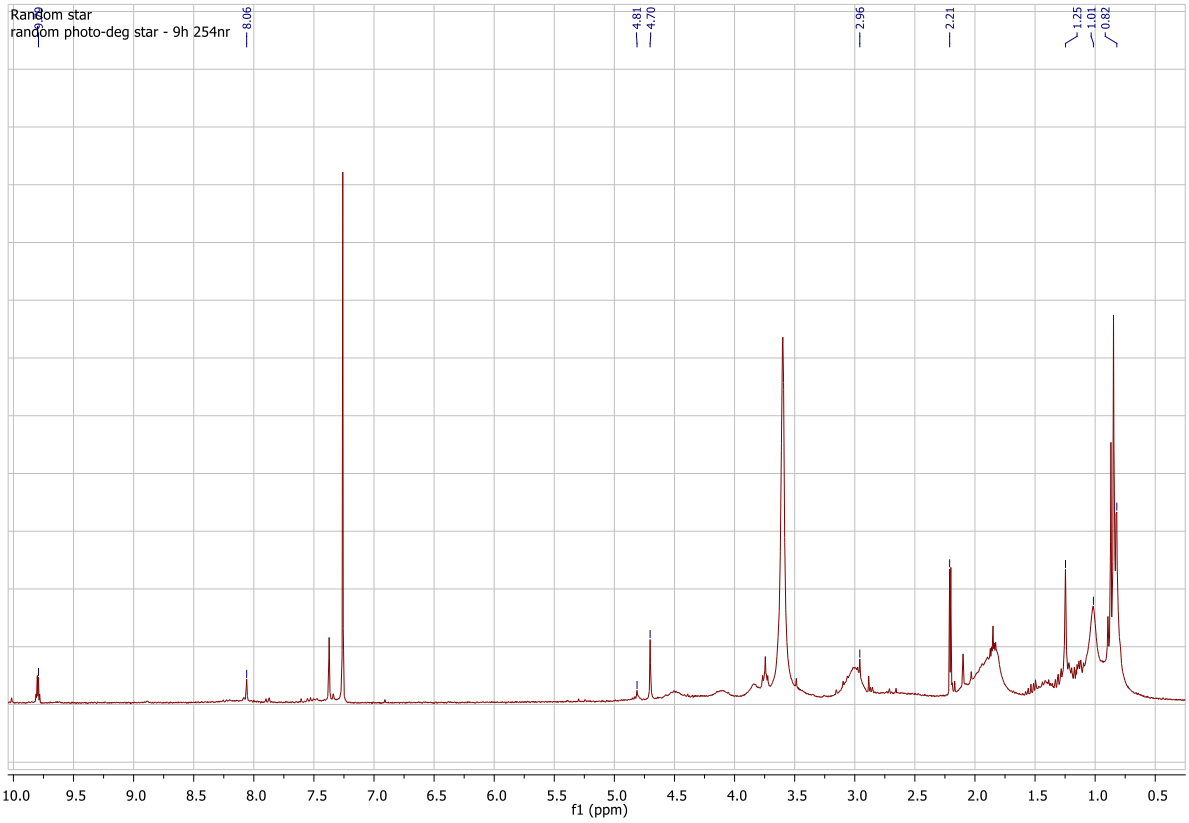

Figure 74 - ^{1}H NMR spectrum of the acid- and photo-degradable random copolymer star after 9h UV irradiation

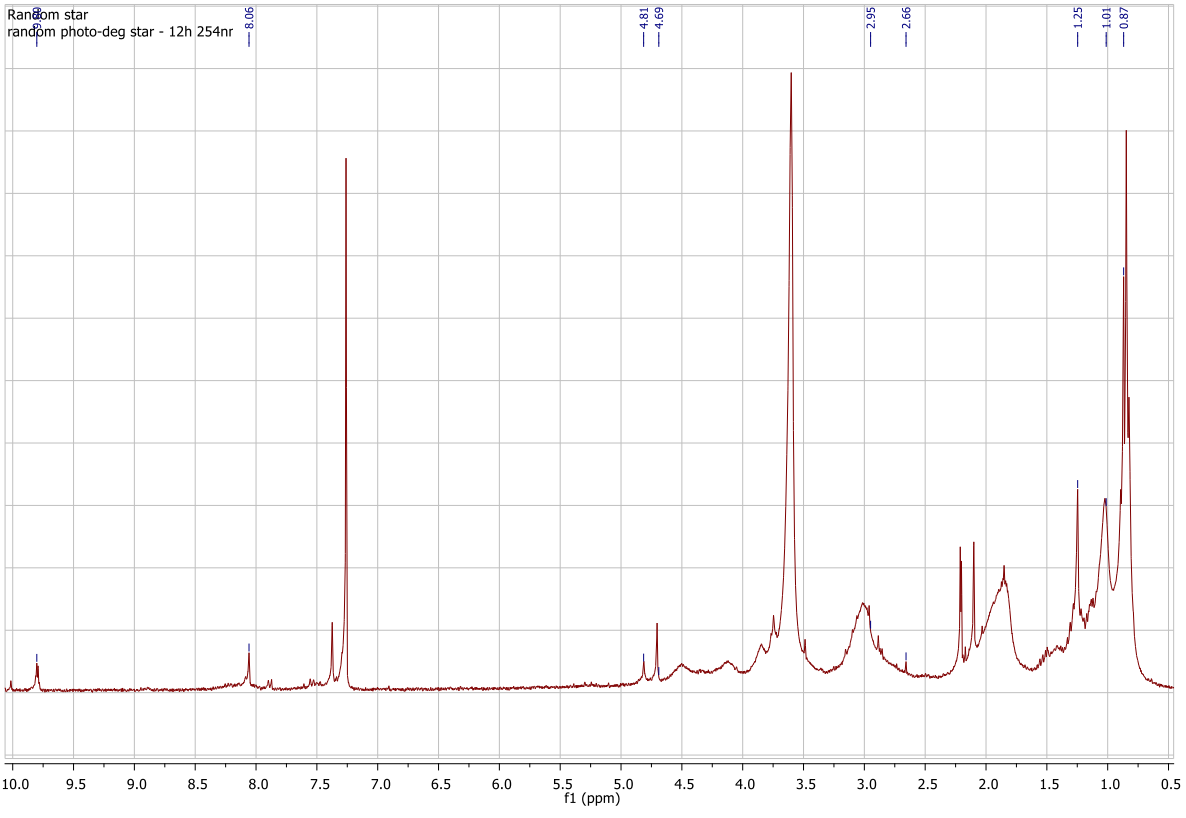

Figure 75 ^{1}H NMR spectrum of the acid- and photo-degradable random copolymer star after 12h UV irradiation

The peak assignment for the above spectra is as follows: 9.79ppm [(CHO), 1H], 8.06ppm [aromatic protons, 4H], 4.81ppm and 4.70ppm [(CH) and (CH_2), 1H and 2H respectively], 2.96ppm [(CH_2), 2H], 2.21ppm [2(OH), 2H], 1.25ppm [(CH_3), 3H] and 1.01ppm and 0.82ppm [(CH_3) on the backbone of the linear chains, 3H]. Again, the absence of the acetal proton peak at 4.82 ppm indicates the beginning of the degradation process, and upon increasing the irradiation times, the proton peaks of the photoproducts become more intense.

3.6.3 Scanning electron microscopy

Samples of the photodegraded polymers were also prepared and analyzed by SEM. The images taken for the photodegraded PDMAEMA$_{30}$-*b*-PMMA$_{70}$-photodegradable star polymer, are presented below (Figure 76).

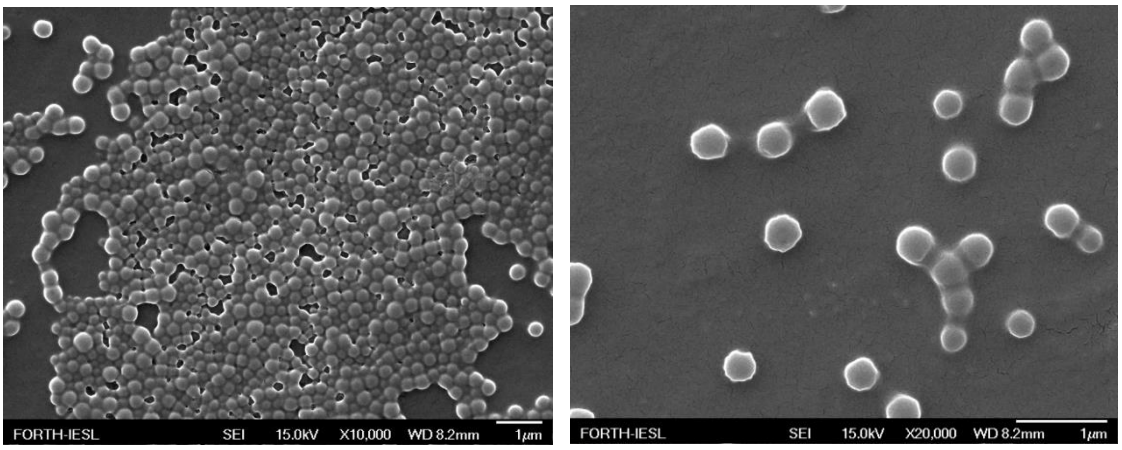

Figure 76 - SEM image of the photodegraded acid- and photo-degradable block copolymer star

As seen in the images above, the photodegraded sample forms spherical particles which are attributed to the self-assembly of the amphiphilic block copolymer arms. The formed particles can either be distinct, or in aggregates consisting of a large number of spheres.

For the photodegraded random PDMAEMA$_{30}$-PMMA$_{70}$-photodegradable star, the images are shown below (Figure 77).

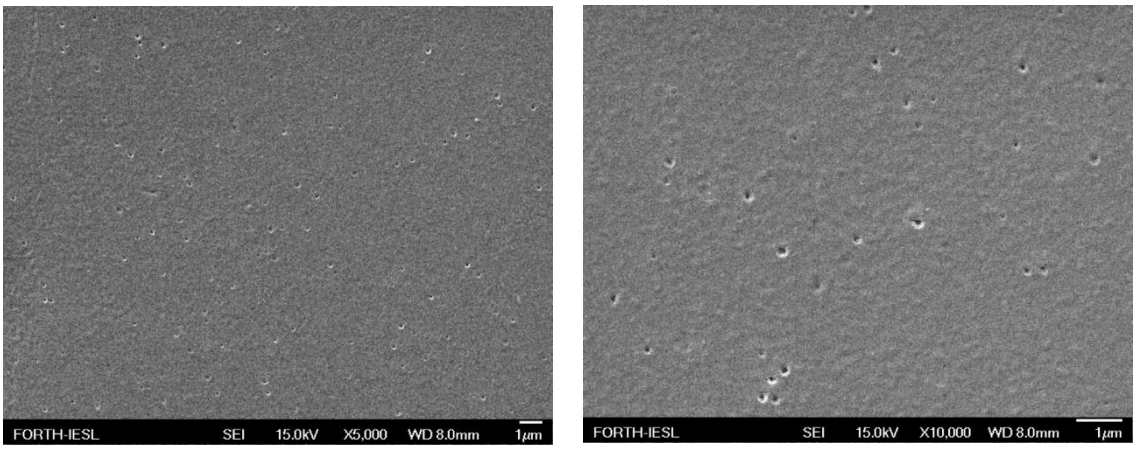

Figure 77 - SEM image of the photodegraded random acid- and photo-degradable star polymer

In this case a uniform film is observed on the substrate and no structures are formed. The lack of any defined structure as those observed in the SEM images of the intact copolymer stars, indicates that the upon UV irradiation the star copolymer effectively degrades to its constituent linear polymer chains that cannot be captured by SEM. The imperfections that are noted on the surface of the sample are attributed to the gold that the sample was sputtered with before imaging and not on the sample itself.

3.7 References

[1] Paul Rempp and Pierre Lutz, Model Macromolecules, *Makromol. Chem., Macromol. Symp.* ***62****, 213-224 (1992)*

[2] Theoni K., Georgiou, Leonidas A. Phylactou, Costas S. Patrickios, *Biomacromolecules* **2006,** 7, 3505-3512

[3] Georgiou, T. K., Vamvakaki, M., Patrickios, C. S., Yamasaki, E. N., & Phylactou, L. A. (2004). Nanoscopic Cationic Methacrylate Star Homopolymers: Synthesis by Group Transfer Polymerization, Characterization and Evaluation as Transfection Reagents. *Biomacromolecules*, 5(6), 2221–2229. doi:10.1021/bm049755e

[4] Maria Rikkou-Kolourkoti, Owen W. Webster, Costas S. Patrickios, Group Transfer polymerization, *Encyclopedia of polymer science and technology*, 2013, vol 99, 1-17, doi: 10.1002/0471440264.pst603

[5] Agarwal, S., Zhang, Y., Maji, S., & Greiner, A. (2012). PDMAEMA based gene delivery materials. Materials Today, 15(9), 388–393. doi:10.1016/s1369-7021(12)70165-7

[6] Pasparakis, G., Manouras, T., Selimis, A., Vamvakaki, M., & Argitis, P. (2011). Laser-Induced Cell Detachment and Patterning with Photodegradable Polymer Substrates. Angewandte Chemie International Edition, 50(18), 4142–4145. doi:10.1002/anie.201007310

[7] Pasparakis, G., Manouras, T., Vamvakaki, M., & Argitis, P. (2014). Harnessing photochemical internalization with dual degradable nanoparticles for combinatorial photo–chemotherapy. Nature Communications, 5(1). doi:10.1038/ncomms4623

[8] Wang, P., Hu, H., & Wang, Y. (2007). Application of the Excited State Meta Effect in Photolabile Protecting Group Design. Organic Letters, 9(15), 2831–2833. doi:10.1021/ol071085c

[9] Wang, P., Hu, H., & Wang, Y. (2007). Novel Photolabile Protecting Group for Carbonyl Compounds. Organic Letters, 9(8), 1533–1535. doi:10.1021/ol070346f

4. Conclusions and future work

Two novel cross-linkers were synthesized in this work for use in acid- and photo-degradable star polymer synthesis. The synthesis of the cross-linkers was achieved via an acid-catalyzed condensation reaction followed by purification via column chromatography. Group transfer polymerization and the arm-first approach was employed in order to synthesize star polymers using these cross-linkers. For the acid-degradable cross-linker, two different star polymers were synthesized, bearing block and random copolymer arms. The first star polymer comprised poly[(2-dimethylamino)ethyl methacrylate] (PDMAEMA) and poly(methyl methacrylate) (PMMA) block copolymer arms, and the second PDMAEMA-co-PMMA random copolymer arms. The produced polymers were purified by fractional precipitation to remove the unattached linear polymer chains that did not incorporate into the stars due to steric hindrance. The molecular weights of the linear precursors and of the star copolymers were determined by size exclusion chromatography. Their molecular structure was verified by nuclear magnetic resonance spectroscopy, their size was measured by dynamic light scattering and last, the star copolymers were imaged by scanning electron microscopy. Following their synthesis, the hydrolysis of the star copolymers under acidic environment was studied and the degradation products were characterized by SEC, ^{1}H NMR, and SEM. Similarly, for the acid- and photo-degradable cross-linker, two star polymers were synthesized via group transfer polymerization following the arm-first synthetic process and comprising block and random copolymer arms of PDMAEMA and PMMA. The star copolymers were purified via fractional precipitation and dried under vacuum. The molecular weight of the star polymers was determined by SEC, and their structure was verified by ^{1}H NMR spectroscopy. The size of the star polymers was measured by DLS and the stars were observed by SEM. Next, the hydrolysis of both star copolymers in acidic environment was verified by SEC, NMR, DLS and SEM. The photo-degradation of the star polymers was also studied following irradiation of the star polymers at 254 nm and the photoproducts were characterized by SEC, NMR and SEM.

Future work on these copolymers could focus on further studying the stability of the stars, as well as their hydrolysis kinetics. The degradation products will be further characterized by TEM and zeta potential measurements. These star copolymers could be further examined as gene transfer agents or drug carriers, since star polymers have already been shown to be promising in such applications. Acid- and photo-degradable stars of different comonomers could be also prepared for use in different fields (i.e. environmental applications for the capture of toxic pollutants).